Rotating black holes in the cubic Galileon theory

Karim van Aelst

▶ **To cite this version:**

Karim van Aelst. Rotating black holes in the cubic Galileon theory. Physics [physics]. Université Paris Cité, 2020. English. NNT : 2020UNIP7043 . tel-03197687

HAL Id: tel-03197687
https://theses.hal.science/tel-03197687

Submitted on 14 Apr 2021

HAL is a multi-disciplinary open access archive for the deposit and dissemination of scientific research documents, whether they are published or not. The documents may come from teaching and research institutions in France or abroad, or from public or private research centers.

L'archive ouverte pluridisciplinaire **HAL**, est destinée au dépôt et à la diffusion de documents scientifiques de niveau recherche, publiés ou non, émanant des établissements d'enseignement et de recherche français ou étrangers, des laboratoires publics ou privés.

Thèse de doctorat en physique

*délivrée par l'*Université de Paris

École doctorale 564 : Physique en Île-de-France

préparée au Laboratoire Univers et Théories - Observatoire de Paris

Rotating black holes in the cubic Galileon theory

présentée par Karim Van Aelst

dirigée par Eric Gourgoulhon

soutenue le 24 juin 2020

devant un jury composé de :

David Langlois, *DR CNRS, Laboratoire Astroparticules et Cosmologie*	Président
Panagiota Kanti, *professeure, University of Ioannina*	Rapportrice
Geoffrey Compère, *professeur, Université Libre de Bruxelles*	Rapporteur
Danièle Steer, *professeure, Laboratoire Astroparticules et Cosmologie*	Examinatrice
Karim Noui, *maître de conférence, Institut Denis Poisson*	Examinateur
Eric Gourgoulhon, *DR CNRS, Laboratoire Univers et Théories*	Directeur
Philippe Grandclément, *CR CNRS, Laboratoire Univers et Théories*	Invité

Remerciements

Ces trois années au LUTh ont été remplies de purs plaisirs d'apprentissage. Elles n'ont pas non plus été dépourvues de quelques moments d'anxiété mais, humainement, je n'imagine pas une thèse pouvant être vécue avec plus de sérénité et de simplicité. Ceci a été permis par de nombreuses personnes, que j'espère nommer ici de manière exhaustive.

Mes premiers remerciements vont naturellement à Eric, pour sa bienveillance, sa disponibilité, sa patience, son attention à rendre ces trois années les plus enrichissantes, formatrices et valorisantes. Evidemment, je veux ensuite remercier Philippe, pour ses conseils et toute son aide dans l'exploitation de l'outil si efficace qu'il a développé. Je dois également un immense merci à Christos Charmousis, d'avoir partagé ses connaissances expertes avec grande gentillesse et participé de manière essentielle à ce projet. Merci à vous, pour tout cela, et d'inspirer à faire bien plus.

Au jour le jour, l'équipe ROC du LUTh a été un environement on ne peut plus paisible pour préparer une thèse. Pour cela, merci beaucoup à Micaela, Jérôme, Alexandre, Aurélien Sourie, Laura, Silvano. Ce cadre est d'autant plus agréable qu'il est partagé avec d'autres étudiants : Antoine, Aurélien, Paul, Jordan, Elise, pour lesquels j'espère bien sûr la plus grande réussite dans la suite de leurs projets.

Cet environement chaleureux ne s'arrête pas à l'équipe ROC : je remercie tout particulièrement Stéphane et Fabrice de l'équipe informatique du LUTh, pour leur gentillesse, disponibilité et aide infaillible dans la résolution de problèmes parfois rébarbatifs. Je dois également de grands remerciements à l'équipe administrative, Nathalie, Annie, Catherine et Marie bien sûr, pour leur gentillesse et leur accompagnement précieux. Un grand merci également à Zakaria, pour son accueil chaleureux dans le laboratoire, et de s'être impliqué dans le suivi du projet.

Ces remerciements ne peuvent pas non plus s'arrêter aux murs du LUTh : je remercie tout d'abord et avec plaisir Gilles Esposito-Farèse et Frédéric Vincent, pour leur temps consacré à plusieurs discussions très utiles. De même, je remercie doublement David Langlois d'avoir très aimablement suivi ce projet dans sa durée jusqu'à en accepter la présidence de jury. *I owe many thanks to Panagiota Kanti and Geoffrey Compère, for the time they devoted to carefully reading the manuscript and making many constructive comments for improvement.* Merci beaucoup à Danièle Steer de porter intérêt à ce projet en acceptant de siéger dans ce jury. Merci à Karim Noui, pour la bienveillance qu'il a manifesté lors de nos quelques rencontres au point d'avoir également accepté le rôle d'examinateur.

Encore un immense merci à toutes ces personnes, fréquentées de près ou de loin, de savoir créer un cadre idéal pour les étudiants.

Quelques mots encore pour les amis proches, qui restent si importants même en ne partageant plus que quelques heures par an. En nommer un serait ridicule sans les nommer tous, ce qui serait aussi ridicule. Se reconnaîtront donc ceux que je retrouve à (quasiment) chaque nouvel an (sous peine de représailles), puis tous les habitants officiels ou clandestins de la chambre 340, et enfin ceux qui ont entendu résonner les murs du chemin de la Butte.

Plus personellement, merci à mon père, ma sœur, et ma mère bien sûr, de toujours vouloir et offrir le meilleur pour moi, et bien plus... Enfin, merci à ma lumineuse Lucie, pour ses encouragements, sa patience, et tout ce qui rend la vie douce et éclatante.

Contents

Introduction

Two weeks before the beginning of the Ph.D. project presently reported, a binary neutron star merger was detected for the first time ever. The confirmation of this exceptional event was based on compatible incoming directions (see figure 1 in reference [1]) and almost equal arrival times (see figure 2 in [1]) of two different types of signals: a gravitational wave labelled GW170817 [2] and a gamma-ray burst labelled GRB170817A [5, 6], respectively detected by the gravitational wave observatories of the LIGO/Virgo collaboration [3, 4] and the gamma-ray space telescopes Fermi [7] and INTEGRAL [8]. Beside the large amount of information carried by these two signals, this "multi-messenger" observation directly implied that the propagation speeds of these two signals, produced by a 43 Mpc distant merger, had to be equal.

Of course, such an experimental fact must be explained in any theory whose application scope includes gravitational and electromagnetic phenomena on supra-galactic scales. Einstein's general relativity (GR) is such a theory, and it does predict the experimental equality of electromagnetic and gravitational waves propagation speeds. Although more than a century old, GR not only solved observational issues at the time, but it still provides the best framework and explanations to most of the astrophysical and cosmological observations realised since then. More than that, GR predicted the existence of new types of gravitational phenomena, which could be observationally confirmed and tested [9, 10] several decades after they were first theoretically characterized. Among such remarkable phenomena, gravitational waves hold a central position, together with black holes, which may form binary systems producing detectable gravitational waves before they merge, just like the binary neutron stars mentioned above. These topics will of course be readdressed in the core of the manuscript.

Most of the experimental successes of GR only probed weak gravitational regimes yet, i.e. phenomena in which gravitation is significantly less intense than in extreme regions like black hole close environments [11]. This is why increasingly strong regimes of gravity are tested by modern, highly accurate instruments. Over the last five years, the interferometer GRAVITY [12] and the Event Horizon Telescope [13] have collected data from objects involved in high energy gravitational processes: coalescing compact objects [2, 4], stars and flares orbiting $Sgr\ A*$ (the central supermassive black hole of the Milky Way) [14, 15], accretion disks and shadows of supermassive black holes [16, 17]. So far, all these observations are consistent with the black hole models of GR. But this observational chase will go on as long as technology and ideas offer new ways to test these regimes.

The rationale motivation of this is that all known theories feature a limited application scope: none of them should expect to be a "theory of everything", and is called instead an "effective" theory [18, 19]. Not only GR had originally no particular reason not to be one of such effective theories but, since then, more precise theoretical argu-

ments, rather than observational facts, have supported the case that the effectiveness of GR should break down in the high energy or strong curvature regimes, mainly in view of its inadequacy to unify with the other fundamental interactions [20, 21]. So far, no observation confirmed these claims. Interestingly, it is instead in the very low energy gravitational regimes that GR may already have revealed its limits. Although one should remain cautious about such claims, GR does suffer from several shortcomings or unresolved questions on galactic and cosmological scales: it does not yet provide satisfactory explanations to the issues of dark matter and dark energy [22, 23].

This all further justifies why both the extremely low and high energy regimes should keep being explored, since knowing the energy scales at which the predictions of GR start failing, and the way they do, will provide precious hints as to how design an alternative theory enjoying a much larger effective scope. Concretely, such a theory would provide answers or alternative solutions to the various shortcomings of GR, while remaining compatible with all the existing observational constraints (such as the equality between electromagnetic and gravitational waves propagation speeds, confirmed by the event GW170817-GRB170817A). In addition, such a theory should fulfill some essential theoretical requirements, such as being predictive (the theory must rely only on a finite number of parameters that can be determined from experiment once and for all), well-posed (knowing exactly the "initial" state of an isolated system "at a given time" must be enough to predict its state at any "future time", which should depend "continuously" on the "initial" state[1]), stable (any physically relevant configuration of a system described by the theory must admit arbitrarily close "perturbed" configurations). All these notions, and terms in quotation marks, actually have precise, non-trivial mathematical formulations, which will be rediscussed in the manuscript.

To realize such a theory, many alternatives to GR are being developed and thoroughly studied [23–27]. Structurally, some of them are slight modifications of GR (called "modified" theories of gravity), while others are based on fundamentally different paradigms (generically called "alternative" theories of gravity). Besides, GR and all alternative theories are often collectively called "theories of gravitation", but it should be clear that most of them also describe other fundamental interactions like electromagnetism, and are for instance expected to recover classical Newtonian mechanics in some consistent limit. Calling them "theories of gravitation" first reminds that they do intend to offer a new consistent description of gravitation, fulfilling most of the theoretical and observational requirements mentioned above. This is indeed worth insisting on, as many physical theories do not even address the challenge to incorporate this problematic interaction. The second reason for this reductive designation is that only the fundamental description of gravity varies between most of these theories. This then has indirect consequences on non-gravitational physics in presence of gravitation, but the theories are equivalent otherwise. "Theories of gravitation" thus not only deal with gravitation, but it actually is their prime reason of existence.

The cubic Galileon theory, which is investigated in this manuscript, belongs to some of the simplest modifications of GR, known as scalar-tensor theories. Although the simplest modified theories, they may yield predictions very different from GR. This is true to the extent that some of them, like Brans-Dicke theory, do not stand the confrontation with observational data, and are thus ruled out for good [10, 28]. This

[1]This additional "continuity" condition makes well-posedness a stricter requirement than determinism.

fact actually provides one more reason to study alternative theories (beside finding a description of the extreme regimes of gravity): within the intermediate regimes of gravity, where GR is so successful, identifying all the modifications of GR that lead to theoretical pathologies, or observational incompatibilies, is a relevant approach to single out the fundamental reasons that explain the undeniable effectiveness of GR in these regimes.

The cubic Galileon theory does yield different predictions than GR too, and the present manuscript will highlight some of them in the case of rotating black holes (the latter are harder to investigate than static black holes, but their observational importance comes from the fact that astrophysical black holes are expected to be rotating). Beforehand, the first part of the manuscript reviews the essential notions involved in discussions on theories of gravitation. Although the latter offer competing descriptions of gravity, most of them share common foundations, which are reviewed in the first two chapters of part I: chapter 1 introduces generic definitions and properties of spacetime, while chapter 2 discusses a few highly regarded principles, such as general covariance and Lorentz invariance, which help refining the framework and tools common to all theories of gravitation, and single out GR in some senses. The following two chapters review some aspects of the latter: chapter 3 recalls the status of GR in regard of the theoretical and observational requirements mentioned above, while chapter 4 introduces two alternative formulations of GR, not to be confounded with alternative theories. In contrast, the latter are addressed in the last two chapters of part I: chapter 5 introduces a few classes of modified theories of gravity connected to topics mentioned in earlier chapters, while chapter 6 makes the transition to part II in focusing on Horndeski theories of gravitation, to which the cubic Galileon belongs. Thus, part I of the manuscript might notably be helpful as an introductory guide through alternative theories, extending a first course on GR.

In view of the program of investigation of all theories of gravitation outlined in the previous paragraphs, part II of the manuscript focuses on the cubic Galileon theory, with the purpose of identifying how it may deviate from GR in some of the strongest possible types of regimes, namely the neighbourhood of (rotating) black holes. To this end, the first three chapters of part II are devoted to the numerical construction of rotating black holes in the cubic Galileon theory: chapter 7 explicitly introduces the theory and derives the equations to be solved, while chapter 8 presents the numerical method used to solve them, and discusses the validity of the numerical solutions, which are finally exposed in chapter 9. Observable signatures of the cubic Galileon theory are then investigated in the three following chapters: based on the numerical solutions constructed in the previous chapters, chapters 10 and 11 compare geodesic motion around black holes in GR and the cubic Galileon theory, while images, produced by an accretion disk orbiting the Galileon black hole solutions, are numerically computed in chapter 12.

The different chapters are unbalanced in terms of length and subsections. Rather than troubling, it is hoped that this helps highlight the progression through distinct notions. Besides, all along the manuscript, original papers on a given topic and hopefully some of the best references presenting it are cited. References cited in a row usually appear in chronological order, so that the last ones should provide the most recent treatment of the topic, in the most modern and familiar language.

Part I

Theories of gravitation

Chapter 1

General framework of physical theories

Contents

In this introductory chapter, we will go over the elementary concepts involved in the formulation of all theories of gravitation: section 1.1 and 1.2 respectively introduce the spacetime manifold and how to define the variations of a physical quantity over it, while sections 1.3, 1.4 and 1.5 respectively cover the specificities of these notions in the example cases of Newtonian physics, special relativity and GR.

Although anachronous, old and recent physical theories are most often taught with concepts that were not available at the time they were first devised. But such modern concepts turned more appropriate to efficiently handle a theory without any former superfluous complication. Expectedly, the present manuscript is no exception in systematically using the language of differential topology and geometry, even e.g. when discussing Newtonian physics. Besides standard, purely mathematical textbooks such as [29–31], the two volumes [32, 33] are a very rich and technical resource with rigorous applications to mathematical physics.

1.1 Topology of spacetime

Eluding centuries of reflexions carried out by philosophers and scientists on the various ways to define physical reality [34], let us here define it as the set of information accessible to measurements made by anyone in the countable set of humans interested in physics. Generally, a physical theory aims at predicting the output of a class of measurements performed by a class of observers on a class of systems. The simplest kind of measurement such a theory may be concerned with is that of the position of a system at a certain time with respect to a given observer. It is performed by the various observers by means of ideal clocks and rulers that were once confirmed to be identical at the same place and date.

Practically, any measurement corresponds to an interaction between the measuring apparatus and the system[2], e.g. a certain point of a ruler touches the system. Then, the actual time t that the observer associates to this measurement is such that the interaction is simultaneous with the ideal clock displaying the date t. However, the clock, carried by the observer, may be far from the system, so that the non-trivial notion of simultaneity at a distance requires a rigorous definition. As will be mentioned in the sections below, such definition varies between theories, as it relies on the assumptions that a given theory makes on the physical reality. Broadly speaking, the time t is always a very complicated function of:

- the reception time t' at which the observer first detects a signal generated by the interaction with the system,
- the very nature of such signal,
- further essential information...

Often, the signal has been purposedly emitted by the observer at an earlier time t_0 to be reflected back when interacting with the system. Then, t_0 may be enough additional information to determine t, but this is not always possible, e.g. for astrophysical observations. In the latter cases, additional information may be provided by the reception times of other signals, or those recorded by other observers[3]. Ultimately though, all definitions of simultaneity must at the very least agree in the trivial limiting case of a measurement made at zero distance from the observer, i.e. on the clock mechanism: in this case, all these complicated functions must yield $t = t'$.

Independently of the definition chosen, consider two observers, each performing a time-position measurement on a system. Call such measurements "equivalent" when their respective interactions with the system happen at the same time for an observer tied to the system. Each equivalence class of such {observer, time, position} measurements is called an event ("the system was here at this time for this observer, or equivalently there at that time for that observer"), and the set of all events is called spacetime. The equivalence relation is indeed independent of the definition of simultaneity since it only relies on the trivial time measurements made by the observer at zero distance to the system. This is a relief as otherwise the mere definition of what an event is would be theory dependent. What the definition of simultaneity does determine is e.g. the situations in which some of the three dates involved in the equivalence relation are equal.

Empirically, any time-position measurement yields finite-accuracy rational numbers. Yet, it is much more profitable to model such a measurement by real numbers in an open set of $\mathbb{R}^4$ in order to benefit from the whole theory of differential calculus on manifolds [39][4]. Indeed, denote $\mathcal{U}_\mathcal{O}$ the set of all events accessible to an observer $\mathcal{O}$.

[2]Classical physics assumes that the resulting disturbance on the system can be made arbitrarily small, while this is fundamentally impossible for most measurements on a quantum system (reduction of the wave packet [35–38]).

[3]The distance travelled by the signal is of course an essential information, but it also comes down to chronometric measurements in the end, since using rulers is obviously unrealistic for astrophysical observations.

[4]See section 3 of this reference for more on this point, and the rest of the article for further discussions on the local and global requirements usually made on spacetime structures to model physical reality.

Since the measurements are now real-valued, observer $\mathcal{O}$ defines a map $\phi_{\mathcal{O}}$ from $\mathcal{U}_{\mathcal{O}}$ to an open set of $\mathbb{R}^4$. By definition, each event $\mathcal{E}$ belongs to at least one set in the countable family of $\mathcal{U}_{\mathcal{O}}$, $\phi_{\mathcal{O}}(\mathcal{E})$ then defines the coordinates of $\mathcal{E}$ with respect to observer $\mathcal{O}$. Furthermore, all maps $\phi_{\mathcal{O}}$ are respectively made continuous on the sets $\mathcal{U}_{\mathcal{O}}$ by equipping spacetime with the initial topology they induce, which fulfills the Hausdorff separation condition. With such a structure, spacetime is a manifold. In addition, all observers were once at the same place and date to take their own copy of the measuring apparatus, or at least were they able to communicate the procedure to build such ideal devices. Spacetime is thus path-connected.

1.2 Preferred frames and derivatives

As one would expect from the title, this section merely ends up with the standard notions of covariant and Lie derivatives. Yet, rather than postulating their axioms, the goal is to provide an empirical introduction to these two aspects of the same natural method that defines variations on a manifold. This should highlight the underlying "preferred" frames, which will be useful all along part I of the manuscript.

Broadly speaking, finding out the physical law ruling the outcome of a measurement, or an intermediate physical quantity Q, amounts to identifying the sources that would cause Q to vary over spacetime. In practice, the variations of a physical quantity Q are evaluated in a given direction, i.e. along a vector tangent to the spacetime manifold $\mathcal{S}$. Recall that a tangent vector d at a spacetime event $\mathcal{E}$ actually corresponds to a particular equivalence class of curves $\mathcal{C}$ through $\mathcal{E}$[5] (as usual, the set of all such classes, i.e. of all tangent vectors at $\mathcal{E}$, will be denoted $T_{\mathcal{E}}\mathcal{S}$). Measuring variations at $\mathcal{E}$ in the direction d thus means recording values of Q along one of the curves $\mathcal{C}$ and differentiate them. But such values, and hence their variations, depend on the way they are measured along $\mathcal{C}$. To illustrate this in less generic terms, figure Q as a n-dimensional vector field over spacetime (in the general sense that, at each spacetime event $\mathcal{E}'$, there exists a n-dimensional vector space $V_{\mathcal{E}'}$ to which $Q(\mathcal{E}')$ belongs). Then, all the possible ways to measure Q correspond to the various vector frames defined along $\mathcal{C}$. Thus, a priori, the explicit formulation of the law requires to specify with respect to what reference apparatus, defined along $\mathcal{C}$, it is expressed.

This is fine, but it would be very practical, e.g. to ease communications between observers, to construct a universal notion of variation along $\mathcal{C}$, i.e. on which all observer would agree. The minimal and most natural way to define such a universal derivative operator $\mathcal{D}_{\mathcal{C}}$ is to arbitrarily pick one, preferred, reference system among all those defined along $\mathcal{C}$. All observers should then convert and differentiate their measures in terms of this preferred system. In the case of Q being a vector field, an observer $\mathcal{O}$ measures the components Q^α of Q along $\mathcal{C}$ with respect to her personal frame $\{q_\alpha\}$ (so that $Q = Q^\alpha q_\alpha$), before converting them to the preferred frame $\{\tilde{q}_\alpha\}$ according to $\tilde{Q}^\alpha = [m^{-1}]^\alpha{}_\beta \, Q^\beta$ where $m \in \mathrm{GL}_n(\mathbb{R})$ is the transition matrix defined by $\tilde{q}_\alpha = m^\beta{}_\alpha q_\beta$. Only then can she differentiate the components $\tilde{Q}^\alpha$ along $\mathcal{C}$, denoted $\dot{\tilde{Q}}^\alpha$. Knowing the matrix m, the observer is finally free to convert the differentiated com-

[5] More precisely, once $\mathcal{E}$ and all such curves $\mathcal{C}$ are respectively identified with a point e and curves c in $\mathbb{R}^4$ through any suitable chart, the curves c have the same tangent vector at e in $\mathbb{R}^4$, in which the notion of tangent vector to a curve is already well-defined.

ponents back to her personal frame, and hence define the components of the universal derivative as

$$(\mathcal{D}_{\mathcal{C}}Q)^{\alpha} = m^{\alpha}{}_{\beta}\,\dot{\tilde{Q}}^{\beta} = m^{\alpha}{}_{\beta}\left(\left[\dot{m}^{-1}\right]^{\beta}{}_{\gamma}\,Q^{\gamma} + \left[m^{-1}\right]^{\beta}{}_{\gamma}\,\dot{Q}^{\gamma}\right) = \dot{Q}^{\alpha} + m^{\alpha}{}_{\beta}\left[\dot{m}^{-1}\right]^{\beta}{}_{\gamma}\,Q^{\gamma}, \tag{1.2.1}$$

so that each observer manipulates a personal formulation of $\mathcal{D}_{\mathcal{C}}$, but the final universal derivative $\mathcal{D}_{\mathcal{C}}(Q^{\alpha}q_{\alpha})$ is independent of the observer because, ultimately, it is always the unambiguously defined vector $\dot{\tilde{Q}}^{\alpha}\tilde{q}_{\alpha}$. The operator $\mathcal{D}_{\mathcal{C}}$ thus defined is $\mathbb{R}$-linear and obeys the Leibniz rule $\mathcal{D}_{\mathcal{C}}(\lambda Q) = \dot{\lambda}Q + \lambda\mathcal{D}_{\mathcal{C}}Q$ for any function λ along $\mathcal{C}$.

Furthermore, note that the last expression of (1.2.1) is invariant under $m \mapsto m \cdot p$ if and only if (*iff*) p is any matrix in $\mathrm{GL}_n(\mathbb{R})$ constant along $\mathcal{C}$. This means that one could have converted to and back from another frame $\tilde{q}'_{\alpha} \equiv p^{\beta}{}_{\alpha}\tilde{q}_{\beta}$, which is thus as a preferred frame as $\{\tilde{q}_{\alpha}\}$. Therefore, a preferred frame always comes with the whole family of frames constantly related to it by the matrices of $\mathrm{GL}_n(\mathbb{R})$[6].

Call "universally transported" along $\mathcal{C}$ the configurations of Q satisfying $\mathcal{D}_{\mathcal{C}}Q = 0$ all along $\mathcal{C}$. They form a vector subspace of all possible configurations of Q along $\mathcal{C}$. One easily sees from (1.2.1) that the preferred frames are precisely all the possible bases of this subspace (which is why, following the Leibniz rule, only the components $\tilde{Q}^{\alpha}$ of Q have to be differentiated in such preferred frames, whereas the basis vectors of non-preferred frames must also be differentiated).

Conversely, if all observers agree on a universal derivative $\mathcal{D}_{\mathcal{C}}$ with reasonable properties[7], there will actually exist a corresponding preferred system. One should find it by adjusting a measuring apparatus along $\mathcal{C}$ until it yields constant measurements on all the universally transported configurations $\tilde{q}$ of Q along $\mathcal{C}$ (there surely exists several such apparatus). This can be stated more precisely in the vector case: most reasonable properties on $\mathcal{D}_{\mathcal{C}}$ are the $\mathbb{R}$-linearity and Leibniz rule expressed above. The corresponding universally transported configurations thus form a vector subspace of all possible configurations of Q along $\mathcal{C}$. Denote $\{\tilde{q}_{\alpha}\}$ one of its bases. Given the first order nature of the last expression in (1.2.1), for any $\mathcal{E}'$ on $\mathcal{C}$, and any $w \in V_{\mathcal{E}'}$, there always exists a universally transported configuration equal to w at $\mathcal{E}'$. This means that $\{\tilde{q}_{\alpha}(\mathcal{E}')\}$ forms a basis of $V_{\mathcal{E}'}$, and hence $\{\tilde{q}_{\alpha}\}$ is a vector frame along $\mathcal{C}$. Since it is also universally transported, it is a preferred frame according to the characterization given above.

Therefore, when Q is a vector quantity, picking a preferred frame along $\mathcal{C}$ is equivalent to constructing a universal $\mathbb{R}$-linear derivative $\mathcal{D}_{\mathcal{C}}$ obeying the Leibniz rule. Then, $\mathcal{D}_{\mathcal{C}}$ naturally extends to the fields of forms acting on the vector spaces $V_{\mathcal{E}'}$ along $\mathcal{C}$ by defining the dual frames $\{\tilde{q}^{\alpha}\}$ as the preferred coframes along $\mathcal{C}$. This finally extends to any tensor product of vectors and covectors by defining the corresponding tensor product of preferred frames and coframes as the preferred tensor frames. Note that the term "observer" has been generically used in the discussion above, but the

[6] In the language of principal and associated bundles [29, 31, 33], a frame $\{\tilde{q}_{\alpha}\}$ along $\mathcal{C}$ defines a lift γ of $\mathcal{C}$ in the (principal) frame bundle $\mathcal{F}$. Choosing it as a preferred frame means that γ outlines the first directions tangent to $\mathcal{F}$ that should be considered horizontal. Realizing that there is necessarily a whole family of $\mathrm{GL}_n(\mathbb{R})$-related preferred frames is realizing the meaning of the $\mathrm{GL}_n(\mathbb{R})$-equivariance that will be later demanded to define a principal connection over $\mathcal{F}$.

[7] In vague terms, it should inherit the properties that hold for all observers when they differentiate with respect to their personal frame.

reasoning does not restrict to realistic observers worldlines[8]: it applies to any spacetime curve. In addition, when Q is actually a tangent vector field, it is absolutely not necessary for the preferred frames to be coordinate frames.

Summing up generically, defining universal variations for Q amounts to systematically expressing it in terms of preferred configurations that were arbitrarily chosen beforehand, in order to define what behaviours should be universally considered as constant along $\mathcal{C}$. From the mathematical point of view, no choice is better than another: given a manifold and a set of fields over it, no universal derivative is more relevant than the others. However, given a physical theory, a practical preferred system might be suggested by a trusted physical law: one would pick a system with respect to which the law takes a simple form (if such a system exists), so that the corresponding universal derivative would be intrinsically adapted to the most essential physical effects.

1.2.1 Covariant derivatives

Based on the above procedure, constructing a covariant derivative ∇ (or "connection") on a set of vector fields over spacetime merely amounts to defining a universal derivative (i.e. a preferred family of frames constantly related by the matrices of $\mathrm{GL}_n(\mathbb{R})$) along any spacetime curve $\mathcal{C}$, subject to the following consistency requirements. If two curves $\mathcal{C}_1$ and $\mathcal{C}_2$ are representatives of the same tangent vector at a given event $\mathcal{E}$ (see footnote 5), then they must satisfy $\mathcal{D}_{\mathcal{C}_1}Q(\mathcal{E}) = \mathcal{D}_{\mathcal{C}_2}Q(\mathcal{E})$ for any vector field Q. This allows the covariant derivative $\nabla_d Q(\mathcal{E})$ of Q at $\mathcal{E}$ in the direction $d \in T_{\mathcal{E}}\mathcal{S}$ to be well-defined as the universal derivative $\mathcal{D}_{\mathcal{C}}Q(\mathcal{E})$ where $\mathcal{C}$ is any representative of d. As a result, for any curve $\mathcal{C}$, $\mathcal{D}_{\mathcal{C}} = \nabla_{\dot{\mathcal{C}}}$. For a field Q, being universally transported along $\mathcal{C}$ is thus equivalent to satisfy $\nabla_{\dot{\mathcal{C}}}Q = 0$ along $\mathcal{C}$, and universal transport is now called parallel transport in the context of connections. Secondly, ∇ is required to be $C(\mathcal{S})$-linear with respect to the direction, where $\mathcal{C}(\mathcal{S})$ denotes the continuous functions over spacetime. This completes the standard set of axioms defining covariant derivatives, since the $\mathbb{R}$-linearity and Leibniz rule with respect to the main argument are inherited from the universal derivative[9]. Furthermore, ∇ naturally acts on any tensor product of vectors and covectors according to the procedure given above for the universal derivative.

Curvature Let us introduce here curvature, gauge transformations and torsion from the point of view developed so far, which will be useful in the rest of part I. Consider two distinct curves $\mathcal{C}_1$ and $\mathcal{C}_2$ joining two distinct events $\mathcal{E}$ and $\mathcal{E}'$, and pick a basis $\{q_\alpha^{\mathcal{E}}\}$ of $V_{\mathcal{E}}$. As mentioned earlier, given the first order nature of the last expression in (1.2.1), there exists a unique parallely transported frame $\{q_\alpha^{(1)}\}$ (resp. $\{q_\alpha^{(2)}\}$) along $\mathcal{C}_1$ (resp. $\mathcal{C}_2$) equal to $\{q_\alpha^{\mathcal{E}}\}$ at $\mathcal{E}$. Then, nothing in the axioms forbids the two bases $\{q_\alpha^{(1)}(\mathcal{E}')\}$ and $\{q_\alpha^{(2)}(\mathcal{E}')\}$ of $V_{\mathcal{E}'}$ to be different. This path-dependence (or "holonomy") of parallel transport is a defining characterization of what is called the curvature of ∇. The latter is entirely

[8] Realistic observer worldlines would correspond to timelike curves if a Lorentzian metric was defined over spacetime, but such a metric is not required at all to define universal derivatives.

[9] In the frame bundle, defining a preferred family along all possible curves compliant with the consistency requirements completed the construction of the horizontal bundle, and hence the principal connection, which induces the covariant derivative on the configurations of Q.

encoded in the Riemann tensor field, defined for instance by

$$^{\nabla}\mathrm{Riem}(Q, d_1, d_2) = \nabla_{d_1}\nabla_{d_2}Q - \nabla_{d_2}\nabla_{d_1}Q - \nabla_{[d_1,d_2]}Q \tag{1.2.2}$$

for any configuration Q and tangent vector fields d_1, d_2 (and where $[\,\cdot\,,\,\cdot\,]$ denotes the Lie bracket).

When curvature vanishes over an open set $\mathcal{U}$, one says that ∇ is flat. This means that one finds the preferred frames by picking any basis $\{q_\alpha^{\mathcal{E}}\}$ at any event $\mathcal{E} \in \mathcal{U}$ and then parallel transport it to any other event $\mathcal{E}' \in \mathcal{U}$. This uniquely defines a field of preferred frames over $\mathcal{U}$ entirely, since parallel transport is now path-independent (all other fields of preferred frames would be obtained with a constant transition matrices over $\mathcal{U}$). In other terms, vanishing curvature over an open set $\mathcal{U}$ is equivalent to saying that the connection has been constructed in the following way: a frame was arbitrarily chosen over $\mathcal{U}$, and its restriction to any curve $\mathcal{C}$ lying in $\mathcal{U}$ defined the preferred frames along $\mathcal{C}$.

Gauge transformations Regarding gauge transformations, consider first an event $\mathcal{E}$, an arbitrary frame $\{e_\rho\}$ of tangent vector fields and an arbitrary frame $\{q_\alpha\}$ of configurations of Q, defined over a neighbourhood of $\mathcal{E}$. The familiar Christoffel symbols $^{\nabla}\Gamma^{\beta}{}_{\alpha\rho}$ of ∇ at $\mathcal{E}$ with respect to those frames are defined by

$$\nabla_{e_\rho} q_\alpha\,(\mathcal{E}) = {}^{\nabla}\Gamma^{\beta}{}_{\alpha\rho}\,(\mathcal{E})\, q_\beta\,(\mathcal{E})\,. \tag{1.2.3}$$

Using relation (1.2.1), one sees that

$$^{\nabla}\Gamma^{\beta}{}_{\alpha\rho}\,(\mathcal{E}) = m^{\beta}{}_{\gamma}\,(\mathcal{E})\left[\dot{m}^{-1}\right]^{\gamma}{}_{\alpha}\,(\mathcal{E})\,, \tag{1.2.4}$$

where the transition matrix m is differentiated along any representative $\mathcal{C}$ of $e_\rho\,(\mathcal{E})$ (this also corresponds to $\nabla_{e_\rho}\left[m^{-1}\right]^{\gamma}{}_{\alpha}$).

However, so far, the transition matrix m depends on $\mathcal{C}$ and hence on e_ρ. A priori, one should thus use a different matrix to compute the Christoffel symbols for a different index ρ. To avoid this, one should continue the preferred frame $\{\tilde{q}_\alpha\}$ over a neighbourhood of $\mathcal{E}$ in the following way. Consider a family $\mathfrak{C}$ of curves through $\mathcal{E}$ covering a neighbourhood W of $\mathcal{E}$ without ever intersecting, and such that any $d \in T_{\mathcal{E}}\mathcal{S}$ is tangent to one and only one of these curves, up to rescaling (meaning that there exists only one curve that can be reparametrized to be an actual representative of d)[10]. In particular, proportional tangent vectors at $\mathcal{E}$ are represented by the same curve of $\mathfrak{C}$, up to reparametrization.

As a result, any event $\mathcal{E}' \in W$ is connected to $\mathcal{E}$ by only one curve of $\mathfrak{C}$. One may then consider the continued frame $\{\tilde{q}_\alpha\}$ (well-)defined over W as parallely transported from $\{q_\alpha\,(\mathcal{E})\}$ to any $\mathcal{E}' \in W$ along the only curve connecting to $\mathcal{E}$. Thus, the matrix m is also naturally continued over W and, for any tangent vector d at $\mathcal{E}$, it provides the transition to a preferred frame along the representative of d in $\mathfrak{C}$. In particular, it can be used to compute the Christoffel symbols for any index ρ in relation (1.2.4). Besides, denoting $e^{\mu}{}_{\rho}$ the transition matrix from a coordinate frame $\{\partial_\mu\}$ to e_ρ, one can now replace differentiation along any representative of $e_\rho\,(\mathcal{E})$ as

$$\left[\dot{m}^{-1}\right]^{\gamma}{}_{\alpha}\,(\mathcal{E}) = e^{\mu}{}_{\rho}\,(\mathcal{E})\,\partial_\mu\left[m^{-1}\right]^{\gamma}{}_{\alpha}\,(\mathcal{E})\,, \tag{1.2.5}$$

[10]The easiest way to construct such a family is to consider a coordinate chart $(\mathcal{U}, \phi)$ containing $\mathcal{E}$, such that $x_0 \equiv \phi(\mathcal{E})$, and define $\mathfrak{C}$ as $\{s \mapsto \phi^{-1}\,(x_0 + sd)\,,\ d \text{ unit vector of } \mathbb{R}^4\}$.

so that (1.2.4) finally rewrites as

$$\nabla\Gamma^{\beta}{}_{\alpha\rho}(\mathcal{E}) = m^{\beta}{}_{\gamma}(\mathcal{E})\, e^{\mu}{}_{\rho}(\mathcal{E})\, \partial_{\mu}\left[m^{-1}\right]^{\gamma}{}_{\alpha}(\mathcal{E}), \tag{1.2.6}$$

which is valid for all indices $\alpha,\ \beta,\ \rho$ with the same matrix field m.

Now change from $\{q_\alpha\}$ to another arbitrary frame $\{q'_\alpha = t^{\beta}{}_{\alpha} q_\beta\}$ according to a transition matrix t. Consider the new preferred frame $\{\tilde{q}'_\alpha\}$ constructed over W according to the previous procedure, i.e. $\{q'_\alpha(\mathcal{E})\}$ is parallely transported along all the curves of $\mathfrak{C}$. As explained earlier, two preferred frames along a curve are related by a constant transition matrix, so that $\{\tilde{q}_\alpha\}$ and $\{\tilde{q}'_\alpha\}$ are related by a constant matrix along any curve of $\mathfrak{C}$. Yet, all these curves contain $\mathcal{E}$, where the preferred frames respectively coincide with the arbitrary frame from which they were parallely transported:

$$\tilde{q}'_\alpha(\mathcal{E}) = q'_\alpha(\mathcal{E}) = t^{\beta}{}_{\alpha}(\mathcal{E})\, q_\beta(\mathcal{E}) = t^{\beta}{}_{\alpha}(\mathcal{E})\, \tilde{q}_\beta(\mathcal{E}), \tag{1.2.7}$$

so that the constant matrix is $t^{\beta}{}_{\alpha}(\mathcal{E})$ for all curves, and hence on all W.

This allows to find the new transition matrix m' from $\{q'_\alpha\}$ to $\{\tilde{q}'_\alpha\}$ on all W:

$$\tilde{q}'_\alpha = t^{\epsilon}{}_{\alpha}(\mathcal{E})\, \tilde{q}_\epsilon = t^{\epsilon}{}_{\alpha}(\mathcal{E})\, m^{\gamma}{}_{\epsilon} q_\gamma = t^{\epsilon}{}_{\alpha}(\mathcal{E})\, m^{\gamma}{}_{\epsilon}\left[t^{-1}\right]^{\beta}{}_{\gamma} q'_\beta, \tag{1.2.8}$$

i.e., using matrix product, $m' = t^{-1} m t(\mathcal{E})$, hence $m'^{-1} = t^{-1}(\mathcal{E})\, m^{-1} t$, and

$$\partial_\mu m'^{-1} = t^{-1}(\mathcal{E})\, \partial_\mu\left(m^{-1}t\right) = t^{-1}(\mathcal{E})\left(\partial_\mu m^{-1}\ t + m^{-1}\partial_\mu t\right). \tag{1.2.9}$$

With an obvious matrix notation for the Christoffel symbols, identity (1.2.6) for the new frame then rewrites

$$\begin{aligned}
\nabla\Gamma'_\rho(\mathcal{E}) &= e^{\mu}{}_{\rho}(\mathcal{E})\, m'(\mathcal{E})\, \partial_\mu m'^{-1}(\mathcal{E}) \\
&= e^{\mu}{}_{\rho}(\mathcal{E})\, t^{-1}(\mathcal{E})\, m(\mathcal{E})\left(\partial_\mu m^{-1}(\mathcal{E})\ \ t(\mathcal{E}) + m^{-1}(\mathcal{E})\, \partial_\mu t(\mathcal{E})\right) \\
&= t^{-1}(\mathcal{E})\, \nabla\Gamma_\rho(\mathcal{E})\, t(\mathcal{E}) + e^{\mu}{}_{\rho}(\mathcal{E})\, t^{-1}(\mathcal{E})\, \partial_\mu t(\mathcal{E}),
\end{aligned} \tag{1.2.10}$$

which is the standard formula of gauge transformations.

Therefore, when changing between two arbitrary frames, the matrix indices $\alpha,\ \beta$ of the Christoffel symbols do not transform as tensor indices when the transition matrix t is spacetime dependent (i.e. $\partial_\mu t \neq 0$). Like changes of coordinates, gauge transformations do not correspond to any modification of the physical situation They merely correspond to a change of frame, so that all observables must be gauge invariant[11].

On the contrary, the last index ρ of the Christoffel symbols is always a tensor index: under a transformation from $\{e_\rho\}$ to another arbitrary tagent frame $\{e'_\rho = u^{\sigma}{}_{\rho} e_\sigma\}$, definition (1.2.3) becomes

$$\nabla\Gamma'^{\beta}{}_{\alpha\rho} q_\beta = \nabla_{e'_\rho} q_\alpha = \nabla_{u^{\sigma}{}_{\rho} e_\sigma} q_\alpha = u^{\sigma}{}_{\rho} \nabla_{e_\sigma} q_\alpha = u^{\sigma}{}_{\rho}\, \nabla\Gamma^{\beta}{}_{\alpha\sigma} q_\beta, \tag{1.2.11}$$

i.e.

$$\nabla\Gamma'^{\beta}{}_{\alpha\rho} = u^{\sigma}{}_{\rho}\, \nabla\Gamma^{\beta}{}_{\alpha\sigma} \tag{1.2.12}$$

even when u is spacetime dependent.

Note however that, when Q is actually a tangent vector field, it is customary that all indices refer to the same frame, i.e. the frames denoted $\{e_\rho\}$ and $\{q_\alpha\}$ above are the same. In such cases, both equations (1.2.10) and (1.2.12) are applied at once when changing to another frame. The whole corresponding formula is still called a gauge transformation.

[11] Expectedly, this principle was central in developing gauge theories such as Yang-Mills theories.

Torsion Finally, still in the case of Q being a tangent vector field, consider the preferred frame $\{\tilde{e}_\rho\}$ built by parallely transporting $\{e_\rho(\mathcal{E})\}$ along all curves in $\mathfrak{C}$. Torsion, defined for any two tangent vector fields d_1, d_2 as

$$^{\nabla}T(d_1, d_2) = \nabla_{d_1} d_2 - \nabla_{d_2} d_1 - [d_1, d_2], \tag{1.2.13}$$

provides a necessary condition for the preferred frame $\{\tilde{e}_\rho\}$ to be a coordinate frame.

By construction, all the frame vectors of $\{\tilde{e}_\rho\}$ are parallely transported in all directions from $\mathcal{E}$, so that $\nabla_{\tilde{e}_\rho}\tilde{e}_\sigma(\mathcal{E}) = 0$ for any two frame vectors, hence

$$^{\nabla}T(\tilde{e}_\rho, \tilde{e}_\sigma)(\mathcal{E}) = -[\tilde{e}_\rho, \tilde{e}_\sigma](\mathcal{E}). \tag{1.2.14}$$

As a tensor, $^{\nabla}T$ vanishes at $\mathcal{E}$ *iff* it vanishes on the basis $\{\tilde{e}_\rho(\mathcal{E})\}$, i.e. *iff* any Lie bracket of the frame vectors vanishes at $\mathcal{E}$. Yet, vanishing Lie brackets is exactly the integrability condition for a frame, i.e. $\{\tilde{e}_\rho\}$ is a coordinate frame around $\mathcal{E}$ *iff* the Lie bracket of any two frame vectors vanishes on a neighbourhood of $\mathcal{E}$. Therefore, a vanishing torsion at $\mathcal{E}$ is a necessary condition, though not sufficient since the Lie bracket might become non-zero in any neighbourhood of $\mathcal{E}$. Furthermore, even if torsion does vanish on some neighbourhood of $\mathcal{E}$, relation (1.2.14) only holds at $\mathcal{E}$ because, anywhere away from $\mathcal{E}$, the frame vectors are no longer parallely transported in all directions.

As mentioned earlier, this would actually be the case *iff* curvature vanished: the bases are all parallely transported to each other independently of the path, hence in all directions. In the flat case, vanishing torsion on some neighbourhood is thus equivalent to the integrability of the preferred frames.

Auto-parallel curves For later use, recall that, for any connection ∇ on tangent fields, a curve $\mathcal{C}$ is called an auto-parallel curve of ∇ *iff*

$$0 = \nabla_{\dot{\mathcal{C}}}\dot{\mathcal{C}} = \left(\ddot{\mathcal{C}}^\rho + {}^{\nabla}\Gamma^\rho{}_{\sigma\mu}\dot{\mathcal{C}}^\sigma\dot{\mathcal{C}}^\mu\right) e_\rho \tag{1.2.15}$$

all along $\mathcal{C}$.

If $\{e_\rho\}$ is a coordinate frame, definition (1.2.13) yields

$$^{\nabla}T^\rho{}_{\sigma\mu} = {}^{\nabla}\Gamma^\rho{}_{\mu\sigma} - {}^{\nabla}\Gamma^\rho{}_{\sigma\mu} = -2\,{}^{\nabla}\Gamma^\rho{}_{[\sigma\mu]}, \tag{1.2.16}$$

so that, with respect to any coordinate frame, torsion is proportional to the antisymmetric part of the Christoffel symbols with respect to their last two indices.

However, one sees from (1.2.15) that only the symmetric part of the Christoffel symbols determines the auto-parallel curves: two connections have the same auto-parallel curves *iff* their symmetric parts are equal in a coordinate frame. Thus the auto-parallel curves are preserved when one modifies the connection by adding any antisymmetric tensor $A^\rho{}_{\sigma\mu} = A^\rho{}_{[\sigma\mu]}$ to the Christoffel symbols, although the torsion of the connection is modified.

1.2.2 Lie derivatives

Consider an event $\mathcal{E}$, a basis $\{e^{\mathcal{E}}_\alpha\}$ of $T_{\mathcal{E}}\mathcal{S}$ and the unique integral curve $\mathcal{C}$ through $\mathcal{E}$ of a tangent vector field d which is at least defined over a neighbourhood of $\mathcal{E}$. Lie-dragging the basis by d defines a frame along $\mathcal{C}$, which can be chosen to be a preferred

frame. This thus defines a universal derivative along $\mathcal{C}$. The latter is called the Lie derivative in the direction d, denoted $\mathcal{L}_d$, and the corresponding universal transport is the Lie-dragging by d.

This can only be done for the integral curves of d, so that the Lie derivative along d is a kind of incomplete, specific covariant derivative. It is only specified in the direction d, but it could be completed in possibly several ways into a connection ∇, which would have the specific property that $\nabla_d = \mathcal{L}_d$, i.e. parallel transport along integral curves of d coincides with Lie-dragging by d. In particular, d is auto-parallel with respect to any such connection, i.e. $\nabla_d d = 0$.

1.2.3 Realistic observer derivative

When discussing curvature and torsion, it was noted that any arbitrary frame defined over an open set $\mathcal{U}$ defines a flat connection over $\mathcal{U}$. In particular, one may use a local tangent frame to define a (flat) local connection ${}^{\mathcal{U}}\nabla$ on tangent vector fields. Moreover, ${}^{\mathcal{U}}\nabla$ has vanishing torsion *iff* the local frame is actually a coordinate frame.

This is exactly the type of derivative that a realistic observer uses: any observer constructs her proper coordinate system by making time-position measurements (sending signals in all directions and recording reception times, as discussed in section 1.1), and then differentiate tangent vector fields by differentiating their components with respect to her coordinate frame. More precise examples of this kind will only be discussed in the next three sections, devoted to concrete cases, as they may rely on structures specific to a theory (e.g. the Fermi-Walker derivative requires the existence of a Lorentzian metric over spacetime to construct an orthonormal frame along the observer worldline).

1.3 Newtonian physics

Topology In Newtonian physics (thoroughly covered in [40]-book 1), simultaneity is trivially defined: it is assumed that the clocks of all the observers remain synchronized, in the sense that the time measurements on a given event yield the same value for all observers, independently of their state of motion or their place in the universe. Equivalently, all the representatives {observer, time, position} of a given event have the same time value. In particular, the times of the three observers involved in the equivalence relation defining events are the same. With such a rigid postulate, time is absolute as it is useless to specify with respect to which observer it is measured, and two events are said simultaneous when they happen at the same absolute time.

Besides, absolute time is assumed to have no beginning nor end, while it is equally assumed that no principle should forbid the rulers of any observer to extend up to infinity. Newtonian spacetime is thus homeomorphic to the whole manifold $\mathbb{R}^4$, from which it inherits e.g. the structure of an affine space (translations between events are globally well-defined and form a vector space).

Preferred frames In Newtonian physics, preferred frames for tangent vector fields, like velocities and accelerations, are suggested by Newton's trusted second law, which takes the simplest form in the inertial frames. The latter are defined by Newton's first law as the frames with respect to which isolated systems have constant velocity. As a consequence, any two inertial frames are related by a matrix of $\mathrm{GL}_4(\mathbb{R})$ constant

over the spacetime $\mathbb{R}^4$. We know from section 1.2.1 that this uniquely defines a flat connection ∇ on tangent fields. Besides, any inertial frame is associated with the global coordinates of an inertial observer. Therefore, ∇ is an example of the flat torsionless connections of realistic observers mentioned in section 1.2.3.

What were generically called essential effects in section 1.2, are thus the inertial effects carried in the covariant derivative and uncovered as non-zero Christoffel symbols in non-inertial frames: consider the respective coordinate frames $\{\tilde{e}_\rho\}$ and $\{e_\rho\}$ of an inertial observer $\mathcal{O}$ and an arbitrary observer $\mathcal{O}'$ (of course, $\{e_\rho\}$ defines a flat torsionless connection as well, but non-inertial). Since Newtonian time is absolute, $\mathcal{O}$ and $\mathcal{O}'$ have the same time coordinate, hence $\tilde{e}_0 = e_0$. Furthermore, the remaining frame vectors $\{\tilde{e}_i\}$ and $\{e_i\}$[12] correspond to the rulers carried by $\mathcal{O}$ and $\mathcal{O}'$, so that their time components are zero. To be more explicit, assume that both spatial frames $\{\tilde{e}_i\}$ and $\{e_i\}$ are orthonormal with respect to the canonical metric on $\mathbb{R}^3$. Then, at any event $\mathcal{E}$, the transition matrix from $\{e_i\}$ to $\{\tilde{e}_i\}$ is a rotation matrix $R(\mathcal{E}) \in \mathrm{SO}(3)$, which actually only depends on the time coordinate t of $\mathcal{E}$. The transition matrix m from $\{e_\rho\}$ to $\{\tilde{e}_\rho\}$ thus writes as

$$m(\mathcal{E}) = \begin{pmatrix} 1 & 0_{1,3} \\ 0_{3,1} & R(t) \end{pmatrix}. \tag{1.3.1}$$

Now consider a tangent vector field Q along a curve $\mathcal{C}$ naturally parametrized by absolute time (for instance, the covariant derivative of Q along $\mathcal{C}$ would be the acceleration of $\mathcal{C}$ if Q was the velocity of $\mathcal{C}$). Denoting $\tilde{Q}^\alpha$ and Q^α the components of Q respectively measured by $\mathcal{O}$ and $\mathcal{O}'$, one already sees from (1.3.1) that $\tilde{Q}^0 = Q^0$, and hence $\dot{\tilde{Q}}^0 = \dot{Q}^0$: absoluteness of time implies absoluteness of the time components. To compute $\nabla_{\dot{\mathcal{C}}} Q$ in terms of quantities measured by $\mathcal{O}'$, one can directly apply formula (1.2.1), which relies on the matrix

$$m\dot{m}^{-1} = \begin{pmatrix} 0 & 0_{1,3} \\ 0_{3,1} & R\dot{R}^T \end{pmatrix}. \tag{1.3.2}$$

This means that the spatial part (which is the only important one, since the time part is absolute and does not enter any Newtonian equation) obeys

$$(\nabla_{\dot{\mathcal{C}}} Q)^i = \dot{Q}^i + [R\dot{R}^T]^i{}_j Q^j. \tag{1.3.3}$$

Since R is orthogonal, $RR^T = Id \Rightarrow R\dot{R}^T = -\dot{R}R^T = -[R\dot{R}^T]^T$. Thus, the 3×3 matrix $\Omega(t) \equiv R\dot{R}^T(t)$ being antisymmetric, there exists $\vec{\omega}(t) \in \mathbb{R}^3$ such that

$$\Omega_{ik}(t) = \epsilon_{ijk}\omega^j(t), \text{ so that } \forall \vec{v} \in \mathbb{R}^3,\ \Omega(t)\vec{v} = \vec{\omega}(t) \times \vec{v}, \tag{1.3.4}$$

where ϵ is the 3-dimensional Levi-Civita symbol.

Expectedly, $\vec{\omega}(t)$ is the instantaneous rotation vector of $\mathcal{O}'$ with respect to $\mathcal{O}$, e.g. for any function θ,

$$R(t) = \begin{pmatrix} 1 & 0 & 0 \\ 0 & \cos\theta(t) & \sin\theta(t) \\ 0 & -\sin\theta(t) & \cos\theta(t) \end{pmatrix} \implies \omega(t) = \begin{pmatrix} \dot{\theta}(t) \\ 0 \\ 0 \end{pmatrix}. \tag{1.3.5}$$

[12] As usual, latin indices are strictly positive integers.

Denoting $\vec{Q}$ the spatial vector having components Q^i, relations (1.3.3) and (1.3.4) finally yield

$$\left(\nabla_{\dot{\mathcal{C}}} Q\right)^i(t) = \left[\dot{\vec{Q}}(t) + \vec{\omega}(t) \times \vec{Q}(t)\right]^i, \tag{1.3.6}$$

which is the familiar formula for differentiating vectors in non-inertial frames. The inertial effects were indeed all encoded in the transition matrix m and hence the Christoffel symbols defined from it according to equation (1.2.6).

Further discussions on Newtonian spacetime and derivatives may be found in chapter 5 of [41], chapter 3 of [42] and part 1 of [40]-book 1.

1.4 Special relativity

Topology When gravitational effects have no measurable influence on the outcome of an experiment, the correct predictions are provided by special relativity[13] (see [48] and [40]-book 2 for thorough introductions and advanced topics on this theory) rather than Newtonian physics, although the errors of Newtonian predictions become significant only when very high velocities are involved in the experiment. In special relativity, constancy of light speed in vacuum with respect to all inertial observers, experimentally highlighted by the Michelson-Morley experiment, leads to a definition of simultaneity different from Newton's. In particular, the times of the three observers involved in the equivalence relation defining events are not the same, which results in time dilation and length contraction effects. All these effects are properly ruled by the fact that transition maps between inertial observers are given by Lorentz transformations. As in Newtonian physics, the clocks and rulers of the inertial observers cover the whole real line, so that the whole spacetime still identifies with the affine space $\mathbb{R}^4$ (and thus inherits all its topological properties). Yet, non-inertial observers may only perform experiments on a subset of the whole spacetime.

Preferred frames Like Newtonian physics, special relativity postulates the existence of global inertial frames, although the orthonormal ones are now related by Lorentz transformations rather than Galilean transformations. The familiar formulations of the laws of special relativity in inertial frames are thus transported to any frame with the help of the Newtonian flat torsionless connection associated with the global coordinates of inertial observers. This is indeed the same covariant derivative as in section 1.3, but now the transition matrix to an arbitrary observer would be more complicated than (1.3.1) because of the non-absoluteness of time and the resulting relativistic effects.

Soon after the first publications of Einstein on special relativity, Minkowski provided an elegant framework to formulate the theory, based on a Lorentzian metric η defined on the whole spacetime and everywhere equal to $\mathrm{diag}(-1, 1, 1, 1)$ with respect to a subclass of inertial frames (hence called orthonormal inertial frames). Let us recall here that,

[13] Famously settled by Einstein from 1905, special relativity originally dealt with classical mechanics and electromagnetism, but was successfully combined to quantum mechanics [35–38] later within the framework of quantized Abelian and non-Abelian Yang-Mills theories [43–47].

given a metric g on spacetime, any connection ∇ on tangent fields uniquely decomposes as

$$\nabla = {}^{g}\nabla + {}^{\nabla}M + {}^{\nabla}C, \tag{1.4.1}$$

where the Levi-Civita connection ${}^{g}\nabla$ associated with g is defined with respect to any coordinate basis $\{\partial_\mu\}$ by the Christoffel symbols

$${}^{g}\Gamma^{\rho}{}_{\sigma\mu} = \frac{1}{2}g^{\rho\tau}(\partial_\sigma g_{\mu\tau} + \partial_\mu g_{\tau\sigma} - \partial_\tau g_{\sigma\mu}), \tag{1.4.2}$$

the tensor ${}^{\nabla}M$ is constructed from the non-metricity tensor ${}^{\nabla}N$ (which is defined by ${}^{\nabla}N_{\lambda\mu\nu} = \nabla_\lambda g_{\mu\nu}$) according to

$${}^{\nabla}M^{\rho}{}_{\sigma\mu} = \frac{{}^{\nabla}N^{\rho}{}_{\sigma\mu}}{2} - {}^{\nabla}N_{(\sigma\mu)}{}^{\rho}, \tag{1.4.3}$$

and the contorsion tensor ${}^{\nabla}C$ is constructed from the torsion tensor ${}^{\nabla}T$ (hence the name) according to

$${}^{\nabla}C^{\rho}{}_{\sigma\mu} = -\frac{{}^{\nabla}T^{\rho}{}_{\sigma\mu}}{2} - {}^{\nabla}T_{(\sigma\mu)}{}^{\rho}, \tag{1.4.4}$$

in which the positions of the indices crucially depend on the conventions used in the definitions (1.2.3) and (1.2.13).

In particular, regarding the last two indices σ, μ when all quantities are expressed with respect to a coordinate frame, torsion (and hence contorsion) contains the whole antisymmetric part of the Christoffel symbols ${}^{\nabla}\Gamma^{\rho}{}_{\sigma\mu}$. On the other hand, the Levi-Civita Christoffel symbols, the tensor ${}^{\nabla}M$ and the second term of (1.4.4) are all respectively symmetric, and their sum corresponds to the whole symmetric part of the Christoffel symbols ${}^{\nabla}\Gamma^{\rho}{}_{\sigma\mu}$. Furthermore, adding any antisymmetric tensor $A^{\rho}{}_{\sigma\mu} = A^{\rho}{}_{[\sigma\mu]}$ to the Christoffel symbols modifies torsion, and hence contorsion. But the symmetric part of the Christoffel symbols, which determines the auto-parallel curves (see section 1.2.1), does not change. This implies that the tensor ${}^{\nabla}M$, and hence non-metricity, changes to compensate the modification in the symmetric part of contorsion, i.e. ${}^{\nabla}M$ is necessarily added the quantity $2A_{(\sigma\mu)}{}^{\rho}$. A connection fulfilling ${}^{\nabla}N = 0$ is called metric-compatible. Changing the torsion of a metric-compatible connection thus generically breaks metric-compatibility.

In the case of special relativity, ∇ is already known to be torsionless, so that ${}^{\nabla}C = 0$. In addition, the Minkowski metric η everywhere writes $\mathrm{diag}(-1, 1, 1, 1)$ with respect to any orthonormal inertial coordinate frame $\{\partial_\mu\}$, so that ${}^{\nabla}N_{\lambda\mu\nu} = \nabla_{\partial_\lambda}\eta_{\mu\nu} = \partial_\lambda\eta_{\mu\nu} = 0$ and hence ${}^{\nabla}M = 0$. The covariant derivative associated with the inertial frames thus reduces to the Levi-Civita connection ${}^{\eta}\nabla$ of the Minkowski metric η.

Flat metric-compatible connections are called Weitzenböck connection. For such connections, $\nabla = {}^{g}\nabla \Leftrightarrow {}^{\nabla}T = 0 \Leftrightarrow$ preferred frames are coordinate frames. For instance, ${}^{\eta}\nabla$ is a torsionless Weitzenböck connection.

The other types of derivatives encountered in special relativity (e.g. concrete examples of the realistic observer derivatives mentioned in section 1.2.3) also appear in the framework of GR, and are thus covered in section 1.5.

Topology, simultaneity and derivatives in special relativity are much further covered in chapters 1 and 3 of [48] and sections 1 and 2 of [40]-book 2.

1.5 General relativity

Topology Between 1907 and 1915, Einstein and collaborators developed GR, which classically describes how gravitational effects are produced, and how they affect non-gravitational phenomena. In particular, it was understood that the Minkowski formulation of special relativity, based on a Lorentzian metric, was an essential step to realize the transition from special relativity to GR: the metric alone was precisely the object that could describe gravitational effects once it was rendered dynamical by appropriate field equations. The proper meaning of "dynamical" and, more generally, the principles invoked to postulate GR from special relativity is the topic of chapter 2.

An important feature of GR is that gravitation, embodied by the metric, is universally coupled to matter, meaning that all non-gravitational phenomena are altered in presence of gravitation. In particular, this applies to the signals and interactions defining time-position measurements, and two signals with different initial directions may eventually cross because of gravitation, making time-position measurements degenerate (a single event might be given two distinct coordinates). As a consequence, it is no longer reasonable to assume that there always exist observers whose clocks and rulers cover the whole real line. Instead, each observer has a restricted perception of spacetime, covered by its bounded coordinate system, like the non-inertial observers in special relativity. Generically, spacetime in GR thus no longer identifies with the affine space $\mathbb{R}^4$ common to Newtonian physics and special relativity.

What can then be be said about the topology of a general relativistic spacetime? The mere existence of a Lorentzian metric clarifies a bit more the structure of spacetime because, although any manifold may be equipped with a Riemannian metric, the existence of a Lorentzian metric is conditioned e.g. by the existence of a nowhere vanishing vector field [49]. Besides, the existence of a Lorentzian metric defines causality relations between events based on the usual notions of spacelike, null and timelike curves. With this causal structure, spacetime may be equipped with a particular topology[14] with respect to which it must be non-compact, as it would otherwise admit closed timelike curves (proposition 4.33 of [50]). Such a topology is coarser than the original topology of spacetime defined in section 1.1, so that the original topology must also be non-compact. Therefore, to model a reasonable spacetime, a manifold must have a non-compact original topology to have a chance to admit a Lorentzian metric without closed timelike curves. Actually, being non-compact (for at least one topology) is enough to admit a Lorentzian metric (theorem 1.8 of [49]), but the latter might still contain closed timelike curves. Finally, Hausdorff separation and existence of a Lorentzian metric imply that spacetime is paracompact (section 3.1 of [51]).

Preferred frames The title of this paragraph must first be clarified in regard of the fact that GR is often said not to feature any preferred frame. This is true and has to do with the inherent absence of absolute objects in GR, as will be discussed in section 2.3. Yet, GR makes use of a covariant derivative ∇ which integrates all the coordinate dependencies of spacetime differentiations, and thus allows to write the equations of the theory in the most general form (thus realizing general covariance, covered in section 2.1). But, as mentioned in section 1.2.1, no connection is mathematically better

[14] The Alexandrov topology is generated by the sets $< \mathcal{E}, \mathcal{E}' >$ of all events lying on a timelike curve joining any two fixed events $\mathcal{E}$ and $\mathcal{E}'$ (see section 4 of [50] or section 6.4 of [51]).

than any other: the theory could be written with any other connection ∇', by adjusting an ad hoc compensating tensor field (the difference between any two connections always is a tensor since the second term in the last expression of (1.2.10) is the same for all connections, while the first is a tensor). Therefore, the preferred frames are defined by ∇, not the theory. Yet, the most elegant formulation of the theory uses the connection that absorbs the ad hoc tensor. In GR, this connection still is the Levi-Civita connection ${}^g\nabla$ (the principles justifying this will be rediscussed in chapter 2).

To picture the preferred tangent frames corresponding to ${}^g\nabla$, consider one of them, denoted $\{\tilde{e}_\rho\}$, along a curve $\mathcal{C}$ (unless $g = \eta$, the Riemann tensor ${}^g\text{Riem}$ of the Levi-Civita connection is non-zero, so that, unlike Newtonian physics and special relativity, the curve supporting a preferred frame must be specified). Because of metric-compatibility, the components of g with respect to $\{\tilde{e}_\rho\}$ are constant along $\mathcal{C}$. Parallel transport of ${}^g\nabla$ thus preserves scalar products. This means that $\{\tilde{e}_\rho\}$ can be assumed to be orthonormal all along $\mathcal{C}$ whereas, for a non metric-compatible connection, a preferred frame orthonormal at a certain event would no longer be orthonormal at some other event.

However, not all orthonormal frames along $\mathcal{C}$ are preferred frames: some of them are related to $\{\tilde{e}_\rho\}$ by a non-constant family of transition matrices of the Lorentz group $\text{O}(3,1)$ along $\mathcal{C}$. Any non-preferred orthonormal frame $\{e_\rho\}$ thus has constant norms and angles between the frame vectors, and yet is non-constant with respect to any othonormal preferred frame: one is naturally tempted to say that it is 4-rotating (the Lorentz group indeed is the generalization of the rotation group to Lorentzian signature). This is why, when $\{e_\rho\}$ actually is an orthonormal frame defined on an open set[15] containing $\mathcal{C}$, rather than on $\mathcal{C}$ only, the Christoffel symbols of ${}^g\nabla$ with respect to $\{e_\rho\}$ are called Ricci rotation coefficients.

Let us come back to the general case such that $\{e_\rho\}$ is only defined along $\mathcal{C}$, and denote $u \equiv \dot{\mathcal{C}}$ and $a \equiv {}^g\nabla_u u$. Since $\{e_\rho\}$ is everywhere orthonormal along $\mathcal{C}$, and ${}^g\nabla$ is metric-compatible, one has

$$0 = {}^g\nabla_u \left(e_\rho \cdot e_\sigma\right) = e_\rho \cdot {}^g\nabla_u e_\sigma + e_\sigma \cdot {}^g\nabla_u e_\rho, \tag{1.5.1}$$

so that $\Omega_{\rho\sigma} \equiv e_\rho \cdot {}^g\nabla_u e_\sigma$ is an antisymmetric tensor satisfying ${}^g\nabla_u e_\rho = \Omega^\sigma{}_\rho e_\sigma$, i.e. it is exactly analogous to the matrix Ω involved in (1.3.4).

Furthermore, along $\mathcal{C}$, Ω decomposes as[16]

$$\Omega_{\rho\sigma} = 2u_{[\rho}a_{\sigma]} + u^\mu \epsilon_{\mu\rho\nu\sigma}\omega^\nu, \tag{1.5.2}$$

where ϵ is the 4-dimensional Levi-Civita symbol, and ω is the rotation 4-vector of $\{e_\rho\}$.

Assume here that $\mathcal{C}$ is the worldline of a realistic observer $\mathcal{O}$ parametrized by her proper time. Then $\{e_\rho\}$ may be constructed by taking e_0 as the 4-velocity u of $\mathcal{O}$, and $\{e_i\}$ as three orthonormal rulers carried by $\mathcal{O}$. Thus constructed, $\{e_\rho\}$ coincides on $\mathcal{C}$ with the frame associated with $\mathcal{O}$'s natural coordinate system, which is locally (well-)defined by the following procedure: assign coordinates $(x^\mu) = (\tau, sd^i)$ to the

[15] Such frames are called tetrad (or vierbein). They can always be constructed locally, by applying either the Gram-Schmidt process to a coordinate frame, or the procedure described in section 1.2.1, i.e. parallely transporting an orthonormal basis from a fixed event along all the curves of a set $\mathfrak{C}$, constructed e.g. according to footnote 10.

[16] See section 3.5 of [48]

event lying at distance s on the spatial geodesic[17] starting from $\mathcal{O}$ at $\mathcal{O}$'s proper time τ in the direction $d^i e_i$ for d in the unit sphere of $\mathbb{R}^3$. This coordinate system can only be valid locally because, as mentioned earlier, gravitation (or $\mathcal{O}$'s acceleration) will cause geodesics to eventually cross. Note that, in general, the corresponding coordinate frame is orthonormal only along $\mathcal{C}$. The associated (flat torsionless) covariant derivative is a general example of a realistic observer derivative.

In this realistic case, the time component of ω with respect to $\{e_\rho\}$ vanishes, while the spatial components are read from suitably arranged gyroscopes carried by $\mathcal{O}$. It is exactly analoguous to the vector ω involved in (1.3.4). Indeed, when rewriting the spatial components of (1.5.2) with respect to $\{e_i\}$, as is the case in (1.3.4), the spatial components of u vanish, while $u^0 = 1$. This yields

$$\Omega_{ik} = \epsilon_{0ijk}\omega^j = \epsilon_{ijk}\omega^j, \tag{1.5.3}$$

where the last ϵ is the 3-dimensional Levi-Civita symbol, hence recovering (1.3.4).

Therefore, $\{e_\rho\}$ will be said to be 3-rotating when $\omega \neq 0$. The decomposition (1.5.2) shows that 4-rotation (i.e. non-parallel transport of an orthonormal frame) does not imply 3-rotation, as 4-acceleration is a form of 4-rotation. When $\mathcal{O}$ indeed does not 3-rotate, but possibly accelerates, the corresponding coordinates constructed above are called Fermi coordinates, and the associated (flat torsionless) covariant derivative is called the Fermi-Walker derivative (and the corresponding parallel transport is called Fermi-Walker transport). Let us finally use equation (1.5.2) to explicitly expand the covariant derivatives of $\{e_\rho\}$ along $\mathcal{C}$:

$$^g\nabla_u u = a^i e_i \tag{1.5.4}$$

$$^g\nabla_u e_k = a_k u + \epsilon^i{}_{jk}\omega^j e_i, \tag{1.5.5}$$

where, numerically, $\epsilon^i{}_{jk} = \epsilon_{ijk}$ because indices are raised and lowered with the metric which equals $\mathrm{diag}(-1,1,1,1)$ in $\{e_\rho\}$ all along $\mathcal{C}$.

Relation 1.5.4 restates the definition of 4-acceleration and hence the fact that the natural coordinate frame of an accelerating observer cannot be a preferred frame along its worldline. Yet, following a geodesic is not sufficient according to 1.5.5. The latter shows that 3-rotation and 4-acceleration cannot compensate each other: if any of them is present, no spatial frame vector $\{e_k\}$ is parallely transported. Therefore, only the Fermi frame of a non-rotating non-accelerating observer $\mathcal{O}$ has zero 4-rotation along $\mathcal{O}$'s worldline, and hence is a preferred frame of $^g\nabla$. In this case, the Fermi-Walker derivative coincides with $^g\nabla$ along the geodesic. When $g = \eta$, the Fermi coordinates of a non-rotating non-accelerating observer are global orthonormal inertial coordinates.

As an additional remark, it is easy to note that, in the general case, Ω actually identifies with the 0^{th} Christoffel matrix $^g\Gamma_0$ along $\mathcal{C}$ of any frame coinciding with $\{e_\rho\}$ along $\mathcal{C}$, because in such a case:

$$^g\nabla_u e_\rho = {}^g\Gamma^\sigma{}_{\rho 0} e_\sigma, \quad \text{i.e.} \quad {}^g\Gamma^\sigma{}_{\rho 0} = \Omega^\sigma{}_\rho. \tag{1.5.6}$$

Relation (1.5.6) is for instance valid for $\mathcal{O}$'s natural coordinate frame, or the orthonormal frame constructed by parallely transporting $\{e_\rho\}$ along the spatial geodesics defining $\mathcal{O}$'s coordinate system (in which case the Christoffel symbols are a case of Ricci

[17] The distance s along a geodesic γ is given by $s[\gamma] = \int_{\xi_i}^{\xi_f} \sqrt{|\dot\gamma(\xi)\cdot\dot\gamma(\xi)|}d\xi$.

rotation coefficients). In addition, the Christoffel symbols of ${}^g\nabla$ are symmetric with respect to the last two indices according to relation (1.4.2), so that only the components ${}^g\Gamma^\sigma{}_{ij}$ depend on the exact frame. It is particularly easy to compute the latter with respect to $\mathcal{O}$'s coordinate frame because all spatial geodesics starting on $\mathcal{O}$'s worldline are represented by the curves $\gamma : \xi \mapsto (\tau, \xi d^i)$ for all d in the unit sphere of $\mathbb{R}^3$. The geodesics equation

$$0 = {}^g\nabla_{\dot\gamma}\dot\gamma^\sigma = \ddot\gamma^\sigma + {}^g\Gamma^\sigma{}_{ij}\dot\gamma^i\dot\gamma^j = {}^g\Gamma^\sigma{}_{ij}d^i d^j \tag{1.5.7}$$

thus holds for any 3-dimensional unit vector d, which requires all ${}^g\Gamma^\sigma{}_{ij}$ to vanish.

Topology in GR is extensively covered in [49–51]. Section 13.6 of [52] or section 24.5.1 of [53] may also be consulted for a thorough treatment of the natural coordinate system of an arbitrary observer, together with chapters 3 and 13 of [48] for a complete discussion of 4-rotation. The latter three references also cover the different types of derivatives involved in GR. Since this last section on GR closes the introductory chapter, let us cite here standard and excellent textbooks not mentioned yet: [54–57] for different expositions of GR, [58–60] devoted to cosmology, and [11, 61, 62] focusing on applications such as the physics of neutron stars and black holes. See also [63] for a rich and original compilation of both historical and technical discussions on GR.

Chapter 2

From special relativity to general relativity

Contents

GR is a relativistic description of gravitation, but also of all classical non-gravitational phenomena in presence of gravitation. This means that GR modifies special relativity to integrate gravitation. Much effort, still ongoing today, has been made, by Einstein himself and many others, in formulating the most reasonable, physically well-founded arguments leading from trusting special relativity to postulating GR. This usually brings up concepts such as general covariance, dynamical fields, diffeomorphism invariance, and equivalence principles. Based on rigorous definitions (which may unfortunately vary between authors), these notions have more than a heuristic interest; they are often invoked as guiding principles in the elaboration of modified theories. Before consulting more complete, yet sometimes confusing, discussions in the literature, the sections below should serve as a simple synthesis disentangling the notions at stake and providing their sharpest definitions.

2.1 General covariance

In section 1.1, spacetime $\mathcal{S}$ was given a definition valid for all physical theories. Then, the first purpose of any physical theory is to define all the sets S_i of objects O_i, mathematically related to spacetime (often fields defined over spacetime), that are necessary to predict all the observations lying in the application scope of the theory. Secondly, the behaviours of those objects are described by physical laws which are mathematical rules $\mathcal{R}_j(\{O_i\})$ (often field equations, which generally involve one of the types of derivatives introduced in section 1.2). A family of objects satisfying all rules is called a solution of the theory.

GR is often praised for being generally covariant, and requiring this property originally stood as very valuable in grasping GR from special relativity. To assess the

legitimacy of this, consider the following general definition of a covariance group.

Definition 2.1.1 (Covariance group)**.** *Denote $G \subset \mathrm{Diff}(\mathcal{S})$ a subgroup of spacetime diffeomorphisms. The rules of a theory are called G-covariant when there exists a faithful*[18] *action Φ_i of G on each S_i in such a way that*

$$\forall g \in G,\ \forall j,\quad \mathcal{R}_j(\{O_i\}) \iff \mathcal{R}_j(\{\Phi_i(g)\cdot O_i\}). \tag{2.1.1}$$

The rules are called generally covariant when G actually equals the whole of $\mathrm{Diff}(\mathcal{S})$.

Often, S_i is a vector space (in which case the action Φ_i is sometimes called a realization [41, 57]). However, Φ_i can be non-linear in the sense that it takes values in the whole of $\mathrm{Diff}(S_i)$, rather than only $\mathrm{GL}(S_i)$ (in which case the realization is usually called a representation). Generically, when the object O_i is a tensor field, the action $\Phi_i(g)$ is the pull-back by the diffeomorphism g.

It must be stressed that definition 2.1.1 really characterizes the rules $\mathcal{R}_j(\{O_i\})$ rather than the physical content of the theory. Indeed, a theory is properly defined as an equivalence class of objects and rules ultimately leading to the same exact predictions. Then, covariance with respect to a given group is a possible property of some representative formulations of the theory, but not necessarily all of them. Therefore, general covariance is only a property of the standard formulation of GR. This is why, as soon as 1917, Kretschmann pointed to Einstein, who firmly defended the "heuristic force" of general covariance, that any theory does admit a generally covariant formulation [64]. In vague terms, one should work out how non-generally covariant rules transform under the action of a generic diffeomorphism g, and redefine objects, or introduce notations, that integrate all possible terms generated from the action of g. In many cases, one would look for geometric objects over spacetime like tensors, and would most probably use covariant derivatives for terms involving differentiation.

This is how the familiar Galilean covariance of Newtonian physics, and Lorentz covariance of special relativity (which characterize their respective formulations with respect to inertial frames), can be promoted to general covariance. For instance, the series of papers [65–68] illustrates the benefits of a generally covariant Newtonian formulation to model neutron stars, while reference [69] develops a generally covariant formulation for Newtonian and special relativistic fluid mechanics. As a side remark, there exists a geometric (i.e. based on geodesic motion in curved spacetime instead of a force in $\mathbb{R}^4$) generally covariant reformulation of Newtonian gravity, known as Newton-Cartan formulation (see section III.5 of [42] or chapter 12 of [52]). The objects and the formulation thus resemble GR even more, but such effort to reformulate Newton's gravitational force as a geometric effect is not necessary to realize general covariance of Newtonian physics.

Going the opposite way, GR admits a non-generally covariant formulation which is always valid[19]: harmonic coordinates (i.e. such that $g^{\sigma\mu}\,{}^{g}\Gamma^{\rho}{}_{\sigma\mu} = 0$) always exist, and the equations of GR formulated in such coordinates expectedly loose their general

[18] In particular, the trivial action is not allowed.

[19] Of course, in particular cases in which a solution is sought with a given symmetry, e.g. stationarity, or homogeneity and isotropy, the equations of GR can be reformulated in coordinates adapted to the symmetry, and thus loose their general covariance, but such equations are far from entirely representing GR.

covariance although they can still describe any physical situation. This seems to further diminish the importance of general covariance in formulating GR.

Yet, retrospectively, it seems unlikely that GR could have been first formulated in harmonic gauge, so that Einstein's strategy to focus only on generally covariant formulations was an efficient formal shortcut, rather than a complicating constraint. Besides, there is no unique way to render a given theory generally covariant, i.e. not all generally covariant generalizations of a theory are representatives of the same theory. This procedure requires choices that can be confronted with experiments and hence face experimental failure (see section 5.5 of [64]). Thus, requiring general covariance is not devoid of physical implications. This then provides an investigation plan, as the choices that it demands may be tested, and hence contribute to developing the theory.

In short, general covariance certainly was a relevant guide in shaping GR: though general covariance in itself says nothing about the physical content of such a relativistic theory including gravitation, the choices made to devise a generally covariant formulation of such a theory from knowledge of special relativity, do fundamentally reveal the essence of GR. These choices are now discussed.

2.2 Einstein's equivalence principle

All observers in spacetime carry a proper time clock and three rulers that they arrange in an orthonormal frame following the same procedure as in the absence of gravity. So far, no metric is defined over spacetime, so that there would be no sense in assessing the orthogonality of the rulers in terms of a such a metric; the latter will only emerge later. No connection is defined either, so that 4-rotation of a frame cannot be defined in any way, only 3-rotation is (as measured by gyroscopes carried by the observers). In Newtonian physics and special relativity, the inertial observers are the non 3-rotating observers who experience no force. Yet, once taken into account, gravitational effects affect any observer ("universal coupling" of gravitation to matter mentioned in section 1.5). Therefore, in this context, inertial observers can only be defined as the non 3-rotating observers experiencing no other influence than gravitation. This generalization does coincide with the Newtonian definition in the absence of gravitation. Actually, since GR will not describe gravitation as a force, the Newtonian definition will remain valid. Furthermore, such generalized inertial observers will feature further common properties with those of special relativity. Again, since no metric is defined yet, there is no sense in trying to relate the worldlines of inertial observers with the geodesics a such a metric; this will only come later.

All the systems, and hence fundamental fields, studied in special relativity are still present over spacetime, and now influenced by gravitation in virtue of universal coupling. Einstein's equivalence principle (EEP) claims that fundamental non-gravitational test[20] physics is not locally affected by the presence of a gravitational field. More concretely, consider an inertial observer $\mathcal{O}$ at any event $\mathcal{E}$. The latter has coordinates $x = (\tau, 0, 0, 0)$ in $\mathcal{O}$'s coordinate system. Consider fundamental test fields in given spatial configurations with respect to $\mathcal{O}$, i.e. they are known at a fixed τ. Then, for any finite accuracy δ, there exists a finite coordinate range $R_\delta = [\tau,\ \tau + T_\delta] \times [-D_\delta,\ D_\delta]^3$ within which no measurement on the test fundamental fields features deviations greater

[20]The gravitational effects generated by the matter fields must be negligible.

than δ with respect to any other inertial observer considering the same set up in her own coordinate system. Since the latter observer may be chosen far from any graviational influence, the measurements in the box R_δ are predicted by the special relativistic laws.

In EEP, the importance of restricting to fundamental fields, rather than including any system, is clearly justified in [70]: "consider an experiment where the distance l between two nearby freely-falling particles is measured, and consider the quantity $\ddot{l}/l$, where a dot denotes the derivative with respect to proper time, or to a convenient laboratory time. In an inhomogeneous gravitational field, this quantity does not vanish, in general, even in the limit $l \to 0$, although it does vanish identically in the absence of a gravitational field [...] in all such cases one is dealing with the behaviour of systems that are not elementary, but composite. Hence, the need to restrict the statement of EEP to fundamental physics". Indeed, the experiment of the two particles, separated by any fixed distance l at time τ, does not rule out EEP at all when the particles are reconsidered as the macroscopic manifestation of a specific configuration of several interacting fundamental fields, because then, the box R_δ does not have to contain the two balls for all δ. Actually, EEP only indicates that D_δ is necessarily smaller than l when δ is chosen smaller than $\ddot{l}/l$, so as to exclude the regions where the fields steeply materialize the two particles, and hence where their configurations evolve differently than in special relativity, since the latter predicts $\ddot{l} = 0$.

For the box R_δ to exist for any δ, the expressions at $x = (\tau, 0, 0, 0)$, in $\mathcal{O}$'s coordinate system, of the general laws ruling the fundamental fields in presence of gravitation must coincide with the expressions at x, in any (Newtonian) inertial coordinate system, of the special relativistic laws ruling these fields. This holds true at any event, so that the expressions of the fundamental laws are known everywhere, with respect to inertial observers. However, for any event $\mathcal{E}'$, the expressions are only valid at the event (actually at all the events on the worldline of a chosen inertial observer crossing $\mathcal{E}'$, and with respect to who the laws are expressed). This makes it impossible to find solutions of the laws, which are generally partial differential equations (PDEs), because one needs to know the expressions of the PDEs on an open set to try integrating them. Ignoring how the expressions change away from x on any open set exactly corresponds to ignoring how gravitation really comes into play on finite scales.

The first and easier step to fix this is to rewrite those expressions in a generally covariant way. This only requires a connection ∇ such that the coordinate frames of the inertial observers are preferred frames along their worldlines. Such worldlines will necessarily be auto-parallel curves of ∇ because the 0^{th} frame vector is the 4-velocity of the inertial observer, and it is parallely transported along the worldline, by definition of ∇. Actually, all the inertial frame vectors are parallely transported along the worldline by definition, so that the 0^{th} Christoffel matrix ${}^{\nabla}\Gamma_0$, expressed in the coordinate frame of an inertial observer, vanish along her worldline.

One may then replace partial differentiation in $\mathcal{O}$'s coordinate system with covariant differentiation by ∇ in the expressions at $\mathcal{E}$. Actually, this procedure, known as minimal coupling[21], is a priori ill-defined for some special relativistic laws. For instance, laws involving second-order crossed derivatives are ambiguous, because the commutator of partial derivatives vanish, whereas that of covariant derivatives involves the Riemann tensor. The same procedure thus yields two expressions differing by curvature-coupling

[21] Or "comma goes to semicolon rule", as partial differentiation $\partial_\mu Q$ and covariant differentation $\nabla_{\partial_\mu} Q$ are often respectively denoted $Q_{,\mu}$ and $Q_{;\mu}$

terms. Such factor-ordering ambiguities may be sorted out with cautious reasonings, or comparison with experiment if need be: see section 16.3 of [52] and section 25.7 of [53] for concrete examples and general rules to determine the right order. Reference [71] should also be consulted for a detailed treatment of minimal coupling based on the Lagrangian formalism.

When such precautions have been taken, one is left with expressions of the laws valid with respect to any vector basis at $\mathcal{E}$. These expressions will be the same at any other event $\mathcal{E}'$, even away from $\mathcal{O}$'s worldline, since the same procedure would have been followed by another inertial observer crossing $\mathcal{E}'$. As a result, the expressions are valid all over spacetime with respect to any frame, without need of introducing any field that was not already present in special relativity. One may then reexpand the generally covariant expressions with respect to $\mathcal{O}$'s coordinate frame. The expressions now involve the Christoffel symbols of ∇, but they take the form of PDEs on the whole open set where $\mathcal{O}$'s coordinate frame is defined. This is reassuring, but does not solve the problem, because the Christoffel symbols are not known. They are merely a notation for the ignorance of the expressions of the laws away from x (away from $\mathcal{O}$'s worldline more precisely). Actually, they do provide the information that gravitational effects are fundamentally described by a connection[22]: what one really needs, as a second step, are the equations determining the appropriate connection ∇ describing how gravitation affects non-gravitational fields in a given physical situation. In practice, one would then identify the inertial observers as the non 3-rotating observers whose worldlines are the auto-parallel curves of ∇.

As mentioned above, deriving working expressions for the fundamental laws in presence of gravitation has been achieved with no further field introduced: the Christoffel symbols were already there in the special relativistic laws expressed in non-inertial frames. Yet, as discussed in section 1.4, they were known to be the Levi-Civita Christoffel symbols of Minkowski metric. In presence of gravitation, one can again relate them to a global Lorentzian metric over spacetime: define g as taking the form $\mathrm{diag}(-1,1,1,1)$ with respect to the coordinate frame of any inertial observer at any event $\mathcal{E}$ on her worldline. This does cover the whole spacetime as there always exist inertial observers crossing any event. But for this construction to be well-defined, any two inertial observers crossing the same event $\mathcal{E}$ must be defining the same metric at $\mathcal{E}$. This is the case *iff* changing from an inertial frame to the other preserves the above diagonal form, i.e. *iff* the transition matrix at $\mathcal{E}$ is part of the Lorentz group. The EEP confirms that it is the case. One can imagine e.g. that all the inertial observers maintain a certain fundamental field in a predefined behaviour close to them, on which other inertial observers can make measurements to determine the transformations relating them. The EEP concludes that those are the Lorentz transformations corresponding to the relative velocity measured by the inertial observers at $\mathcal{E}$.

Clearly, inertial observers' worldlines are timelike with respect to g. And for any unit timelike vector d at any event $\mathcal{E}$, there always exists an inertial observer crossing $\mathcal{E}$ with 4-velocity d. For any inertial observer $\mathcal{O}$, the components of g are constant along $\mathcal{O}$'s worldline $\mathcal{C}$ with respect to $\mathcal{O}$'s coordinate frame, which is a preferred frame of ∇ along $\mathcal{C}$. Therefore, $\nabla_d g = 0$ for any timelike vector. Yet, any vector can be decomposed as the sum of two timelike vectors: any spacelike (resp. null) vector has components $(0,a,0,0) = (a,a/2,0,0) + (-a,a/2,0,0)$ (resp. $(a,a,0,0) =$

[22] As opposed to a metric (again, the latter will only emerge later).

$(3a, a, 0, 0) + (-2a, 0, 0, 0))$ in some orthonormal frame such that the 0^{th} frame vector is the timelike one. Thus, ∇ is metric-compatible as it is linear with respect to the direction (and thus admits othonormal preferred frames along any curve, as exposed in 1.5). According to decomposition (1.4.1), the remaining difference between ∇ and the Levi-Civita connection ${}^g\nabla$ is a contorsion tensor C (and the orthonormal preferred frames of ∇ 4-rotate with respect to those of ${}^g\nabla$ *iff* $C \neq 0$).

The class of "metric theories", to which GR belongs, then requires that freely-falling test objects, like inertial observers, follow the geodesics of g. As a result, ∇ has the same timelike auto-parallel curves as ${}^g\nabla$. According to section 1.2.1, this requires them to have same symmetric parts in coordinate frames, and hence ${}^{\nabla}T_{(\sigma\mu)}^{\ \ \ \rho} d^\sigma d^\mu = 0$ for all timelike directions d. One can hardly make further exact statements about the relation between ∇ and ${}^g\nabla$. But the spirit of metric theories actually is to describe gravitation only in terms of a metric, so that a connection that would not be entirely determined by the metric is not allowed. This finally sets $\nabla = {}^g\nabla$, and hence identifies the inertial frames as the preferred frames of ${}^g\nabla$ along the geodesics of g, i.e. the non-accelerating non 3-rotating frames, as discussed in section 1.5. As a result, the equations on the connection ∇ that had to be devised to describe gravitation on finite scales, must actually rule the dynamics of a metric g, from which ∇ is constructed as ${}^g\nabla$.

Reference [72] should be consulted for richer discussions on metric theories and the EEP, together with [10, 28], which also covers experimental tests of EEP and the alternative versions of the equivalence principle. There is indeed a great variety of statements similar to EEP, but featuring either weaker, stronger, or simply different implications. For instance, some of them are general enough to allow non-metricity [73]. References [70] and section 5.2 of [74] precisely examine the rigourous, or conjectured, relations between numerous versions of equivalence principles. For instance, the weak equivalence principle (WEP) states that the trajectory of any freely-falling test body with negligible compactness[23] is independent of its internal structure, i.e. only determined by its initial kinematic conditions[24]. It is clearly implied by EEP, but Schiff's conjecture claims that it is actually equivalent under reasonable assumptions (see e.g. section 2.5 of [28] for details, and section 5.2 of [74] for cases in which Schiff's conjecture was proved or disproved, thus refining its assumptions).

Theoretical and experimental tests of the equivalence principles are still very lively topics. For instance, reference [75] suggests a new criterion to test the gravitational WEP (defined by no longer requiring a negligible compactness in the WEP) to handle the fact that actual bodies always have non-zero compactness and hence do not necessarily follow exact geodesics. Besides, the WEP has recently been experimentally confirmed down to a precision of 10^{-14} by the space mission MICROSCOPE [76–78]). This means that we potentially have access to a priviledged family of curves over spacetime, which, in metric theories, are the geodesics of the metric. Yet, many metrics share the same geodesics. For instance, two metrics related by a constant conformal factor have the same Levi-Civita connection, and hence same geodesics. But is it the only possibility? References [79–81] thus address implications of the WEP in classifying most possibilities.

[23] Compactness is the dimensionless ratio of the mass to the characteristic size. A very light black hole would be a test body, but would still have the greatest possible compactness.

[24] In Newtonian gravity, this is famously implied by the equality bewteen inertial and gravitational masses.

2.3 Absolute objects and invariance

Absolute and dynamical objects So far, discussing general covariance and EEP missed the central point of any theory of gravitation, which is to describe gravitational effects on finite scales. In section 2.2, it became clear that this would be achieved by devising equations ruling the Christoffel symbols of a connection on a neighbourhood of any event. In the framework of metric theories, these equations come down to rule a metric, since the Christoffel symbols are required to be those of a Levi-Civita connection. Unlike special relativity, such equations must intuitively render the metric dynamical instead of a fixed absolute object.

However, ruling an object with a PDE is not sufficient to make it dynamical. For instance, instead of postulating the existence of observers with respect to who physical laws take their usual expressions in inertial coordinates, special relativity admits the following equivalent (generally covariant) formulation: there exists a Lorentzian metric g over spacetime ruled by ${}^g\mathrm{Riem} = 0$, and the physical laws are postulated in the forms obtained by replacing partial derivatives with the Levi-Civita connection in their usual "inertial" expressions. Yet, the solutions of the metric equation are known to be all the expressions of the Minkowski metric η with respect to the frames defined on open sets. Therefore, the object g of the above formulation of special relativity is qualified as an absolute rather than dynamical object. In the general case, one thus relies on the following equivalence class to disclose absolute objects hidden in "deceptive" PDEs such as ${}^g\mathrm{Riem} = 0$.

Definition 2.3.1 (Equivalent objects)**.** *When the objects of a given set S_i are fields, any two of them O and O' are said equivalent when, $\forall \mathcal{E} \in \mathcal{S}$, there exists a neighbourhood U of $\mathcal{E}$ and a diffeomorphism $g : U \to U$ such that $[\Phi_i(g) \cdot O]_{|U} = O'_{|U}$.*

In practice, this equivalence relation can be adapted to any set S_i, according to its specificities: since any object is mathematically related to spacetime, restriction to a given neighbourhood can always be given a sense.

One then naturally distinguishes absolute and dynamical objects as follows.

Definition 2.3.2 (Absolute and dynamical objects)**.** *For a given set S_i, consider the subset of all the objects O_i appearing in any solution of the theory. When all such objects are equivalent, they are called absolute. Otherwise, they are called dynamical.*

In the first formulation of special relativity above, one sticks to the inertial frames, so that the metric is fixed: it is always numerically the same in all solutions although other fields such as the electromagnetic tensor are not. Generically, absolute elements of a theory often appear as fixed fields in some family of formulations. Conversely, objects that appear fixed in a given formulation clearly are absolute objects and would be unveiled in any other (possibly deceptive) formulation by the defining criteria 2.3.1 and 2.3.2. Yet, in the first ("inertial") formulation of special relativity, the metric rather is a practical tool than a proper object: one can forget it and consider the formulations of the laws used before Minkowski introduced the metric. Thus, in the first formulation, absoluteness actually resides in the inertial frames: all the inertial frames involved in the solutions of this formulation are locally (actually globally) diffeomorphic, by means of Lorentz transformations. Of course, all the theories relying on the rigid framework of special relativity, such as quantum field theories or string theory, feature these absolute objects.

Invariance Identifying the absolute objects of a theory allows to properly distinguish covariance (definition 2.1.1) and invariance, defined below. Indeed, since it was noted that special relativity admits a generally covariant formulation, what is usually meant by "Lorentz invariance of special relativity"? It is surely not only about the Lorentz covariance of its "inertial" formulation: it has to do with the physical fact that the same experiment conducted with respect to any two inertial frames yields the same results in both frames. One can extract such physical invariances with the following definition, which requires that the dynamical objects and absolute objects have already been identified according to definitions 2.3.1 and 2.3.2.

Definition 2.3.3 (Invariance group)**.** *Consider a generally covariant formulation of the rules of a theory. The invariance group of a family of objects* $\mathcal{F} = \{O_k\}_{k\in K}$ *is the set* $I_\mathcal{F} \subset \mathrm{Diff}(\mathcal{S})$ *such that*

$$\forall g \in I_\mathcal{F},\ \forall j,\quad \mathcal{R}_j(\{O_k\}_{k\in K} \cup \{O_l\}_{l\notin K}) \iff \mathcal{R}_j(\{\Phi_k(g)\cdot O_k\}_{k\in K} \cup \{O_l\}_{l\notin K}). \quad (2.3.1)$$

It is called the invariance group of a given object O_i *when* $\mathcal{F}$ *only contains* O_i*.*

The invariance group I *is the invariance group of the family containing all the dynamical objects. The theory is called diffeomorphism-invariant when* I *actually equals the whole of* $\mathrm{Diff}(\mathcal{S})$*.*

There is indeed a physical content in the fact that any solution actually generates a whole family of solutions by acting only on certain objects (the dynamical ones). Besides, one sees that, when there are no absolute objects, the invariance group equals the covariance group, so that the theory is automatically diffeomorphism-invariant. Conversely, it is common to think that requiring diffeomorphism invariance is too constraining to allow any absolute object.

More generally, the general covariance relation (2.1.1) shows that I also equals the invariance group of the family containing all the absolute objects. Besides, the invariance group of any family clearly contains the intersection of the invariance groups of each of its objects. Furthermore, given the wide variety of phenomena $\mathcal{R}_j$ that the rules describe, they are often injective in the sense that, when $\mathcal{F}$ reduces to a single object O_k, relation (2.3.1) implies $\Phi_k(g)\cdot O_k = O_k$. The latter relation exactly defines the elements of the stabilizer of O_k, which clearly is always included in the invariance group of O_k. With injective rules, the invariance group of an object thus equals its stabilizer. In special relativity for instance, the Minkowski metric is the only absolute object and its stabilizer is the Lorentz group, hence the Lorentz invariance. In the context of theories of gravitation, Lorentz invariance refers to the property that inertial frames at an event are related by the Lorentz trasformation corresponding to the relative velocity measured by the inertial observers, as claimed by EEP (this property is thus rather called "local Lorentz invariance"). Indeed, when it is the case, one can construct a Lorentzian metric over spacetime (as was done earlier) whose stabilizer at any event is, by definition, the Lorentz group.

Background objects and action-reaction principle Based on the criteria 2.3.1 and 2.3.2, the metric equation to be devised should make the metric a dynamical object. Together with the equations ruling the non-gravitational fields, obtained with EEP, the theory will thus realize diffeomorphism invariance. Yet, this does not completely characterize the specifities of most theories of gravitation like GR. One further

criterion should be imposed to forbid an unphysical metric equation such as the following (diffeomorphism-invariant) model:

$$ {}^{g}\mathrm{Ric} = 0, \tag{2.3.2} $$

$$ {}^{g}\Box\phi = 0, \tag{2.3.3} $$

where ϕ is a scalar field, and ${}^{g}\mathrm{Ric}$ and ${}^{g}\Box$ are respectively the Ricci tensor and the d'Alembert operator associated with g.

The metric equation (2.3.2) clearly admits non-equivalent solutions in regard of criterion 2.3.1, e.g. the whole Kerr-Newman family. Solving equation (2.3.3) then yields non-equivalent scalar configurations as well. Hence all fields are dynamical. The issue is that the metric can be completely determined first, independently of the scalar field: g acts on ϕ through ${}^{g}\Box$, but is not back-reacted upon by ϕ, as if all possible scalar configurations were test fields to the metric, and the latter an independent background to ϕ. Such "one-way coupling" is unphysical in view of a fundamental action-reaction principle: a field A is involved in the equation of motion of a field B *iff* B is involved in A's equation of motion. Fields enforcing this principle could be called "proper dynamical objects", or "acting-reacting objects", as opposed to "background objects", of which absolute objects are the most rigid representatives. The example (2.3.2)-(2.3.3) shows that the intersection between background objects and dynamical objects is not empty; it contains the "dynamical backgrounds".

Much more complete discussions on general covariance, invariance, and absolute, dynamical and background objects are conducted in chapter 4 of [41], chapter II of [42], part IV of [82], section 3.5 of [57] and the articles [83–85].

2.4 Lovelock theorem

After such discussions, the metric g is clearly identified as not only being dynamical, but entirely determined by the back-reaction of the physical situation that it influences. Yet, what PDE can be devised to rule such a proper dynamical metric? There are actually not so many choices according to Lovelock's theorem, originally established in [86, 87], and extending former results exposed in [88, 89].

Theorem 2.4.1 (Lovelock)**.** *Given a metric g over a D-dimensional manifold ($D \geq 2$), any second-rank symmetric tensor $E_{\mu\nu}$ that is divergence-free (${}^{g}\nabla_\nu E^{\mu\nu} = 0$) and constructed only from the metric and its partial derivatives up to order 2 writes as*

$$ E^{\mu}_{\nu} = \sum_{m=0}^{\lfloor \frac{D-1}{2} \rfloor} c_m \delta^{\mu\rho_1\sigma_1\ldots\rho_m\sigma_m}_{\nu\alpha_1\beta_1\ldots\alpha_m\beta_m} \prod_{i=1}^{m} {}^{g}\mathrm{Riem}^{\alpha_i\beta_i}{}_{\rho_i\sigma_i}, \tag{2.4.1} $$

where $\lfloor \cdot \rfloor$ denotes the integer part, δ is the generalized Kronecker delta, and the c_m are any constants (and, conventionally, $\prod_{i=1}^{0} = 1$).

Furthermore, this tensor actually corresponds to the Euler-Lagrange expressions of the action

$$ S[g] = \int d^D x \sqrt{|g|} \sum_{m=0}^{\lfloor \frac{D-1}{2} \rfloor} c_m \delta^{\rho_1\sigma_1\ldots\rho_m\sigma_m}_{\alpha_1\beta_1\ldots\alpha_m\beta_m} \prod_{i=1}^{m} {}^{g}\mathrm{Riem}^{\alpha_i\beta_i}{}_{\rho_i\sigma_i}. \tag{2.4.2} $$

The sums in (2.4.1) and (2.4.2) stop at $\lfloor \frac{D-1}{2} \rfloor$ because further analogous terms beyond would vanish anyway. The $m = 0$ term is proportional to δ^μ_ν in (2.4.1), and is a constant in (2.4.2). The $m = 1$ term (for $D \geq 3$) is proportional to the Einstein tensor ${}^g G^\mu{}_\nu \equiv {}^g\mathrm{Ric}^\mu{}_\nu - {}^g R \delta^\mu_\nu/2$ (where ${}^g R$ is the Ricci scalar associated with g through ${}^g\nabla$) in (2.4.1), and is proportional to the latter in (2.4.2). Those are the only terms for $D = 3$ and $D = 4$.

Such a theorem is particularly interesting because fundamental laws are expected to be second-order PDEs (Newton's second law being the prototypical example). In particular, this guarantees the theory to be free of any unphysical Ostrogradsky instability [90, 91]. Section 7.1 of [54] details further arguments allowing to guess the structure of the metric equations from their expected weak-field approximation. In particular, the metric equations should involve an energy-momentum tensor $T_{\mu\nu}$ containing the properties of matter that should generate gravitational effects. An energy-momentum tensor, synthesizing the properties of matter fields, is already well-defined, symmetric and divergence-free in the framework of special relativity (see e.g. section 2.8 of [54] or chapters 19 and 20 of [48]). Expecting the same properties in presence of gravitation (in agreement with EEP), one may first consider metric equations in the form $E_{\mu\nu} = T_{\mu\nu}$, where $E_{\mu\nu}$ would gather all the terms involving only the metric and its partial derivatives up to order 2, while $T_{\mu\nu}$ would contain any term involving any other field of the theory (hence possibly metric terms coupled to other fields). Then, $E_{\mu\nu}$ is necessarily symmetric and divergence-free, hence expressed by (2.4.1). In four dimensions, the latter exactly reduces to the $m = 0$ and $m = 1$ terms detailed above, yielding metric equations in the form

$$G_{\mu\nu} + \Lambda g_{\mu\nu} = \frac{8\pi G_N}{c^4} T_{\mu\nu}, \tag{2.4.3}$$

where the constants c_0 and c_1 (with further numerical factors) are reinterpreted in terms of the cosmological constant Λ, Newton's constant G_N and the speed of light in vacuum c.

Besides, if the field equations of the theory are to be derived from an action principle, the part of the action involving only the metric and its derivatives should be given by expression (2.4.2). In four dimensions, the $m = 0$ and $m = 1$ terms yield the Einstein-Hilbert action with the cosmological constant:

$$S_{EH}[g] = \frac{c^4}{16\pi G_N} \int d^4x \sqrt{|g|} \left({}^g R - 2\Lambda \right). \tag{2.4.4}$$

The rest of the complete action would then describe matter fields: it should take a form suggested by the minimal coupling procedure applied to the Minkowski action of matter, up to factor-ordering ambiguities (although second-order derivatives are unusual in Lagrangians to prevent from the Ostrogradsky instability ealier mentioned). This will couple matter fields to metric terms emerging from the Christoffel symbols of the Levi-Civita covariant derivative. The Euler-Lagrange expressions of these coupled terms with respect to the metric then define the energy-momentum tensor $T_{\mu\nu}$.

Chapter 3

General relativity

Contents

As stated in the introduction, the actual applicability of any theory is not only assessed from compatibility with existing observational constraints, but also from purely theoretical criteria. This chapter recaps the status of both kinds of viability conditions in GR.

3.1 Theoretical viability

Predictivity The Einstein's field equations (2.4.3) only involve three free parameters: Λ, G_N and c, which are to be determined from experience once and for all before making any prediction. With such a (small) finite number of parameters valid for the whole application scope of the theory, GR is a priori predictive. Of course, the energy-momentum tensor may also rely on free parameters describing the properties of matter, but then, it will rather be a requirement on $T_{\mu\nu}$ not to spoil predictivity to be considered an admissible energy-momentum tensor. These are only straighforward considerations (yet not holding for all physical models), but any prediction on a system not only is a function of the free parameters but also requires sufficient knowledge of the state of the system. Identifying precisely the amount of required knowledge, and whether it is reasonable, defines the "well-posed" formulation of a problem.

Well-posedness Most of the time, the main rules of a theory are PDEs satisfied by fields defined over spacetime. A realistic system is thus generically described by a set of functions f_k defined over a spacetime domain $\mathcal{U}$, and solving a certain set of PDEs. Finding solutions to the PDEs generally starts by prescribing restrictions $f_{k_{|\mathcal{H}}}$ which seem to describe the system on a certain subset $\mathcal{H} \subset \mathcal{U}$. However, some restrictions are inappropriate in that they do not yield a unique solution: they may either underdetermine or overdetermine the system. In light of this, Hadamard formalized in 1907 [92] the notion of well-posedness: a problem is well-posed when a subset $\mathcal{H} \subset \mathcal{U}$ has been identified such that prescribing the restrictions $f_{k_{|\mathcal{H}}}$ does yield a unique solution f_k, which smoothly depend on the $f_{k_{|\mathcal{H}}}$.

When one has interest in a stationary system, $\mathcal{U}$ may be reduced to a spatial domain. In a laboratory experiment, the experimenter would most easily influence the system defined over $\mathcal{U}$ by fixing its conditions at the boundaries of $\mathcal{U}$. If the system always adopt the same stationary behaviour for given boundary conditions, one would expect the laws of the system to be well-posed with $\mathcal{H}$ identified as the boundary $\partial\mathcal{U}$ of $\mathcal{U}$. Yet, it is not forbidden for an experimenter to fix conditions on another domain $\mathcal{H}'$ strictly inside $\mathcal{U}$ if she can, and then infer whether the corresponding mathematical problem should be well-posed. For systems evolving in time, the experimenter prepares the system in a known configuration at an inital time ("Cauchy data"). With the same approach as for the boundary problem, she would then investigate the initial value problem ("Cauchy problem"). Moreover, for spatially bounded systems, she may again tune the conditions of the system on its spatial boundaries ("Cauchy-boundary problem"). Beside any textbook on PDEs, reference [93] is a synthetic review of the existing mathematical results on these subjects.

Trust in determinism, and continuity with respect to appropriate knowledge of any system, requires physical theories to have well-posed Cauchy problems. This has been investigated in GR for several systems. Let us briefly illustrates how this is formalized in the vacuum case: Λ and $T_{\mu\nu}$ are set to zero, so that the system reduces to the spacetime metric g. Consider a coordinate system (t, x^i) such that ∂_t is timelike and the ∂_i are spacelike (this is always possible, since realistic observers' coordinates fulfills these conditions). Denote n the (unique timelike) unit future-oriented vector field normal to the (spacelike) constant t hypersurfaces $\mathcal{H}_t$. Then, a relevant family of functions f_k describing the system is formed by the spatial (Riemannian) metric γ induced by g on the hypersurfaces $\mathcal{H}_t$, the extrinsic curvature $K = -\mathcal{L}_n\gamma/2$, the lapse function $N = (-g^{00})^{-\frac{1}{2}}$ and the shift vector $\beta = \partial_t - Nn$, from which the metric g is reconstructed as

$$g_{\mu\nu}dx^\mu dx^\nu = -N^2dt^2 + \gamma_{ij}(dx^i + \beta^i dt)(dx^j + \beta^j dt). \tag{3.1.1}$$

Though one is a priori ready to prescribe the configurations of (N, β, γ, K) on a fixed hypersurface $\mathcal{H}_0 = \mathcal{H}_{t_0}$, analysis of the Einstein's equations (2.4.3) actually shows that these initial configurations cannot be freely chosen: they are themselves constrained to solve the so-called Hamiltonian and momentum constraints, which are respectively scalar and vector equations on $\mathcal{H}_0$ (reference [94] should be consulted for much more on the "3+1" decomposition (3.1.1) and these constraints). Furthermore, the lapse N and shift β turn out to carry information only about the coordinate system (t, x^i) rather than the physical degrees of freedom of the metric. Besides, causality requires that knowledge of (N, β, γ, K) on $\mathcal{H}_0$ should only determine g on the set of events $\mathcal{E}$ such that either all the future-directed, or all the past-directed causal curves from $\mathcal{E}$ intersect $\mathcal{H}_0$ exactly once. If this set actually corresponded to the whole spacetime, such $\mathcal{H}_0$, uniquely determining the metric everywhere, would be called a Cauchy hypersurface. To admit such a Cauchy hypersurface is one among several equivalent definitions of the globally hyperbolic spacetimes [49].

So far, the point of view based on the coordinate system (t, x^i) could only be a first step to figure out some necessary conditions for the existence and uniqueness of a solution to the Einstein's equations (2.4.3), because we assumed from the start that the solution metric was already present on spacetime, for instance to consider causality relations between events. Therefore, to properly formalize the problem, one

must consider the hypersurface $\mathcal{H}_0$, and the corresponding restrictions of (N, β, γ, K), independently of any embedding spacetime. The only properties to retain are that $\mathcal{H}_0$ is a $D-1$ dimensional manifold equipped with a Riemannian metric γ and a symmetric second-rank tensor K fulfilling the Hamiltonian and momentum constraints on it. Such a triple $(\mathcal{H}_0, \gamma, K)$ thus constitutes a Cauchy data for the vacuum evolution problem. The latter was shown to be locally and globally well-posed in the senses of theorems 3.1.2 and 3.1.3 below, which rely on the following two definitions.

Definition 3.1.1 (Developments and extensions)**.** *Call development of $(\mathcal{H}_0, \gamma, K)$ a Lorentzian spacetime $(\mathcal{S}, g)$ such that g satisfies the vacuum Einstein equation ${}^g\mathrm{Ric} = 0$, and there exists an embedding $\Theta : \mathcal{H}_0 \to \mathcal{S}$ such that:*

- *$\Sigma \equiv \Theta(\mathcal{H}_0)$ is a Cauchy hypersurface of $\mathcal{S}$ (which is hence globally hyperbolic),*
- *$\gamma = \Theta^* g$,*
- *$K = \Theta^{*\,\Sigma}K$, where ${}^\Sigma K$ is the extrinsic curvature of Σ.*

Call extension of $(\mathcal{S}, g)$ a development $(\mathcal{S}', g')$ such that the corresponding embedding satisfies $\Theta' = \psi \circ \Theta$ where $\psi : \mathcal{S} \to \mathcal{S}'$ is an embedding.

Theorem 3.1.2 (Local well-posedness)**.** *There always exist developments of a given Cauchy data, and any two developments are extensions of a common development.*

Theorem 3.1.3 (Global well-posedness)**.** *There always exists a maximal development (in the sense that it is an extension of all developments), which is unique up to isometries.*

Such result was established in 1969 by Choquet-Bruhat and Geroch [95]. For more details on these subjects, one could first consult section 3.8 of [57], before going through [96] for a complete mathematical treatment (of non-vacuum cases as well).

Black hole solutions Proving the well-posedness of evolution problems in GR are great mathematical achievements, and important criteria ensuring that the theory is physically viable. However, this generally does not provide any method to actually construct solutions of the theory. Actually, several solutions of GR were discovered long before well-posedness was proved. Most known analytical solutions are exposed in the different textbooks on GR cited so far. Of course, different solutions often apply to different physical situations, from the neighbourhood of planets to cosmological scales. Given the topic of part II of this manuscript, let us only recall a few important results on black hole solutions in GR.

First of all, black holes are rigorously defined with the notion of conformal completion of a Lorentzian spacetime, which is properly defined in section 4.3.1 of [97]. In particular, a conformal completion provides a boundary $\mathcal{I}$ to spacetime. Then, the black hole region of spacetime is defined as the set of events such that no future-directed causal curve from them ever reaches $\mathcal{I}$.

Despite this general definition, several results have tended to prove that the black hole solutions of GR are very limited, and actually restrict to the explicitly known Kerr-Newman family. Historically, the first striking results of this kind were obtained by Israel, who demonstrated that the Schwarzschild [98] (resp. Reissner-Nordström [99])

metric was the unique asymptotically flat static solution under a few reasonable assumptions. Then Carter [100], Hawking [101] and a final argument by Robinson [102], established the uniqueness of the Kerr family, yet under the well-known unphysical requirement of analyticity.

Such uniqueness results have come to be named no-hair theorems as they picture black holes as devoid of any distinctive character (other than a finite, actually very small number of parameters). These results have since then pushed physicists to look for reasonable conditions in which different black hole solutions could be obtained. Such "hairy" black holes can indeed be found, either within the framework of GR, or that of alternative theories, as will be discussed in section 6.2.

Reference [103] provides proofs of the no-hair theorems mentioned above (and history of the improvements made on their assumptions), while the review [104] covers more uniqueness results. Much more on the Kerr solution and black holes in general is to be found in references [105–111] and the textbooks and lecture notes [97, 112–115].

Stability One further important criterion for the viability of a theory is the stability of its solutions, meaning the existence of "perturbed" configurations arbitrarily close to the solutions. Firstly, the most trivial solution of GR is the Minkowski metric with vanishing matter fields. Yet, demonstrating its global stability against all types of perturbations (not only linear) was utterly non-trivial, as established by Christodoulou, Klainerman and Nicolo in [116, 117]. Such a result actually considers perturbations of the metric "only", while all matter fields remain unperturbed. A first extension in this direction has been achieved in [118, 119], where stability against all types of perturbations of the metric and massive scalar fields is proved.

Regarding black hole solutions, the linear stability of the Schwarzschild solution against metric perturbations has been discussed and obtained in several studies [120–122]. Regarding the Kerr family, several restricted results exist [123, 124]. One may also consult section 4.9 of [113] and section 10.2.5 of [115] for more details.

Well-defined physical quantities New theories often questioned and even disputed concepts and representations of former well-established theories. In some cases though, one may legitimately expect that some fundamental physical quantities should find clear generalizations in all theories. In the case of GR, the very notions of mass and angular momentum actually raise non-trivial issues and enjoy several definitions specific to different situations. These are exposed in [125], and in [126] in even greater detail.

3.2 Observational tests

As mentioned in the introduction, GR passed many experimental tests, predicting e.g. the correct perihelion precession of Mercury, deflection of light by the sun, Shapiro time delay. These are thoroughly reviewed in [10, 127]. In particular, detection of gravitational waves (GW) by the LIGO and Virgo observatories [3, 4] are among the most recent tests of GR. These are highly difficult observations to realize due to the very low amplitudes of GW signals. Extraction of GW patterns from brut data thus demands several signal processing steps and notably to be able to generate a large database of all possible patterns. The most common (and the only ones observed so

far) sources of GW are mergers of compact objects. In this case, patterns are generated with the help of different techniques, each one being appropriate for a specific phase of the merger. The inspiralling phase is modelled with post-Newtonian [128, 129] and effective-one-body [130] techniques, which rely on perturbative expansions in terms of the velocities of the compact objects. The last merging orbits require numerical approaches [131, 132]. Finally, the post-merger (or ringdown) phase, which is even harder to extract from observations, requires investigation of the quasi-normal modes of the final black hole [133, 134]. This is achieved by sudying pertubations around the expected equilibrium metric. Up to now, all GW detections are consistent with GR but better precision seems to be required to distinguish between patterns of GR and alternative theories.

A second type of modern tests is the monitoring of supermassive black holes lying at the center of galaxies. For instance, the interferometer GRAVITY [12] accurately records the trajectories of stars orbiting the central supermassive black hole of the Milky Way (*Sgr A**) [14]. It is also capable of following variable hot spots ("flares"), suspected to originate from magnetic processes in the accretion disk of *Sgr A**, over time scales of an hour [15]. Both stars and flares are expected to follow geodesics, so that the corresponding astrometric measurements provide precious information about very strong-field regions. The Event Horizon Telescope [13] is a worldwide realization of very-long baseline interferometry, which allowed to investigate the emision structure of *Sgr A** [16], or to reconstruct the image of the accretion disk of the supermassive black hole *M87** [17]. Such observational data is produced in strong gravitational fields and carried by photons following null geodesics. It is thus another valuable source to test strong gravity. Again, both types of observations are compatible with GR so far, and improved accuracy would be required to set strong constraints on alternative theories.

References [131, 132] and [11] respectively cover the possibilities offered by GW astronomy and astrophysical black holes to test the strongest regimes of gravity.

Chapter 4

Alternative formulations

Contents

Before turning to alternative theories of gravity, this chapter briefly introduces two alternative frameworks classically[25] equivalent to GR: the tetradic formulation, notably in the case of teleparallelism, and the Palatini formulation.

4.1 Tetradic formulation

Consider an arbitrary frame $\{e_\rho\}$ and a tetrad (see footnote 15)

$$\{e_\alpha\} = \{e_\alpha = e^\rho{}_\alpha e_\rho\} \tag{4.1.1}$$

defined over an open set.

A tetrad is an orthonormal frame, so that $g_{\rho\sigma}\, e^\rho{}_\alpha\, e^\sigma{}_\beta = \eta_{\alpha\beta}$, where η merely denotes the matrix $\mathrm{diag}(-1,1,1,1)$. Denoting $\hat{e}^\alpha{}_\rho$ the inverse matrix of $e^\rho{}_\alpha$, one recovers the metric in the arbitrary frame as

$$g_{\rho\sigma} = \eta_{\alpha\beta}\hat{e}^\alpha{}_\rho\hat{e}^\beta{}_\sigma. \tag{4.1.2}$$

One may actually use relation (4.1.2) as the definition of the metric, and instead regard the tetrad transition matrix $e^\rho{}_\alpha$ as a more fundamental field: consider a spacetime, so far devoid of any metric, but equipped with an invertible second rank tensor e. Then, construct a metric $g[e]$ according to (4.1.2), where η merely is a notation for the diagonal matrix $\mathrm{diag}(-1,1,1,1)$, i.e. it should not be seen as a fundamental object of the tetrad formulation (very much like the Minkowski metric in the "inertial" formulation of special relativity, discussed in section 2.3). In particular, all the frames defined by (4.1.1) will be orthonormal frames with respect to the newly defined metric $g[e]$. Furthermore, relation (4.1.2) yields $\det g = -\det{}^2 e$, so that the Einstein-Hilbert action (2.4.4) rewrites as

$$S_{\text{tetrad}}[e] = \frac{1}{16\pi G_N}\int d^4x|e|\left({}^{g[e]}R - 2\Lambda\right), \tag{4.1.3}$$

[25] Subtle differences may appear when trying to quantize these formulations: see e.g. sections 3.2.1 and 3.2.2 of [135], and [136, 137].

where the speed of light c is set to 1 from now on.

Note that this formulation is more than a curiosity as it is very often used to introduce spinor fields in the matter action (see e.g. section 9.1 of [135]). Yet, this is not the only way to handle spinors over spacetime (see section 15.1 of [63]).

Teleparallelism Teleparallelism further reformulates action (4.1.3) based on the following approach. Consider the connection ∇ whose preferred frames are the tetrad defined by (4.1.1) (in such a case, the tensor field e exactly corresponds to the transition matrix m used in section 1.2). Such a connection ∇, called a Lorentz connection, is flat (see section 1.2.1), but may admit a non-trivial torsion ${}^{\nabla}T$. This would only mean that the tetrad is not integrable. Furthermore, ∇ would be compatible with the metric (4.1.2), as the latter takes the constant form $\mathrm{diag}(-1,1,1,1)$ in the tetrad. It would therefore be an example of a Weitzenböck connection (see the end of section 1.4). Then, remarkably, it is possible to reformulate the Ricci scalar ${}^{g[e]}R$ of the Levi-Civita connection ${}^{g[e]}\nabla$ in terms of the torsion ${}^{\nabla}T$ only, yielding the teleparallel action

$$S_{\text{tele}\parallel}[e] = \frac{1}{16\pi G_N}\int d^4x|e|\left(\frac{1}{4}{}^{\nabla}T_{\alpha\beta\rho}\,{}^{\nabla}T^{\alpha\beta\rho} + \frac{1}{2}{}^{\nabla}T_{\alpha\beta\rho}\,{}^{\nabla}T^{\beta\alpha\rho} - {}^{\nabla}T_{\alpha}\,{}^{\nabla}T^{\alpha}\right), \tag{4.1.4}$$

where indices are raised and lowered with the metric (4.1.2), and the torsion vector ${}^{\nabla}T_{\alpha}$ is the quantity ${}^{\nabla}T^{\beta}{}_{\alpha\beta}$.

Beside this reformulation, teleparallelism really uses the tensor e as the only fundamental field describing gravitation, in that it renounces to describe gravity with the help of ${}^{g[e]}R$. In particular, motion of free particles can no longer be described as geodesics. Instead, the effect of gravity is equivalently described by a force term in the action of free particles (analogous to the Lorentz term in presence of an electromagnetic potential): teleparallelism is not a geometric description of gravity.

All the technical steps needed to realize this consistent reformulation of GR, and much more on teleparallel gravity, are exposed in [138–140]. One may also consult the technical exchanges between the articles [141–143].

4.2 Palatini formulation

The Palatini formulation is a first step towards metric-affine theories of gravity, which will be introduced in section 5.1. The principle is to consider a situation such that the connection ∇, from which the Ricci scalar is defined in the Einstein-Hilbert action (2.4.4), is not necessarily the Levi-Civita connection, but still is torsionless. According to decomposition (1.4.1), ∇ is actually a sum ${}^{g}\nabla + M$, where M is a new argument of the action, with components $M^{\rho}{}_{\sigma\mu}$ symmetric in the last two indices. With such a construction, the Ricci tensor of ∇ is a composite of the two arguments of the action

$$S_{\text{Palatini}}[g,M] = \frac{1}{16\pi G_N}\int d^4x\sqrt{|g|}\left({}^{\nabla}R - 2\Lambda\right). \tag{4.2.1}$$

If the rest of the action does not involve ∇ (i.e. uses the Levi-Civita connection to describe the dynamics of matter), then the Euler-Lagrange expressions with respect to

the metric are structurally the same as Einstein's field equations, yet the Ricci tensor (and hence the Ricci scalar) are constructed from $\nabla = {}^g\nabla + M$ rather than ${}^g\nabla$. However, it turns out that the Euler-Lagrange expressions with respect to the components ${}^{\nabla}M^{\rho}{}_{\sigma\mu}$ ultimately amount to requiring $\nabla = {}^g\nabla$ (i.e. equating the Christoffel symbols of ∇ to the expressions (1.4.2)): metric-compatibilty ensues from the action principle.

Reference [144] discusses the Palatini approach in much more details and a more general framework. Note also that the tetrad and Palatini formulations are very often combined, although these two sections show that they are not entangled in principle.

Chapter 5

Alternative theories

Contents

The number of alternative theories of gravity is considerable. It is only legitimate here to introduce a few models which directly connect to topics mentioned in the previous chapters and to part II.

5.1 Metric-affine gravity

Metric-affine gravity generalizes the approach of the Palatini formalism (section 4.2) in allowing the connection ∇ to be arbitrary (i.e. non-metricity and torsion are allowed), and to be used in the matter action (i.e. it is no longer constrained to be only involved in the construction of the Ricci scalar ${}^{\nabla}R$). In particular, the Ricci tensor ${}^{\nabla}\mathrm{Ric}$ of ∇ is now completely independent from the metric, so that g only contracts with ${}^{\nabla}\mathrm{Ric}$ to construct ${}^{\nabla}R$. As a result, no derivative of the metric is involved in the action, whereas the Einstein-Hilbert action (2.4.4) contains second-order derivatives of g for sure. The latter is thus known as a second-order formulation, while metric-affine models are called first-order formulations. Actually, the gravitational part (which gathers all the terms involving only the metric and the connection) of such theories is allowed to be much more complex than a Ricci scalar, e.g. functions of it.

General discussions on this type of theories are provided in [145, 146].

Einstein-Cartan In section 2.2, EEP suggested that gravitational effects would be described by a connection ∇. Before restricting to the framework of metric theories and hence the Levi-Civita connection, ∇ had only been shown to be compatible with the metric constructed by copying the Minkowski metric in the inertial coordinate frames attached to inertial observers' worldlines. According to decomposition (1.4.1), a contorsion tensor ${}^{\nabla}C^{\rho}{}_{\sigma\mu}$ was still allowed. Einstein-Cartan theory precisely considers

this possibility, while still using a Ricci scalar alone in the gravitational part of the action. The structure of the action is thus the same as Palatani's action (4.2.1), yet ∇ is constrained to be metric-compatible instead of torsionless.

More explicitly, the second argument of the action, which was made of a tensor ${}^{\nabla}M^{\rho}{}_{\sigma\mu}$ symmetric in the last two indices, is replaced by a torsion tensor ${}^{\nabla}T^{\rho}{}_{\sigma\mu}$, i.e. a third-rank tensor with antisymmetric last two indices. Any occurence of ∇ in the matter action actually denotes the sum ${}^{g}\nabla + {}^{\nabla}C$, where ${}^{\nabla}C$ is the contorsion tensor of ${}^{\nabla}T$ defined by relation (1.4.4). Therefore, with such a construction of ∇, the Ricci tensor is a composite of the two arguments of the action (g and ${}^{\nabla}T$).

With respect to the metric, the Euler-Lagrange equations yield analogues of Einstein's field equations. With such connection and torsion, conservation laws still ensue from Bianchi identities, but do not necessarily take the form of a divergence-free energy-momentum tensor. With respect to torsion, the Euler-Lagrange equations establish a direct algebraic equation giving the explicit form of the torsion in terms of a tensor interpreted as the internal angular momentum density of matter ("spin density tensor").

References [147, 148] review Einstein-Cartan theory.

5.2 Higher-dimensional models

Higher-dimensional models arise in many contexts. Below are introduced only three standard examples.

Lanczos-Lovelock theories In the previous chapters, Lovelock theorem 2.4.1 was another hint at alternative theories. It was indeed useful to guess the structure of the left-hand side of Einstein's equations (2.4.3), but it also suggested that, for every dimension D, these equations have a natural generalization sharing same properties: the left-hand side is given by the expression (2.4.1) while the energy-momentum tensor has exactly the same form as in four dimensions.

These models are reviewed in [149].

Higher-dimensional GR Higher-dimensional GR truncates the Lanczos-Lovelock expansion (2.4.1) at $m = 1$ for any dimension, so that the Einstein's equations are considered in the exact same form (2.4.3) independently of the dimension. These models have received a lot of attention, notably regarding black holes. In 1963 (same year as the discovery of the Kerr solution [150]), Tangherlini obtained a generalization of the Schwarzschild family for any higher dimension D [151]. Actually, by adding flat dimensions to this solution, new black holes (usually known as "black branes") with exotic horizon topologies can also be constructed. However, such solutions are generically unstable ("Gregory-Laflamme instability"). In 1986, Myers and Perry obtained a black hole generalization of the Kerr family for any higher dimension [152]. Yet, unlike the Kerr family, those generalizations are not subject to a general no-hair theorem.

Much more details on higher-dimensional black holes are exposed in references [153, 154].

Kaluza-Klein models Kaluza-Klein models are characterized by the existence of coordinate systems (x, y) with respect to which the metric takes the form

$$g_{MN}(x,y) = \begin{pmatrix} g_{\mu\nu}(x) & v_\nu(x) \\ v_\mu(x) & \phi(x) \end{pmatrix}, \tag{5.2.1}$$

where x denotes coordinates on a $(D-1)$-dimensional spacetime, and y is one further coordinate on a compact dimension from which all metric components are independent.

Then, consider the higher-dimensional Einstein-Hilbert action (2.4.4). One may decompose the D-dimensional metric determinant and Ricci scalar in terms of the $(D-1)$-dimensional analogue quantities constructed from the metric $g_{\mu\nu}$, together with non-trivial terms generated by the $(D-1)$-vector v^μ and the scalar field ϕ. One may then integrate over the compact dimension of the action to recover a $(D-1)$-dimensional Einstein-Hilbert action added with vector and scalar actions (see e.g. section 10.2.1 of [155] for an explicit example of such "dimensional reduction"). In some 5-dimensional cases considered in the original works of Kaluza [156] and Klein [157, 158], the final vector action may be interpreted as Maxwell's action, so that both 4-dimensional GR and electromagnetism can be recovered from model (5.2.1).

The implications of Kaluza-Klein inspired models are covered in references [159–161].

5.3 Massive gravity

It has been mentioned in the introduction that GR does not fit in the quantum formalism of particle physics [20, 21]. In such a perspective, the metric would be the classical manifestation of a quantum field whose perturbations are interpreted as fundamental spin-2 particles called graviton. When one follows this approach, the gravitons turn out to be massless particles: their Lagrangian lack a term analogue to the $\mu\phi^2$ or $\mu v_\mu v^\mu$ terms of scalar and vector fields, where μ would be the mass of the corresponding particles.

In view of this, it became interesting for several reasons to try to provide gravitons a mass, one of them being related to the unexplained accelerated expansion of the universe ("dark energy problem" [22, 23]): roughly speaking, massive particles mediate interactions whose amplitude decreases as $e^{-\mu r}/r$ with distance r. The effective range of the interaction is thus limited to scales below approximately $1/\mu$, which becomes infinite in the limit of massless particles like gravitons. As a result, a small but non-zero graviton mass would annihilate gravitational effects on very large scales, which could provide a natural solution to the dark energy problem.

In 1939, Fierz and Pauli developed a simple (yet unique under a few consistency requirements) theory of a non self-interacting (linear field equations) massive spin-2 field [162, 163]: they expanded the Einstein-Hilbert action to quadratic order in a perturbation h of the Minkowski metric η, and added a mass term in the form $\mu^2[h_{\mu\nu}h^{\mu\nu} - (\eta_{\mu\nu}h^{\mu\nu})^2]$. In 1970, it was shown, notably by van Damn, Veltman and Zakharov, that the Fierz-Pauli theory could not reproduce solar system predictions of GR in the limit $\mu \to 0$ (a result known as the "vDVZ discontinuity"), and was hence incompatible with observations [164–166]. In 1972, Vainshtein understood that the vDVZ discontinuity was caused by the linear nature of Fierz-Pauli theory [167]: the

latter can be appropriately completed in a non-linear theory free of vDVZ discontinuity, which becomes strongly coupled in the vanishing mass limit, in the sense that it cannot be consistently approximated by a truncated perturbative expansion like Fierz-Pauli theory. As mentioned above, such massive theories modify GR on large scales, and yet coincide with GR on solar system scales. This means that there exists a certain radius, known as Vainshtein radius, where a transition operates. The property of these non-linear completions of Fierz-Pauli theory (NLFP) to recover the predictions of GR when $r \to 0$ is known as the Vainshtein mechanism or Vainshtein screening[26].

To construct the gravitational action of NLFP theories, it is clear that at least one assumption of the Lovelock theorem 2.4.1 must be evaded, otherwise perturbations around any background will describe a massless graviton. Yet, the assumption of less than second-order derivatives is maintained, firstly to keep preventing the Ostrogradsky instability, and secondly because mass terms are actually not expected to arise from derivative terms. It is therefore required that the gravitational action involves another field than the metric. The most studied situation is to use a second metric field f, although matter fields remain coupled only to the first metric g. Standard massive gravities take f to be flat and non-dynamical (i.e. it is an absolute background according to section 2.3), while bi-metric models take f to be properly dynamicals. Many interaction terms between f and g are then allowed to realize NLFP theories.

Unfortunately, curing the vDVZ discontinuity with the Vainshtein mechanism characterizing NLFP theories was followed by another issue, raised a few months later by Boulware and Deser [168]: NLFP theories appeared to generically suffer from an instability known as the Boulware-Deser ghost. This reduced interest for massive gravity until the Dvali-Gabadadze-Porrati (DGP) model was developed in 2000 [169]. The DGP model is a 5-dimensional theory of gravity such that all matter fields are restricted to a 4-dimensional subspace $\mathcal{H}$ (the usual spacetime):

$$S_{DGP} = M^3 \int d^5X \sqrt{|{}^{(5)}g|}\, {}^{(5)}R + M_P^2 \int_{\mathcal{H}} d^4x \sqrt{|g|}\, [R + \mathcal{L}_m]\,, \tag{5.3.1}$$

where M and M_P are constants (the 5 and 4-dimensional Planck masses), $\mathcal{L}_m$ is the Lagrangian of matter fields and ${}^{(5)}R$ (resp. R) is the Ricci scalar constructed from the 5-dimensional (resp. 4-dimensional) metric ${}^{(5)}g$ (resp. g).

In this model, gravity induced on $\mathcal{H}$ is effectively mediated by a continuum of massive gravitons [170] featuring a Vainshtein screening [171] and generically free of ghost [172]. This suggested that ghost-free NLFP should actually exist in spite of the arguments of Boulware and Deser, and realize well-behaved massive gravities simpler than the DGP model. This was explicitly proved in 2011 by de Rham, Gabadadze and Tolley (dRGT models, or "ghost-free massive gravity") [173].

Motivations, issues and implications of massive gravity are covered in much greater detail in the reviews [170, 174, 175]. More specifically, reference [175] reviews black holes in (ghost-free) massive gravity. One may also be interested in the series of papers [176–179] which numerically confirmed the recovery of GR below the Vainshtein radius in different models of massive gravity. Reference [180] and section 2 of [181] may also be consulted for more on the different types of screening mechanisms.

[26] This is notably named after the idea that three out of the five degrees of freedom enjoyed by massive gravitons get hidden by non-linear effects below the Vainshtein radius, in order to explain the manifest reduction to the two degrees of freedom of GR massless gravitons.

5.4 Non-minimally coupled fields

Scalar-tensor theories As illustrated above with the NLFP, Lovelock theorem 2.4.1 provides a useful method to construct modified theories in an organized way. It suggests that the only consistent approach to modify GR in four dimensions is to integrate new fields into the gravitational action. Such gravitational fields should couple to the metric in an essential way, i.e. such that they could not be equivalently interpreted as matter fields. The minimal coupling procedure, discussed in section 2.2 as a (possibly ambiguous) way to implement EEP, generates interaction terms between any matter field χ and the metric from the covariant derivatives[27] $\nabla\chi$ of χ (which do involve the metric within the Levi-Civita Christoffel symbols) or contractions of the metric with χ or $\nabla\chi$. Gravitational fields should thus feature interaction terms with the metric that not fall in these categories.

Of course, the simplest candidates to consider as a non-miminally coupled fields are scalar fields. Actually, such reasoning based on Lovelock theorem is not the only motivation encountered so far to consider gravitational scalar fields. As mentioned in section 5.2, scalar terms may naturally emerge from dimensional reduction over compact dimensions in higher dimensional models of gravity. This was the case for the Kaluza-Klein example, but it is actually true for the DGP model too, as will be recalled in chapter 6. One more motivation (actually also related to higher dimensions) is the systematic appearence of a scalar field, known as the "dilaton", in all string theories [182].

A popular family of scalar-tensor theories (sometimes known as Bergmann-Wagoner theories) is defined by the gravitational action

$$S_{\text{S-T}}[g,\phi] = \int d^4x\sqrt{|g|}\left[\phi R - \frac{\omega(\phi)}{\phi}g^{\mu\nu}\partial_\mu\phi\partial_\nu\phi - V(\phi)\right], \tag{5.4.1}$$

where ω and V are arbitrary functions.

It actually is the most general gravitational action with one scalar field, which is at most quadratic in derivatives of the fields [25]. The case of constant ω and $V = 0$ is known as Brans-Dicke theory. The latter, and actually the whole family (5.4.1), will be mentioned again in 6.2 as the subjects of important theorems.

Scalar-tensor theories are the subject of the textbook [183], but several reviews on the topic will be cited in chapter 6, which focuses on a much larger class of scalar-tensor theories, known as Horndeski theories. Actually, an even larger class known as "degenerate higher-order scalar-tensor theories" has recently been developed and studied [184], yet it will not be further mentioned.

Vector-tensor theories Expectedly, the next non-minimally coupled candidates are vector fields. An important example of this kind is the Einstein-Æther theory, whose gravitational action is

$$S_{\text{Æther}}[g,v,\lambda] = \int d^4x\sqrt{|g|}\left[R + K^{\alpha\beta}_{\mu\nu}\nabla_\alpha v^\mu\nabla_\beta v^\nu + \lambda\left(v^\mu v_\mu + 1\right)\right], \tag{5.4.2}$$

[27] From now on, the only connection considered will be the Levi-Civita connection, so that the pre-exponent notations ^{g} are abandoned for all quantities constructed from the metric and the connection.

where the field λ clearly is a Lagrange multiplier constraining the Æther vector v to be timelike, and

$$K^{\alpha\beta}_{\mu\nu} = c_1 g^{\alpha\beta} g_{\mu\nu} + c_2 \delta^\alpha_\mu \delta^\beta_\nu + c_3 \delta^\alpha_\nu \delta^\beta_\mu - c_4 v^\alpha v^\beta g_{\mu\nu}, \tag{5.4.3}$$

where the c_i are any constants.

The founding article [185] of the theory very clearly states the purposes of the theory and the choices required to achieve them. In particular, Einstein-Æther theory was constructed as a model for Lorentz-violating theories: the Æther, though dynamical, induces preferred frame[28] effects spoiling Lorentz invariance.

Reference [186] reviewed this model, but it should be noted that it was proved to be well-posed since then [187]. Observable signatures of the theory in gravitational waves and quasi-normal modes are respectively studied in [188] and [189].

Tensor-vector-scalar theories Of course, non-minimally coupled scalar and vector fields can be combined. Such models include the so-called TeVeS theory, developed by Bekenstein in 2005 [190] as a relativistic generalization of the modified newtonian dynamics (MoND) introduced by Milgrom in 1983 [191–193] to explain dark matter, i.e. the large unobserved amount of matter required to explain several gravitational phenomena [22, 23].

Observable signatures of such theories in gravitational waves are also studied in [188].

These different types of theories are subject to violate certain versions of the equivalence principle (see section 3.1.2 of [10]). Specific formalisms have been developed to theoretically investigate this question for large classes of theories, e.g. the $TH\epsilon\mu$ formalism (see section 2.2 of [10]). In the same spirit, the parametrized post-Newtonian formalism uses ten constant coefficients, introduced in several places of post-Newtonian expansions in a way that covers all possible deviations from GR of a large class of theories up to fixed orders (see chapter 4 of [28] for a thorough exposition). These allow to quickly and clearly identify the differences between theories and interpret them physically.

5.5 Approaches to quantum gravity

Such overview of modified theories of gravity should at least mention the most popular attempts to describe gravity within a quantum formalism: string theory (which unifies all the interactions, including gravity, in a quantum formalism) [182, 194–196], loop quantum gravity (which primarily realizes a canonical quantization of GR) [135, 197, 198], the effective field theory treatment of GR [18, 199, 200], asymptotic safety [201], causal set theory [202, 203], noncommutative geometry [204, 205], twistor theory [206]. Their large number indicates that none stood out in obtaining fully satisfactory results so far.

Beside, one could note that the standard model of particle physics, which met great success in describing the non-gravitional interactions within a quantum formalism, is

[28] Here, preferred frames are intrinsically singled out by the theory, independently of the connection (which is still the Levi-Civita connection).

not devoid of several defects either, e.g. the relatively large number of free parameters (about twenty, which is seen as unphysical, compared e.g. to the three parameters of GR discussed in section 3.1) or the assumption of zero neutrino masses which is in tension with observations. Like GR, solutions are sought in modified theories, involving e.g. supersymmetry [155, 207], which still has not found clear experimental confirmations.

Chapter 6

Horndeski theories

Contents

In 1974, Horndeski considered a general Lagrangian involving a metric tensor, a scalar field and their derivatives up to an arbitrary order p over a 4-dimensional spacetime [208]. Requiring the corresponding Euler-Lagrange equations to be second-order, he showed that these could be derived from a Lagrangian such that $p = 2$, which he provided the explicit expression. In other terms, Horndeski theories are the most general 4-dimensional scalar-tensor theories leading to second-order field equations. This latter fact being a valuable property preventing from Ostrogradsky instability, these theories received a renewed interest from 2012 [209].

6.1 Overview

Denoting $\phi_\mu = \partial_\mu\phi$, $X = -\frac{1}{2}\phi_\mu\phi^\mu$, and $\phi_{\mu\nu} = \nabla_\nu\nabla_\mu\phi$, Horndeski theories are all the linear combinations of the Lagrangians

$$\mathcal{L}_2 = G_2(\phi, X), \tag{6.1.1}$$

$$\mathcal{L}_3 = G_3(\phi, X)\Box\phi, \tag{6.1.2}$$

$$\mathcal{L}_4 = G_4(\phi, X)R + G_{4,X}\left((\Box\phi)^2 - \phi_{\mu\nu}\phi^{\nu\mu}\right), \tag{6.1.3}$$

$$\mathcal{L}_5 = G_5(\phi, X)G_{\mu\nu}\phi^{\mu\nu} - \frac{G_{5,X}}{6}\left((\Box\phi)^3 - 3\phi_{\mu\nu}\phi^{\nu\mu}\Box\phi + 2\phi_{\mu\nu}\phi^{\nu\sigma}\phi_\sigma{}^\mu\right), \tag{6.1.4}$$

where $G_{\mu\nu}$ is the Einstein tensor introduced in section 2.4, the G_i are arbitrary functions, and $G_{i,X}$ denotes differentiation with respect to their second argument.

More recently, another large family of theories, known as (covariantized generalized) Galileons, and defined in all dimensions, turned out to coincide with Horndeski theories in four dimensions [210]. This family was constructed in several steps. First of all, an effective formulation of the DGP model (5.3.1) on the 4-dimensional spacetime $\mathcal{H}$ was shown to generate scalar terms in a physically consistent "decoupling" limit [211, 212]. Such a scalar thus reproduces the effects of massive gravity, inducing deviations

from GR on cosmological scales, but recovering the latter on small scales through a Vainshtein mechanism. Reference [213] then determined the most general scalar action sharing such properties on a flat background. The resulting theories featured the so-called Galilean symmetry

$$\phi \to \phi + constant, \;\; \nabla\phi \to \nabla\phi + constant\ vector \tag{6.1.5}$$

and were hence named (flat) Galileons.

It was further argued that such theories were the most general theories on flat spacetime whose Euler-Lagrange equations only contained second-order derivatives. Generalized (flat) Galileons were then constructed as the most general family on flat spacetime whose Lagrangian and Euler-Lagrange equations contain derivatives of order two or less. They were finally covariantized in the unique way that preserves such properties over any curved spacetime, which required the addition of non-minimally coupled terms [214].

These steps and the equivalence with Horndeski theories in four dimensions are clearly reviewed in [215].

6.2 No-scalar-hair theorems

The no-hair theorems mentioned in section 3.1 have aroused interest for black hole solutions different than the Kerr family. To obtain such hairy solutions, one or several assumptions from those theorems had to be evaded. A natural idea was to consider a scalar field interacting with the metric. Yet, even in such contexts, so-called no-scalar-hair theorems proved that the scalar field had to be trivial, so that the metric reduced to the GR vacuum black holes.

Minimally coupled hair The first no-scalar-hair theorem was established by Chase in 1970 [216], finding general conditions within which no static massless scalar field could be coupled to a static asymptotically flat black hole metric. In a series of papers [217–219], Bekenstein generalized this result to stationary massive scalar, vector and second-rank fields, while the remaining possibilities are known to exist: the Maxwell field of the Kerr-Newman family provides massless vector hair, and the perturbations of a Kerr metric would constitute massless second-rank tensor hair. In 1997, Peña and Sudarsky established one further no-scalar-hair theorem applying to spherically symmetric metric coupled to a complex scalar field [220]:

$$S[g,\Psi] = \int d^4x\sqrt{|g|}\left(\frac{R}{16\pi G_N} - \nabla_\mu\Psi^*\nabla^\mu\Psi^* - \mu^2\Psi^*\Psi\right), \tag{6.2.1}$$

where μ is the scalar field mass.

Only recently, stationary, rotating, asymptotically flat black holes with non-trivial scalar hair were numerically constructed in the model (6.2.1) by evading the assumption that the complex scalar field should also be stationary [221, 222]. In a coordinate system (t, r, θ, ϕ) adapted to stationarity and axisymmetry, the following scalar ansatz was considered:

$$\Psi = \phi(r,\theta)e^{i(m\phi-\omega t)} \tag{6.2.2}$$

where ϕ is a real function, m an integer and ω strictly positive.

It was then crucial to note that such ansatz remains compatible with the assumption of a stationary metric. Indeed, the harmonic time-dependence of the scalar field completely cancel out in the energy-momentum tensor of Ψ, so that the metric could legitimately, and successfully, be constructed in a stationary form, yielding solutions known as "Kerr black holes with scalar-hair" (although the metrics deviate from any member of the Kerr family).

Non-minimally coupled hair Given the strong results of Bekenstein in the framework of GR, scalar hair was also sought within modified theories, i.e. as non-minimally coupled scalar fields. Even in this case, several no-scalar-hair theorems were established. One of the first was formulated by Hawking for stationary black holes in the Brans-Dicke theory [223], earlier defined below equation (5.4.1). Since then, a profusion of no-scalar-hair theorems have been demonstrated in different frameworks [224–227]. In particular, Hawking's no-scalar-hair theorem for Brans-Dicke was extended to the larger family of scalar-tensor theories (5.4.1) by Faraoni and Sotiriou in 2012 in the asymptotically flat case [228, 229]. The reviews [230, 231] cover many of them and techniques used to prove them.

What about the whole class of Horndeski theories (6.1.1)-(6.1.4) rather than the subfamily (5.4.1) ? In 2013, Hui and Nicolis established a no-scalar-hair theorem [232] applying to almost[29] all shift-symmetric Horndeski theories, i.e. theories whose action features the shift-symmetry[30] $\phi \to \phi + constant$. In such models, the scalar field equation actually coincides with the current conservation associated with the shift-symmetry. Contrary to the theorem by Faraoni and Sotiriou, this new theorem only applies to the static and spherically symmetric case (see yet [236] for an extension to slow rotation and [237] for stars).

The existence of such a theorem could have strongly reduced the interest for the black holes of shift-symmetric theories because, ultimately, the attractive feature of hairy solutions is to induce observable deviations from GR[31]. Instead, it was rapidly shown that slightly violating one of the hypotheses of the no-hair theorem [232], namely the stationarity of the scalar field [238], allowed to obtain static and spherically symmetric black holes different from GR solutions [239]. This also suggested that rotating black holes in shift-symmetric theories might significantly deviate from the Kerr solution, which motivated the work reported in part II, the cubic Galileon being shift-symmetric.

More explicitly, the hairy solutions exhibited in [238, 239] showed that such deviations exist in shift-symmetric theory whenever the staticity of the scalar field is replaced by a linear time-dependence:

$$\phi = qt + \Psi(R), \tag{6.2.3}$$

where q is a non-zero constant, t a time coordinate and R a radial coordinate.

The structure (6.2.3) actually arises in a cosmological context from the assumption of a slow cosmological dynamics [240], and it has been considered in several contexts [240–

[29] Important precisions mentioned below were given in [233–235].

[30] This symmetry actually is a remnant of the more general "Galilean" symmetry (6.1.5) enjoyed by the flat Galileons discussed in section 6.

[31] Actually, one could have still been interested in the perturbations of such GR black holes within these modified theories, as they would probably differ from GR despite a common background.

244] due to the following interesting properties. Recall that the scalar field only contributes to the action through its derivatives (hence the shift-symmetry). As a result, the linear time-dependence of (6.2.3) does not bring any actual time-dependence into the action nor the field equations, in which only the constant q appears. This explains why Ansatz (6.2.3) is harmless in regard of instabilities that generically come with ever-growing fields: the perpetual increase with time cannot appear in any physical quantity. Moreover, it is thus rigorously possible for the metric to be static and spherically symmetric, and yet dressed with a scalar field not sharing all these symmetries. Furthermore, the ansatz (6.2.3) does not spoil the self-consistency of the field equations in the static and spherically symmetric case; this means that one is left with as many unknown functions as independent ordinary differential equations [239].

This is in some sort very similar to the trick used to evade Bekenstein's no-scalar-hair theorem mentioned in the beginning of the section, consisting in providing a clever time-dependence to the scalar field, which cancel in the energy-momentum tensor in order to construct stationary rotating black hole metrics. In this former case, the time-dependence had to be harmonic rather than linear. Last but not least, it has been shown for cases where analytical expressions are known [235, 238], that the linear time-dependence (6.2.3) renders the scalar field regular at the event horizon by precisely cancelling out the radial divergence in $\Psi(R)$.

Finally, note that, besides the hairy solutions of references [238, 239], several other cases, constructed by breaking one of the hypotheses of the no-hair theorem [232], were found for different terms of Horndeski theories [233, 234, 245]. Although these hairy solutions are obtained for different higher order Horndeski terms, they can be separated in two generic classes: those in which spacetime is very close to that of GR, characterized by an additional parity symmetry $\phi \leftrightarrow -\phi$ and often dubbed as stealth solutions; and those with no parity symmetry and significant deviations from GR metrics. For the former case, a rotating stealth black hole was recently analytically constructed [246], making use of an analogy with geodesic congruences of Kerr spacetime [106]. In the latter class, on the other hand, belong the Gauss-Bonnet black holes.

Actually, scalar-Gauss-Bonnet theories have been particularly investigated over the last decades. Their action involve the Gauss-Bonnet scalar $\hat{\mathcal{G}}$, which is entirely built from the metric and quadratic in the curvature scalars:

$$\hat{\mathcal{G}} = \mathrm{Riem}_{\alpha\beta\mu\nu}\mathrm{Riem}^{\alpha\beta\mu\nu} - 4\mathrm{Ric}_{\mu\nu}\mathrm{Ric}^{\mu\nu} + R^2. \tag{6.2.4}$$

In four dimensions, this term is a topological invariant, so that it must be coupled to another field to yield non-trivial contributions to the equations of motion. This is why scalar-Gauss-Bonnet theories consider couplings of the form $f(\phi)\hat{\mathcal{G}}$, where f is any non-trivial function of a scalar field. Such theories were shown to belong to Horndeski family [210] and arise in some low-energy effective formulations of string theories [195, 196]. In the latter case, the scalar field is usually called the "dilaton", and $f(\phi) = \alpha \exp(\beta\phi)$ for some constants α, β. Exact static and spherically symmetric hairy black hole solutions of the dilaton model were first studied numerically in [247, 248], and shown to be linearly stable [249, 250]. Rotating generalizations were later constructed in [251, 252]. All these solutions are notably characterized by a minimal mass and secondary hair, meaning that the scalar field is entirely determined by the black hole charges such as mass and angular momentum.

The linear coupling $f(\phi) = \alpha\phi$, for some constant α, is another interesting case.

As $\hat{\mathcal{G}}$ is a topological invariant in four dimensions, the model is shift-symmetric (and comes as the first non-trivial term in the expansion of the dilaton coupling). Yet, the no-hair theorem [232] does not apply to this specific type of shift-symmetric coupling, as was first pointed out in [233]: static and spherically symmetric black holes different from any GR black hole could be explicitly constructed in this shift-symmetric theory [234]. Their rotating generalizations were numerically constructed and studied in [253]. They featured some common properties with the dilaton case, such as the mass gap with respect to Minkowski spacetime.

Actually, the existence of hairy solutions for both the dilaton and shift-symmetric couplings (despite the no-hair theorem in the latter case) is a consequence of the conclusion drawn in reference [254]: under a simple condition on the derivative of the coupling function f at the horizon, asymptotically flat hairy black holes always exist. This was explicitly illustrated in reference [255] for different forms of f, while asymptotically anti-de Sitter hairy solutions were constructed in [256].

6.3 Viability

Well-posedness Through the different works [257–259], Horndeski theories have very recently been proved to admit a well-posed Cauchy problem in so-called modified harmonic coordinates, and under the assumption of weak coupling. As explained in the last article, the latter does not require the fields themselves to be weak, e.g. well-posedness does apply to a large class of black hole formation problems.

Observational constraints As mentioned in the introduction, the gravitational wave detection GW170817 and its electromagnetic counterpart GRB170817A set uptight constraints on the speed of gravitational waves. Consequently, it seems that only restricted families of many modified theories of gravity are explicitly compatible with these constraints, notably within Horndeski theories (it is the case e.g. of sectors (6.1.1) and (6.1.2), whereas (6.1.3) and (6.1.4) would be ruled out) [260–263]. Yet the rigorous interpretation of these constraints involves subtleties which might protect more models from being ruled out than initially thought [264].

Part II

Investigation of cubic Galileon black holes

Chapter 7

The cubic Galileon model

Contents

The cubic Galileon theory is of particular interest among Horndeski theories discussed in chapter 6. For a start, it is the simplest of Galileons with higher order derivatives. It is also well-known for being related to the DGP model (see section 5.3), from which all (flat) Galileon theories originate (see section 6.1). Recall that the DGP model is a 5-dimensional theory of gravity such that all non-gravitational fields are restricted to a 4-dimensional subspace (the usual spacetime), on which gravity is induced by a continuum of massive gravitons. In this framework, the decoupling limit of an effective formulation of gravity on the 4-dimensional spacetime generates a scalar term corresponding to the cubic Galileon action [211, 212]. Actually, this term also arises from Kaluza-Klein compactification of higher dimensional metric theories of gravity (see for example [265, 266]).

On the observational side, the cubic Galileon is compatible with the observed speed of gravitational waves (see the references of section 6.3). Regarding cosmology, the cubic Galileon enters the family of theories featuring "kinetic gravity braiding" [267], which inherit infrared modifications of gravity from the DGP model. These provide self-accelerating scenarios whose cosmological viability has been investigated in several studies, either assuming convergence of the Galileon to a common "tracker" solution [268, 269] or more agnostic scenarios [270–272]. The latter references highlighted strong tensions between the dark energy models of the cubic Galileon and observational data including e.g. the integrated Sachs-Wolfe effect[32]. Note though that the standard ΛCDM model may be recovered in the cubic Galileon, in which case such conclusions do not apply, in particular when the canonical kinetic term is not included.

On the theoretical side, various issues have been tackled within the framework of the cubic Galileon theory or larger theories including it: accretion onto a black hole [241,

[32]This cosmological effect describes the overall redshift caused by large-scale variations of the gravitational potential along photon paths; it is introduced e.g. in chapter 6 of [60].

273], types of coupling to matter [274], laboratory tests [275], cosmological dynamics [242, 244], structure formation [276], stability of cosmological perturbations [277, 278], well-posedness [257–259, 279, 280].

In the present and next two chapters (which correspond to reference [281]), we concentrate on the numerical construction of rotating[33] black holes in the cubic Galileon theory, finding significant deviations from the GR Kerr spacetime. First, the field equations of the cubic Galileon theory are presented in section 7.1. Based on section 6.2, the ansatz used for the scalar field in the rotating case is introduced in section 7.2 along with the circular ansatz used for the metric. The resulting expressions of the field equations and the boundary conditions to impose are respectively exposed in sections 7.3 and 7.4. The numerical setup is presented in chapter 8, while the numerical solutions are analysed in chapter 9.

7.1 Dynamics

The vacuum action of the cubic Galileon involves the Einstein-Hilbert term (with a cosmological constant Λ) and the usual scalar kinetic term for the scalar field ϕ along with an additional nonstandard term:

$$S[g,\phi] = \int d^4x\sqrt{|g|}\left[\zeta(R-2\Lambda) - \eta(\partial\phi)^2 + \gamma(\partial\phi)^2\Box\phi\right], \tag{7.1.1}$$

where $(\partial\phi)^2 \equiv \nabla_\mu\phi\nabla^\mu\phi$, $\Box\phi = \nabla_\mu\nabla^\mu\phi$ and ζ, η and γ are coupling constants.

The non-standard term $(\partial\phi)^2\Box\phi$ realizes a non-minimal coupling with the metric (and the adjective "cubic" comes from the three copies of ϕ present in this term). It is actually known to emerge from the decoupling limit of an effective formulation of the DGP model [211, 212]. As an additional legacy from the DGP model, the cubic Galileon is subject to the Vainshtein mechanism [167, 282], like all Galileon models which were originally designed to possess this property [213]. As mentioned in section 5.3, this mechanism is based on nonlinear terms of the scalar Lagrangian that screen the non-GR degrees of freedom on scales smaller than a certain Vainshtein radius around a spherical matter source. It has been studied in different contexts such as massive gravity [178, 179] and Galileons [283, 284]. For instance in the cubic Galileon theory, the dimension of the Solar System is smaller than the Vainshtein radius of the Sun, below which GR is recovered. Hence in generic situations, local Solar System experiments and PPN methods cannot set constraints on the parameters of the theory [285]. Yet, the Vainshtein mechanism was shown not to hold for black holes [282, 286].

For the case of the cosmological Galileon however, note that there are some subtleties due to kinetic gravity braiding, which is the fact that both scalar and metric equations involve second-derivatives of both g and ϕ in any conformal frame (see for instance cubic Galileon equations (7.1.2) and (7.1.4) below). More precisely, the higher order nature of the Galileon operators, and in particular the presence of curvature in the scalar field equation, can invoke local constraints as explained in the careful analysis of [242]. Yet these are evaded in the framework in which the work exposed below is set, notably due to asymptotic flatness (see sections 7.4 and 9.1.1).

[33] Besides the theoretical interest lying in generalizing the hairy static solutions introduced in section 6.2, recall that the observational importance of rotating black holes comes from the fact that astrophysical black holes are expected to be (rapidly) rotating.

Explicitly, the metric equations in the cubic Galileon theory take the form

$$G_{\mu\nu} + \Lambda g_{\mu\nu} = 8\pi T^{(\phi)}_{\mu\nu} \tag{7.1.2}$$

where

$$\begin{aligned} 8\pi T^{(\phi)}_{\mu\nu} = &\frac{\eta}{\zeta}\left(\partial_\mu\phi\partial_\nu\phi - \frac{1}{2}g_{\mu\nu}(\partial\phi)^2\right) \\ &+ \frac{\gamma}{\zeta}\left(\partial_{(\mu}\phi\partial_{\nu)}(\partial\phi)^2 - \Box\phi\partial_\mu\phi\partial_\nu\phi - \frac{1}{2}g_{\mu\nu}\partial^\rho\phi\partial_\rho[(\partial\phi)^2]\right) \end{aligned} \tag{7.1.3}$$

does contain second derivatives of ϕ.

As mentioned in section 6.2, the scalar field equation actually coincides with the current conservation associated with the shift-symmetry $\phi \to \phi + constant$ of action (7.1.1):

$$\nabla_\mu J^\mu = 0, \tag{7.1.4}$$

where

$$J_\mu = \partial_\mu\phi\left(\gamma\Box\phi - \eta\right) - \frac{\gamma}{2}\partial_\mu\left(\partial\phi\right)^2, \tag{7.1.5}$$

which does generate second derivatives of the metric in (7.1.4).

One can see from the field equations (7.1.2) and (7.1.4) that any solution of vacuum GR along with a constant scalar field[34] is a solution to the cubic Galileon theory (see [287] for general results on the theories featuring this property and their relations with other shift-symmetric theories). The no-scalar-hair theorem [232] introduced in section 6.2 establishes the converse result in the case of an asymptotically flat, static, spherically symmetric black hole metric and a scalar field featuring the same symmetries and a standard kinetic term (i.e. $\eta \neq 0$ in (7.1.1)): under such hypotheses, the solutions to the cubic Galileon theory can only be those of GR with a constant scalar field. The proof, and an extension to the case $\eta = 0$ (relevant for the work presented here, as detailed in section 7.4), are given in appendix A in the restricted case of the cubic Galileon.

Yet, the attractiveness of a given modified theory is to feature deviations away from GR at least in some circumstances, otherwise there would be no interest in studying its black holes. As mentioned in section 6.2, the solutions exhibited in [239] showed that such deviations exist in the cubic Galileon theory whenever the staticity of the scalar field is replaced by a linear time-dependence (6.2.3). This motivated the scalar Ansatz introduced in section 7.2.

7.2 Ansätze and assumptions

The goal is to construct stationary, rotating (i.e. axisymmetric with a non-zero angular velocity), asymptotically flat black hole spacetimes. In addition, a simplifying assumption is made: the spacetime geometric structure is assumed to be circular, or "t, φ-orthogonal" (see [103, 108–110, 112, 288, 289] and references therein for further

[34] This is equivalent to cancel everywhere due to the shift-symmetry of the theory.

details on the statements reported in this section). The accuracy of this hypothesis will be evaluated in section 8.2.

Denoting ξ and χ the Killing vectors associated with stationarity and axisymmetry respectively, circularity amounts to requiring that there exists a coordinate system (t, x^1, x^2, φ) such that $\xi = \partial_t$, $\chi = \partial_\varphi$ and the transformation $(t, \varphi) \mapsto (-t, -\varphi)$ leaves the metric unchanged. This is equivalent to complete integrability of the codistribution $(dt, d\varphi)$, i.e. the existence of a foliation of spacetime by 2-surfaces (called meridional surfaces) everywhere orthogonal to ξ and χ. Using Frobenius theorem, this property takes the form

$$d\xi \wedge \xi \wedge \chi = d\chi \wedge \xi \wedge \chi = 0, \tag{7.2.1}$$

where the vectors are identified with their corresponding 1-form by metric duality.

Since the surfaces of transitivity (i.e. the orbits of the combined actions of ξ and χ) are orthogonal to the meridional surfaces, the metric components (tx^1), (tx^2), (φx^1) and (φx^2) vanish in coordinate systems having the aforementioned properties. A judicious choice of coordinates (x^1, x^2) within the meridional surfaces allows to cancel $g_{x^1x^2}$ as well so that the metric reads[35]

$$ds^2 = -N^2 dt^2 + A^2 \left(dr^2 + r^2 d\theta^2\right) + B^2 r^2 \sin^2\theta \left(d\varphi - \omega dt\right)^2, \tag{7.2.2}$$

where N, A, B and ω are only functions of the coordinates r and θ.

Such a coordinate system is naturally called quasi-isotropic. It can be global for a starlike object, or cover the domain from the horizon to infinity for a black hole spacetime. In the case of spherical symmetry, the four functions only depend on r, while $\omega = 0$ and $A = B$ (so that the coordinates are merely called isotropic).

In a circular spacetime, Ricci-circularity holds, i.e.

$$\mathrm{Ric}(\xi) \wedge \xi \wedge \chi = \mathrm{Ric}(\chi) \wedge \xi \wedge \chi = 0, \tag{7.2.3}$$

where Ric is the Ricci tensor.

In stationary, axisymmetric, asymptotically flat spacetimes, the converse result is true, i.e. (7.2.3) $\Rightarrow$ (7.2.1). Then, within GR, the Einstein equations allow to substitute the Ricci tensor with the energy-momentum tensor T[36], so that an asymptotically flat black hole is circular *iff* the following holds (generalized Papapetrou theorem):

$$T(\xi) \wedge \xi \wedge \chi = T(\chi) \wedge \xi \wedge \chi = 0. \tag{7.2.4}$$

This indicates that circularity may be interpreted in terms of the physical dynamics of matter rather than purely geometric statements. More precisely, the relations (7.2.4) indicate that the source of the gravitational field has purely rotational motion about the symmetry axis and no momentum currents in the meridional planes. Hence assuming circularity is very standard in numerical relativity to handle rapidly rotating stars since such objects have negligible convective meridional flows compared to rotation-induced circulation [290]. For instance, circularity allowed to model rotating proto-neutron stars in GR [291]. In the case of a scalar field, circular rotating boson stars were also constructed numerically [292]. Finally, circularity is very relevant to describe rotating

[35] When such a choice is made, x^1 and x^2 are rather denoted r and θ respectively.

[36] Because one always has $g(\xi) \wedge \xi \wedge \chi = g(\chi) \wedge \xi \wedge \chi = 0$.

black holes: the Kerr solution is circular[37] and numerical metrics of rotating black holes were successfully computed in Einstein-Yang-Mills theory [294, 295] and in the dilatonic Einstein-Gauss-Bonnet theory [251, 252] based on circularity.

Regarding the scalar field, the successful ansatz (6.2.3) is rehashed, with a mere additional angular dependence, in order to connect with the solutions of [239] in the non-rotating limit:

$$\phi = qt + \Psi(r, \theta). \tag{7.2.5}$$

7.3 Equations in quasi-isotropic gauge

Injecting the ansätze (7.2.2) and (7.2.5) into the metric equations (7.1.2) yields eight non-trivial equations rather than ten since the components (r, φ) and (θ, φ) of the three tensors appearing in (7.1.2) all separately vanish. These eight metric equations are combined to form four coupled, independent equations[38] adding to the scalar equation (7.1.4) to solve for the four metric functions N, A, B, ω and the scalar function Ψ.

Every quantity is then made dimensionless using the free parameters of the theory, which are the scalar velocity q, the cosmological constant Λ, the coupling constants ζ, η and γ, and the event horizon radial coordinate $r_{\mathcal{H}}$ (in quasi-isotropic coordinates, the event horizon is always located at a constant radial coordinate):

$$\bar{\Lambda} \equiv \Lambda r_{\mathcal{H}}^2, \qquad \bar{\eta} \equiv -q^2 r_{\mathcal{H}}^2 \frac{\eta}{\zeta}, \qquad \bar{\gamma} \equiv q^3 r_{\mathcal{H}} \frac{\gamma}{\zeta}, \tag{7.3.1}$$

$$\bar{r} \equiv \frac{r}{r_{\mathcal{H}}}, \qquad \bar{\omega} \equiv r_{\mathcal{H}} \omega, \qquad \bar{\Psi} \equiv \frac{\Psi}{q r_{\mathcal{H}}}, \tag{7.3.2}$$

and all the functions are manipulated as functions of $\bar{r}$.

Using the notations

$$\Delta_2 = \partial^2_{\bar{r}\bar{r}} + \frac{1}{\bar{r}} \partial_{\bar{r}} + \frac{1}{\bar{r}^2} \partial^2_{\theta\theta}, \tag{7.3.3}$$

$$\Delta_3 = \partial^2_{\bar{r}\bar{r}} + \frac{2}{\bar{r}} \partial_{\bar{r}} + \frac{1}{\bar{r}^2} \partial^2_{\theta\theta} + \frac{1}{\bar{r}^2 \tan\theta} \partial_\theta, \tag{7.3.4}$$

$$\tilde{\Delta}_3 = \Delta_3 - \frac{1}{\bar{r}^2 \sin^2\theta}, \tag{7.3.5}$$

the four metric equations eventually take the schematic form

$$N^2 \Delta_3 N = \mathcal{S}_N, \tag{7.3.6}$$

$$N^3 \Delta_2 [NA] = \mathcal{S}_A, \tag{7.3.7}$$

$$N^2 \Delta_2 [NB\bar{r} \sin\theta] = \mathcal{S}_B, \tag{7.3.8}$$

$$N \Delta_3 [\bar{\omega} \bar{r} \sin\theta] = \mathcal{S}_{\bar{\omega}}, \tag{7.3.9}$$

where the explicit expressions of the right-hand side terms and the steps to derive them are presented in appendix B.

[37] The corresponding expressions of the metric functions N, A, B and ω (and the transformation from the usual Boyer-Lindquist coordinates to quasi-isotropic coordinates) are given in appendix C; reference [293] may also be consulted.

[38] These combinations of the equations (displayed below and in appendix B) are generically used in GR as they feature classical elliptic operators, well-suited for iterative numerical methods.

Once again, recall that the cubic Galileon theory features the shift-symmetry $\phi \to \phi + constant$, meaning that only the first derivatives of ϕ are physically meaningful. The numerical approach presented in section 8 below concretely makes use of this fact: within the numerical code, the scalar field is only manipulated through its first derivatives $\bar{\Psi}' \equiv \partial_{\bar{r}}\bar{\Psi}$ and $\bar{\Psi}_\theta \equiv \partial_\theta \bar{\Psi}$. More precisely, $\bar{\Psi}'$ and $\bar{\Psi}_\theta$ are first introduced as independent functions, just like N, A, B and $\bar{\omega}$. The fact that these functions actually arise from a common scalar field is then implemented through imposing $\partial_\theta \bar{\Psi}' = \partial_{\bar{r}}\bar{\Psi}_\theta$ (symmetry of second-derivatives) in addition to the equations {(7.3.6)−(7.3.9), (7.1.4)}.

The complete set of equations to solve then is

$$N^2\Delta_3 N = \mathcal{S}_N, \tag{7.3.10}$$
$$N^3\Delta_2[NA] = \mathcal{S}_A, \tag{7.3.11}$$
$$N^2\Delta_2[NB\bar{r}\sin\theta] = \mathcal{S}_B, \tag{7.3.12}$$
$$N\Delta_3[\bar{\omega}\bar{r}\sin\theta] = \mathcal{S}_{\bar{\omega}}, \tag{7.3.13}$$
$$\partial_\theta \bar{\Psi}' = \partial_{\bar{r}}\bar{\Psi}_\theta, \tag{7.3.14}$$
$$\nabla_\mu \bar{J}^\mu = 0, \tag{7.3.15}$$

where the explicit expression of the scalar equation (7.3.15) is also given in appendix B.

Of course, if a circular black hole exists in the cubic Galileon theory, then it satisfies the system (7.3.10)-(7.3.15). But any solution to this system does not necessarily satisfy all the metric equations of motion (7.1.2) since only four independent combinations of the latter are solved instead of eight. Hence each numerical solution to (7.3.10)-(7.3.15) was reinjected into the whole set of metric equations (7.1.2) to assess the relevance of the circularity hypothesis a posteriori (see section 8.2).

7.4 Boundary conditions

Equations (7.3.10)-(7.3.15) form a system of first (equation (7.3.14)) and second order coupled partial differential equations (PDE) involving the six functions N, A, B, $\bar{\omega}$, $\bar{\Psi}'$ and $\bar{\Psi}_\theta$. It must then be provided with boundary conditions suitable for the search for black hole solutions with non-trivial scalar hair. More precisely, the system is defined on a meridional surface (all of them are equivalent due to circularity) between the intersections of the latter with the black hole event horizon and spacetime infinity. As mentioned in section 7.3, the event horizon is located at $\bar{r} = 1$, while spacetime infinity corresponds with the limit $\bar{r} \to \infty$. Boundary conditions must then be prescribed for both limits.

First, in quasi-isotropic coordinates, the function N must vanish on the event horizon (see for instance [293] for the case of Kerr). This induces an important alteration of the nature of the equations (7.3.10)-(7.3.13) since all the second-order operators acting on the metric functions thus cancel at $\bar{r} = 1$. This kind of degeneracy actually reduces the required number of boundary conditions.

The other crucial condition at the horizon is the value of the function $\bar{\omega}$. The weak rigidity theorem states the existence of a constant $\Omega_\mathcal{H}$ such that $\xi + \Omega_\mathcal{H}\chi$ is (a Killing vector field) normal to the horizon [103, 109, 110]. On the horizon, the function $\bar{\omega}$ necessarily equals the constant $\bar{\Omega}_\mathcal{H} \equiv r_\mathcal{H}\Omega_\mathcal{H}$, called the dimensionless angular velocity of the horizon.

Regarding conditions at infinity, the only case considered in the present work is asymptotic flatness. This is not meant to fit with observations of the Universe based on which a small positive value is credited to an effective cosmological constant, which is usually modelled by asymptotically de Sitter models such as the dark energy scenarios of the Galileons mentioned in the introduction. Rather, the prime objective here is to construct the strong-field region of rotating black holes in the simplest Galileon with higher-order derivatives. This actually prepares for the investigation of their geodesics in chapter 11 and the imaging of an emitting accretion torus surrounding them in chapter 12, which concerns scales much smaller than a potential cosmological horizon. Furthermore, asymptotic flatness is a standard hypothesis made to study isolated black holes and establish no-hair theorems [228]. In particular, it leads to construct hairy black holes that escape the no-hair theorem of [232] in a minimal way.

Yet, in the cubic Galileon theory, imposing asymptotic flatness in static and spherical symmetry is incompatible with Ansatz (6.2.3) unless $\eta = \Lambda = 0$. To picture this, it is easier to consider the Schwarzschild-like coordinates (t, R, θ, φ) used in [239], with respect to which the static and spherically symmetric line element takes the form

$$ds^2 = -h(R)dt^2 + \frac{1}{f(R)}dR^2 + R^2\left(d\theta^2 + \sin^2\theta d\varphi^2\right). \tag{7.4.1}$$

Using the scalar ansatz (6.2.3), all the relevant equations are the following (the (tR) equation[39], a combination of the (tR) and (RR) equations, and a combination of the (tR), (RR) and (tt) equations respectively):

$$\gamma(R^4h)'fh\Psi'^2 - \gamma q^2R^4h' - 2\eta R^4h^2\Psi' = 0, \tag{7.4.2}$$

$$\frac{\eta}{2\zeta}(fh\Psi'^2 - q^2) + \frac{fh'}{R} + h\left(\frac{f-1}{R^2} + \Lambda\right) = 0, \tag{7.4.3}$$

$$f\Psi'^2\left[\eta R^2\sqrt{\frac{h}{f}} - \gamma\left(R^2\sqrt{fh}\Psi'\right)'\right] = 2\zeta Rh\left(\sqrt{\frac{f}{h}}\right)', \tag{7.4.4}$$

where a prime denotes differentiation with respect to the unique variable R.

As mentioned in section 6.2, one can note that the Schwarzschild-(Anti-)de Sitter metric along with $\Psi' = 0$ and $q = 0$ (i.e. $\phi = constant$) must be a solution to the system (7.4.2)-(7.4.4) since it is a static and spherically symmetric vacuum solution of GR:

$$h(R) = f(R) = 1 - \frac{\mu}{R} - \frac{\Lambda}{3}R^2, \tag{7.4.5}$$

where μ appears as an integration constant

According to [239], injecting asymptotic expansions in powers of $1/R$ for h, f and Ψ into (7.4.2)-(7.4.4) yields the following asymptotic behaviours if $\eta \neq 0$:

$$h(R) = -\frac{\Lambda_{\text{eff}}}{3}R^2 + 1 + O\left(\frac{1}{R}\right), \tag{7.4.6}$$

$$f(R) = -\frac{\Lambda_{\text{eff}}}{3}R^2 + c + O\left(\frac{1}{R}\right), \tag{7.4.7}$$

$$h(R)\Psi'(R) = \frac{\eta R}{3\gamma} + \frac{c'}{R} + O\left(\frac{1}{R^2}\right), \tag{7.4.8}$$

[39] In this context, the (tR) equation implies the scalar equation [239].

where c and c' are some fixed constants and Λ_{eff} is an effective cosmological constant made from a combination of the bare cosmological constant Λ and the kinetic coupling η.

Therefore, if $\Lambda_{\text{eff}} \neq 0$, spacetime is asymptotically (anti-)de Sitter. Asymptotic flatness thus requires $\Lambda_{\text{eff}} = 0$, which is impossible whenever $\eta \neq 0$ (see the relations (4.10) of [239]). Then, setting η to 0 in (7.4.3) yields

$$f\left(\frac{h'}{Rh} + \frac{1}{R^2}\right) = \frac{1}{R^2} - \Lambda, \tag{7.4.9}$$

while asymptotic flatness (i.e. vanishing Riemann tensor when $R \to \infty$) requires the following asymptotic behaviours:

$$\frac{h'}{h} = o\left(\frac{1}{R}\right), \tag{7.4.10}$$

$$f \longrightarrow 1, \tag{7.4.11}$$

so that Λ must be 0 as well as η.

As mentioned in section 6.2, it is shown in appendix A that, for the cubic Galileon, the no-hair theorem still holds if $\eta = 0$. Therefore, the asymptotically flat, static, spherically symmetric hairy solutions constructed in [239] with $\eta = \Lambda = 0$ evade the no-hair theorem in a minimal fashion since only the staticity of the scalar field is abandoned.

It is reasonable to think that asymptotic flatness requires vanishing η and Λ even in the rotating case, although there is no proof of such a claim. Regardless of the actual answer, η and Λ are set to zero in the numerical work exposed here in order to connect with the solutions of [239] in the non-rotating limit.

Chapter 8

Numerical treatment

Contents

This chapter briefly introduces the numerical method used to solve the PDE system (7.3.10)-(7.3.15), and discusses the validity of the numerical solutions that will be presented in chapter 9 in regard of the circularity assumption (7.2.1).

8.1 Spectral methods and Newton-Raphson algorithm

The numerical approach to solve the problem (7.3.10)-(7.3.15) comprises two steps implemented within the library *Kadath*[40] [296]. First, the system is discretized within the framework of spectral methods. This amounts to projecting each function N, A, B, $\bar{\omega}$, $\bar{\Psi}'$ and $\bar{\Psi}_\theta$ onto a set of basis functions defined as the products of (Legendre or Chebyshev) polynomials T_i with trigonometric functions, e.g. for the function A:

$$A(r,\theta) = \sum_{i=0}^{m_r} \sum_{j=0}^{m_\theta} \tilde{A}_{ij} T_i(r) \cos(2j\theta), \tag{8.1.1}$$

where m_r and m_θ are integers defining the resolution of the discretization[41]. All the information about the unknown function A is then encoded into the spectral coefficients $\tilde{A}_{ij}$. Moreover, the projection of any of its partial derivative is also given in terms of these coefficients. Applying this procedure to each unknown function N, A, B, $\bar{\omega}$, $\bar{\Psi}'$ and $\bar{\Psi}_\theta$ in the system (7.3.10)-(7.3.15) transforms the latter into a nonlinear algebraic system S, whose unknowns are suitable combinations of the spectral coefficients ensuring regularity conditions [296].

Secondly, the discretized system S is solved with a Newton-Raphson algorithm. The vector $\tilde{X}$ gathering all the relevant combinations of the spectral coefficients should satisfy

$$S(\tilde{X}) = 0. \tag{8.1.2}$$

[40] https://kadath.obspm.fr/

[41] For class C^∞ functions, the convergence of the spectral series towards the original function is exponential in the resolution.

Starting with an initial guess $\tilde{X}^{(0)}$ and denoting $\tilde{X}^{(n)}$ the vector gathering the coefficients at step n, $\tilde{X}^{(n+1)}$ is built as the solution to

$$S(\tilde{X}^{(n)}) + dS_{\tilde{X}^{(n)}}(\tilde{X}^{(n+1)} - \tilde{X}^{(n)}) = 0, \tag{8.1.3}$$

which requires inverting the Jacobian matrix $dS_{\tilde{X}^{(n)}}$.

Under appropriate conditions, such an iterative process converges towards the exact solution of S. In particular, a good initial guess is an important condition of success. This merely means that the closest to the exact solution the process starts, the more chance it has to converge to the solution (while starting too far away from it induces risks to leave the neighbourhood of the solution after a few iterations and eventually diverge). This is the reason why the existence of the static and spherically symmetric black hole solutions of [239] is particularly useful since reconstructing these solutions numerically (for a fixed choice of the coupling constants) provides ideal initial guesses to reach slowly rotating solutions, which in turn serve as initial guesses to reach slighlty more rapidly rotating solutions and so on.

Finally, let us mention that, in the rotating cases, an additional condition was implemented in order to avoid a conical singularity [288]. It consists in imposing $A = B$ on the symmetry axis $\theta = 0, \pi/2$[42], which guarantees that the metric could be regularly well-defined on an open chart containing the axis. For instance, this condition was also imposed in [251, 252] to construct rotating black holes in the dilatonic Einstein-Gauss-Bonnet theory, but for rotating bosons stars [292], the field equations alone imply $A = B$ on the symmetry axis.

8.2 Accuracy of the code

As explained in section 7.3, all the numerical solutions to the system (7.3.10)-(7.3.15) were reinjected into the whole set of metric equations (7.1.2) in order to assess the validity of the code. Writing the metric equations (7.1.2) as $E_{\mu\nu} = 0$, the error on each equation corresponds to its maximum spectral coefficent (in absolute value). Six out of the eight non-trivial[43] metric equations feature a fast decrease of the error as the resolution increases, which confirms that these equations are properly solved numerically. Figure 8.1a illustrates this fact in the case of equation $E_{r\theta}$ for various angular velocities at fixed coupling $\bar{\gamma} = 1$.

On the other hand, the error on the two metric equations E_{tr} and $E_{t\theta}$ is independent of the resolution, as illustrated on Fig 8.1b, revealing that there exists an actual violation of non-numerical origin. The cause of this violation can be identified a bit more precisely. In quasi-isotropic coordinates, the components (tr) and $(t\theta)$ of both the metric and Ricci tensors are zero. As a result, the metric equations $E_{tr} = E_{t\theta} = 0$ reduce to $T^{(\phi)}_{tr} = T^{(\phi)}_{t\theta} = 0$. Actually, these last two equations coincide with the two non-trivial circularity conditions provided by the generalized Papapetrou theorem (7.2.4). The latter can be applied to $T^{(\phi)}$ because the metric equations $E_{\mu\nu} = 0$ have an Einstein-like structure.

[42] In the static and spherically symmetric cases, A spontaneously equals to B everywhere (as it should in spherical symmetry) through the numerical process without being imposed anywhere.

[43] See section 7.3.

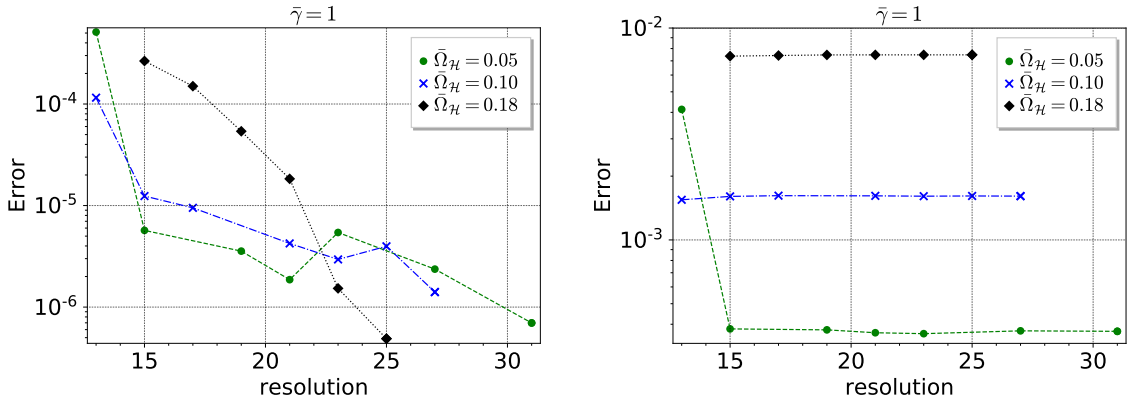

(a) Validation of equation $E_{r\theta}$ (the error decreases with the resolution).

(b) Violation of equation E_{tr} (the error is independent of the resolution).

Figure 8.1: Errors on the metric equations with respect to the resolution $m_r = m_\theta$. The error is measured in horizon units ($\bar{r} = 1$).

This yields

$$\left(T^{(\phi)}(\partial_t) \wedge \partial_t \wedge \partial_\varphi\right)_{tr\varphi} = T^{(\phi)}_{t[t}\,(\partial_t)_r\,(\partial_\varphi)_{\varphi]} \propto T^{(\phi)}_{tr}, \tag{8.2.1}$$

$$\left(T^{(\phi)}(\partial_t) \wedge \partial_t \wedge \partial_\varphi\right)_{t\theta\varphi} = T^{(\phi)}_{t[t}\,(\partial_t)_\theta\,(\partial_\varphi)_{\varphi]} \propto T^{(\phi)}_{t\theta}. \tag{8.2.2}$$

Therefore the errors on E_{tr} and $E_{t\theta}$ estimate the validity of the circularity hypothesis. More precisely, in the expression (7.1.3) of $T^{(\phi)}_{tr}$ (resp. $T^{(\phi)}_{t\theta}$), the only non-trivial terms are those proportional to $\partial_t\phi\partial_r\phi$ (resp. $\partial_t\phi\partial_\theta\phi$) and $\partial_{(t}\phi\partial_{r)}(\partial\phi)^2$ (resp. $\partial_{(t}\phi\partial_{\theta)}(\partial\phi)^2$) which are non-zero only if ϕ depends on both t and r (resp. t and θ). This means that non-circularity is caused by combined time and radial, or time and angular, dependences of the scalar field. Yet, the ansatz (6.2.3) used in [239] to derive static and spherically symmetric solutions does feature both time and radial dependences. But these solutions were obtained taking advantage of the fact that E_{tR} (in the Schwarzschild-like coordinates (7.4.1)) implies the scalar equation. Thus, solving $E_{tR} = 0$ instead of the scalar equation automatically fulfilled the circularity condition (8.2.1) since $E_{tR} \propto T^{(\phi)}_{tR} \propto T^{(\phi)}_{tr}$ (where the last relation holds because the transformation (9.2.8) from Schwarzschild-like coordinates to quasi-isotropic coordinates relates only the coordinates R and r in spherical symmetry).

But as soon as one looks for rotating solutions and thus adds an angular dependence to all functions, including the scalar field according to the ansatz (7.2.5), the equations are too complex to benefit from a similar simplification. Therefore the system (7.3.10)-(7.3.15) based on the circular metric (7.2.2) and the ansatz (7.2.5) is not exactly self-consistent. Yet, the violation of circularity in the dimensionless setup is less than 10^{-2}, meaning that it is fairly small with respect to the scale given by the radial coordinate $r_{\mathcal{H}}$ of the event horizon in a dimensional physical configuration. In addition, Fig 8.1b expectedly confirms that the violation continuously goes to zero with the angular velocity (since in this limit the solutions are exactly circular), so that it seems reasonable to believe that the solutions presented in the next sections still provide precise approximations to rotating black hole solutions of the cubic Galileon theory.

Chapter 9

Black hole solutions

Contents

In this chapter, the numerical configurations of asymptotically flat rotating black holes in the cubic Galileon theory are presented. These black holes are endowed with a non-trivial scalar field and exhibit a non-Schwarzschild behaviour: faster than $1/r$ convergence to Minkowski spacetime at spatial infinity and hence vanishing of the Komar mass. The metrics are compared with the Kerr metric for various couplings and angular velocities. Their physical properties are extracted and show significant deviations from the Kerr case.

9.1 Metric functions

9.1.1 Static and spherically symmetric black holes

First, the existing static, spherically symmetric black hole solutions reported in [239] have been reconstructed in the quasi-isotropic gauge (instead of the Schwarzschild-like coordinates used in [239]) in order to later serve as initial guesses to compute rotating solutions. As mentioned in 6.2, these solutions were obtained in [239] by numerical integration of the ordinary differential equations (7.4.2) – (7.4.4). In addition, the value of h' was prescribed at the horizon in order to obtain the desired asymptotic behaviour (shooting method). In the present work, these solutions are generated with the numerical treatment presented in section 8, i.e. as solutions to the PDE system (7.3.10)-(7.3.15). In addition, boundary conditions are prescribed both at infinity and at the horizon; in particular, staticity is imposed by setting the dimensionless angular velocity $\bar{\Omega}_{\mathcal{H}}$ to zero. The resulting numerical solutions feature spherical symmetry ($A = B$, $\bar{\omega} = 0$ everywhere, and no angular dependence) although such symmetry is not imposed anywhere in the numerical process.

As explained in section 8, the numerical process requires initial guesses. Conveniently, the test-field solution given in [239] (relations (4.12)-(4.13)) provides the very first of them. This configuration merely comes out from solving the scalar equation (7.1.4) on a Schwarzschild background metric with the scalar ansatz (6.2.3), which physically

amounts to neglecting the back-reaction of the scalar field onto the metric, i.e. taking the limit $\gamma \to 0$ (η being already set to zero).

Actually, only the expression of Ψ' is given for this test-field solution:

$$\Psi'(R) = \frac{\pm q}{\left(1 - \frac{R_H}{R}\right)\sqrt{\frac{4R}{R_H} - 3}}, \tag{9.1.1}$$

where R_H is the Schwarzschild radius. As stated earlier, this is sufficient because, due to the shift-symmetry of the theory, only the first derivatives of ϕ are meaningful (and hence only Ψ' in static and spherical symmetry).

One can see from the action (7.1.1) that flipping the sign of both γ and ϕ of a given solution provides another solution to the theory. This fact holds true in the limit $\gamma \to 0$, which is why equation (9.1.1) offers two test-field solutions with opposite signs. Moreover, it is thus sufficient to seek solutions for positive γ only.

Once the Schwarzschild metric and the test scalar field (9.1.1) are reexpressed in terms of the quasi-isotropic coordinates, the numerical process may converge to a solution of the system (7.3.10)-(7.3.15) in which the coupling $\bar{\gamma}$ is set to a slightly non-zero value. In turn, such solution serves as an initial guess to reach a solution with a slightly greater coupling $\bar{\gamma}$ and so on. Note that due to the Vainshtein mechanism (see section 7.1) and the absence of kinetic term (see section 7.4), no constraint can be inferred on the values of the parameters of the problem either from Solar System tests or cosmological arguments. Therefore the values of $\bar{\gamma}$ picked for the graphs displayed in the present and later sections are only chosen so as to highlight with sufficient clarity how the results depend on $\bar{\gamma}$.

The resulting solutions are displayed in figure 9.1. Due to spherical symmetry, one has $B = A$, $\bar{\omega} = 0$ and $\bar{\Psi}_\theta = 0$ everywhere, so that only the radial profiles of N, A and $\bar{\Psi}'$ are non-trivial. Actually, $Z \equiv N\bar{\Psi}'$ is plotted instead of $\bar{\Psi}'$ because the former is finite on the horizon contrary to the latter.

For the function N (figure 9.1a), the boundary values $N = 0$ at the horizon and $N = 1$ at infinity are enforced according to section 7.4. On the contrary, the values of A and Z on the horizon are not imposed due to the degeneracy of the equations. Yet, it can be seen from the right-hand side (B.6) of equation (7.3.11) that this degeneracy spontaneously imposes $A^2 = Z^2$ on the horizon, which is manifest on figures 9.1b and 9.1c (and confirmed numerically).

One can also note that the greater the coupling $\bar{\gamma}$ is, the faster the funtions N, A and Z converge towards their respective limits which correspond to a flat spacetime. Then, when travelling from the horizon towards infinity, spacetime looks flat more rapidly for stronger coupling values $\bar{\gamma}$. In other terms, the more the scalar field back-reacts on the metric, the more it hides the deformations induced by the black hole. This fact is further examined in section 9.2.1 below when discussing the extraction of a mass for these black hole solutions.

9.1.2 Rotating black holes

The Kerr metric is usually parametrized by two parameters M (the mass) and a (the reduced angular momentum). The radial coordinate $r_{\mathcal{H}}$ of the event horizon may then

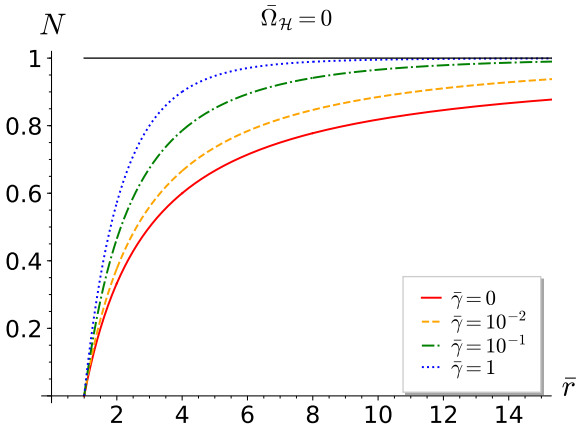

(a) Metric function N

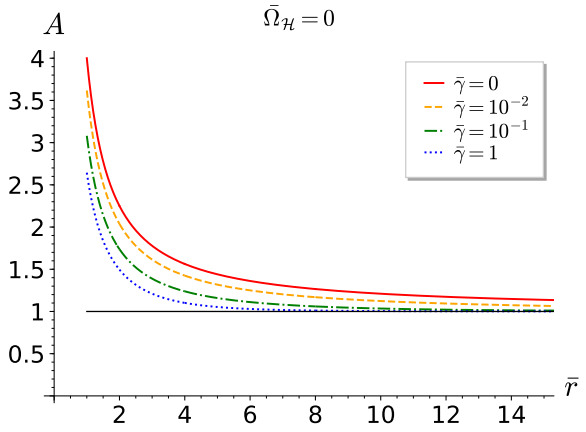

(b) Metric function A

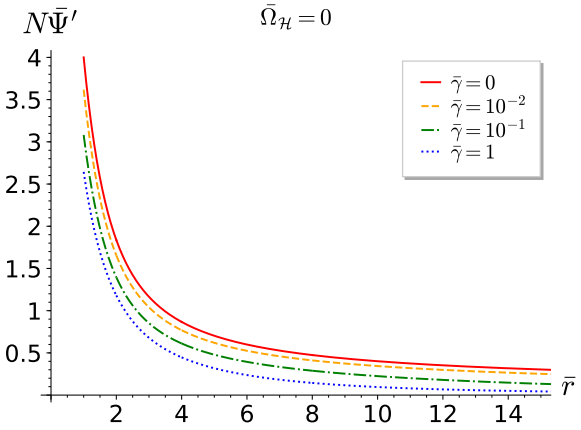

(c) Regular scalar radial derivative $Z \equiv N\bar{\Psi}'$

Figure 9.1: Radial profiles in the static and spherically symmetric case ($\bar{\Omega}_{\mathcal{H}} = 0$) for values of $\bar{\gamma}$ ranging from 0 to 1. When it is not zero, the limit at infinity is represented by a black, solid, horizontal asymptote.

be expressed in terms of these two parameters:

$$r_{\mathcal{H}} = \frac{M}{2}\sqrt{1-\left(\frac{a}{M}\right)^2}. \tag{9.1.2}$$

Once $r_{\mathcal{H}}$ is used to make all the quantities dimensionless and all the metric components are expressed in terms of $\bar{r} \equiv r/r_{\mathcal{H}}$, the dimensionless Kerr solution is only parametrized by one quantity, which can be chosen to be $\bar{\Omega}_{\mathcal{H}}$. Of course, one such quantity might not be enough to parametrize the whole set of black hole solutions of the cubic Galileon theory with a scalar field structured as (7.2.5). Yet, the numerical approach employed here only reaches the solutions that continuously connect to Schwarzschild, by increasing $\bar{\gamma}$ first and then $\bar{\Omega}_{\mathcal{H}}$. This is why, once $\bar{\gamma}$ is fixed, $\bar{\Omega}_{\mathcal{H}}$ is also the only quantity that parametrizes the solutions presented here.

Figure 9.2 displays the radial profiles of all six functions N, A, B, $\bar{\omega}$, $\bar{\Psi}'$ and $\bar{\Psi}_\theta$ at fixed $\bar{\gamma} = 1$ for various values of $\bar{\Omega}_{\mathcal{H}}$. For $\bar{\Omega}_{\mathcal{H}} = 0$ and 0.07, the corresponding dimensionless Kerr solution is plotted for comparison: in the case of N, A and B, the Kerr curve has the same color and linestyle as the Galileon curve corresponding to the same parameter $\bar{\Omega}_{\mathcal{H}}$, and in the case of $\bar{\omega}$, it is the thick dotted curve having the same value at the horizon with its Galileon analog. As for Z and $\bar{\Psi}_\theta$, no Kerr analog is displayed since no test-field solutions are known in the rotating case (i.e. solutions to the scalar equation (7.1.4) on a Kerr background with the scalar ansatz (7.2.5)) and such solutions could not be obtained numerically.

For the other values of $\bar{\Omega}_{\mathcal{H}}$ (0.12 and 0.18), the Galileon solutions displayed in figure 9.2 do not admit a Kerr analog. The reason is that the cubic Galileon admits solutions with dimensionless angular velocities greater than the maximum $\bar{\Omega}_{\mathcal{H}}$ that can be obtained from the Kerr metric. More precisely, at fixed mass M, the angular velocity $\Omega_{\mathcal{H}}$ of the Kerr black hole cancels at $a/M = 0$ and monotonically increases towards a finite value at $a/M = 1$, while the radial quasi-isotropic coordinate $r_{\mathcal{H}}$ of the event horizon is finite at $a/M = 0$ and monotonically decreases towards 0 at $a/M = 1$ according to equation (9.1.2). Then, $\bar{\Omega}_{\mathcal{H}} = r_{\mathcal{H}}\Omega_{\mathcal{H}}$ is a positive function of the dimensionless ratio $a/M \in [0,1]$ cancelling both at 0 and 1:

$$\bar{\Omega}_{\mathcal{H}} = \frac{1}{4}\frac{\frac{a}{M}}{1+\left(1-\left(\frac{a}{M}\right)^2\right)^{-\frac{1}{2}}}, \tag{9.1.3}$$

which is plotted on figure 9.3. In particular, this function has a maximum value $\bar{\Omega}_{\mathcal{H},\max} \simeq 0.075$ at $a/M \simeq 0.8$, which actually turns out to be possible to exceed in the cubic Galileon theory. This will appear clearly in section 9.2 when extracting the angular momentum and the surface gravity of these black hole solutions.

Going back to figure 9.2, one first notes that, although the global behaviours are the same, there are non-negligible gaps near the horizon between the Galileon solution and Kerr for any fixed dimensionless angular velocity. Naturally, for both the Galileon and Kerr, increasing $\bar{\Omega}_{\mathcal{H}}$ tends to slow the convergence towards the asymptotic values (at fixed radial coordinate, it is expected that spacetime looks less flat if the hole is rotating). One last remark to make is that, although these solutions feature quite rapid rotation ($\bar{\Omega}_{\mathcal{H}} = 0.07$ corresponds to $a/M \simeq 0.65$ for Kerr), the angular variations of the various functions are quite moderate for both the Galileon and Kerr; this is manifest on figure 9.4 which displays the angular profile of the function A on the horizon.

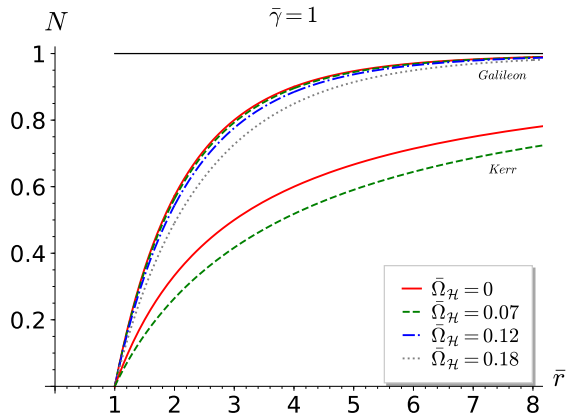

(a) Metric function N at $\theta = \pi/2$

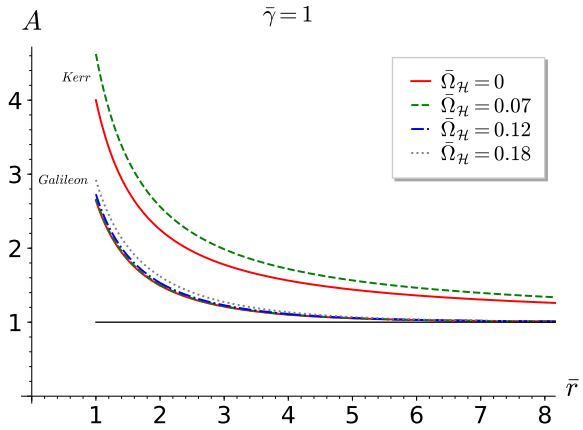

(b) Metric function A at $\theta = \pi/2$

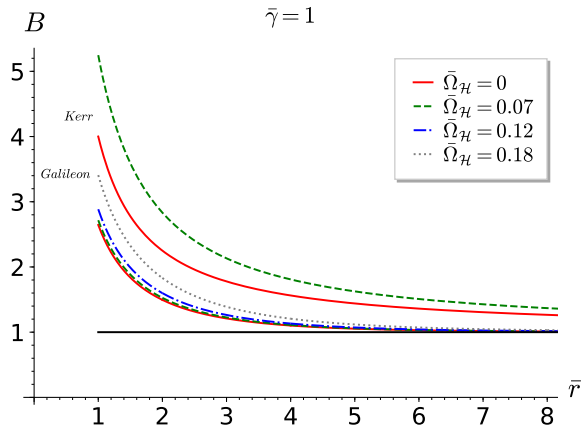

(c) Metric function B at $\theta = \pi/2$

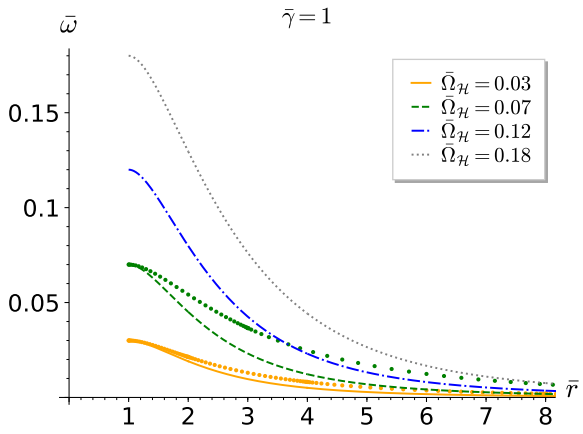

(d) Metric function $\bar{\omega}$ at $\theta = \pi/2$

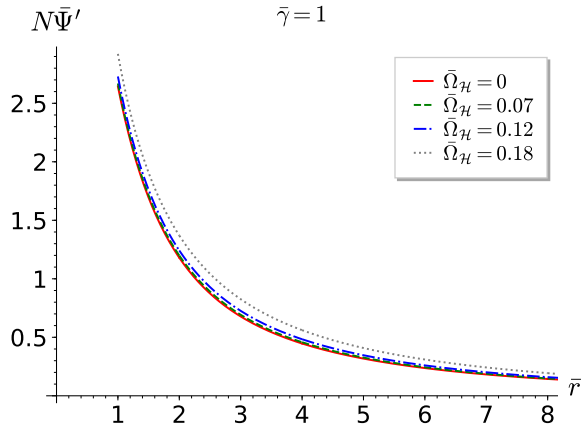

(e) Regular scalar radial derivative $Z \equiv N\bar{\Psi}'$ at $\theta = \pi/2$

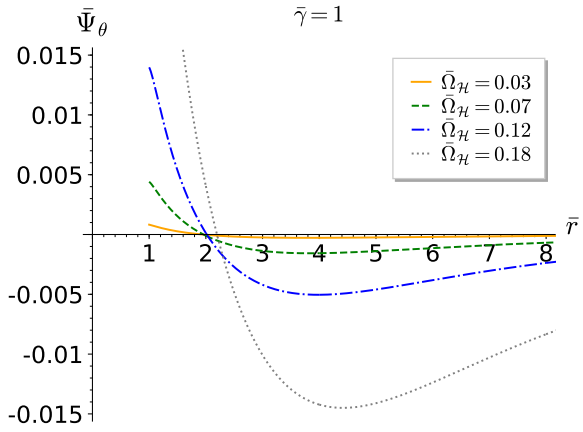

(f) Scalar angular derivative $\bar{\Psi}_\theta$ at $\theta = \pi/4$

Figure 9.2: Radial profiles at fixed coupling $\bar{\gamma} = 1$ and different $\bar{\Omega}_{\mathcal{H}}$. When it is not zero, the limit at infinity is represented by a black, solid, horizontal asymptote.

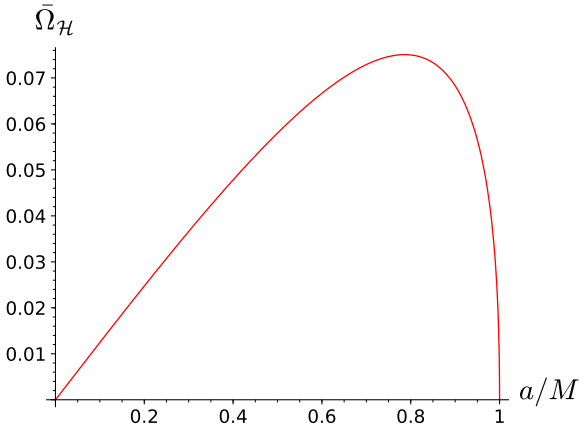

Figure 9.3: $\bar{\Omega}_{\mathcal{H}}$ with respect to a/M for Kerr black holes.

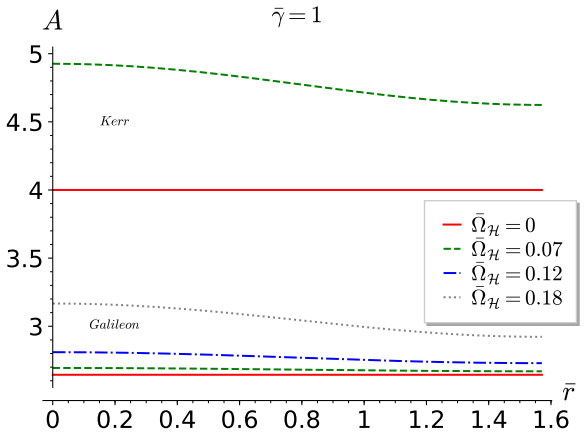

Figure 9.4: Angular profile of A at the horizon.

9.2 Physical properties

9.2.1 Mass

The general definition of the Komar mass of an asymptotically flat stationary spacetime, equipped with a foliation $(\Sigma_t)_{t\in\mathbb{R}}$ by spacelike hypersurfaces, is [94, 288]

$$M_{\text{Komar}} \equiv -\frac{1}{8\pi}\int_{\mathcal{S}} *d\xi, \tag{9.2.1}$$

where ξ is the stationary Killing vector here identified with its metric dual form, $*$ is the Hodge star and $\mathcal{S} \subset \Sigma_{t_0}$ (for some $t_0 \in \mathbb{R}$) is a closed spacelike 2-surface containing the intersection of Σ_{t_0} with the support of the energy-momentum tensor. In GR, the Einstein equations guarantee that the Komar mass does not depend on the choice of such 2-surface $\mathcal{S}$.

In practice, one then usually uses a 2-surface $\mathcal{S}$ lying at spatial infinity. In particular, in quasi-isotropic coordinates, the Komar mass may be computed from the following integral:

$$M_{\text{Komar}} = \frac{1}{2}\lim_{r\to\infty}\int_0^\pi \partial_r N\; r^2 \sin\theta d\theta. \tag{9.2.2}$$

Therefore, if N has the following asymptotic behaviour:

$$N = 1 + \frac{N_1}{r} + o\left(\frac{1}{r}\right), \tag{9.2.3}$$

where N_1 is a constant, then

$$M_{\text{Komar}} = -N_1. \tag{9.2.4}$$

In the cubic Galileon theory, the contribution from the scalar field into equation (7.1.2) does not allow to guarantee that the expression (9.2.1) is independent of the 2-surface $\mathcal{S}$. Yet, as is usually done, one may try to extract a mass from the relation (9.2.4). This can be done explicitly in the static and spherically symmetric case.

To do so, it is simpler to first switch back to the Schwarzschild-like coordinates (7.4.1) used in section 7.4 to extract the asymptotic behaviours (7.4.6)-(7.4.8) when $\eta \neq 0$. Repeating the same procedure in the case of asymptotic flatness, i.e. injecting expansions in $1/R$ into (7.4.2)-(7.4.4) with $\eta = \Lambda = 0$, one finds the following asymptotic behaviours:

$$h(R)\Psi'(R) = \frac{d}{R^2} + O\left(\frac{1}{R^5}\right), \tag{9.2.5}$$

$$h(R) = 1 - \frac{d^2}{q^2R^4} + O\left(\frac{1}{R^7}\right), \tag{9.2.6}$$

$$f(R) = 1 - \frac{4d^2}{q^2R^4} + O\left(\frac{1}{R^7}\right), \tag{9.2.7}$$

where d is some fixed constant. Note here that the test field approximation (9.1.1) gives a wrong indication about the asymptotic behavior of $\Psi'(R)$ since it behaves as $1/\sqrt{R}$

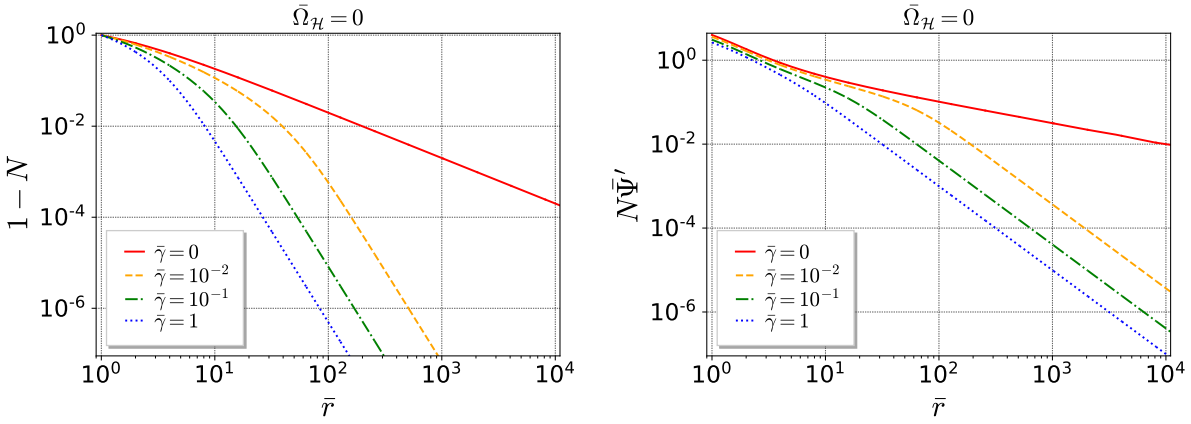

(a) log-log graph of $1 - N$.

(b) log-log graph of $Z \equiv N\bar{\Psi}'$.

Figure 9.5: Asymptotic behaviours in the static and spherically symmetric case.

although, according to equation (9.2.5), it behaves as $1/R^2$ as soon as the coupling γ is non-zero, no matter how small. Yet this did not prevent the test-field solution from being useful as an initial guess in the numerical procedure.

Now, the change of coordinates from the Schwarzschild-like coordinates (t, R, θ, φ) to the quasi-isotropic coordinates (t, r, θ, φ) is merely given by the positive function $R(r)$ defined on $[r_{\mathcal{H}}, +\infty)$ such that

$$rR'(r) = R(r)\sqrt{f\left(R(r)\right)}. \tag{9.2.8}$$

From this, one can infer the same types of asymptotic behaviours as (9.2.5)-(9.2.7) for the functions Z, N and A:

$$Z(r) = \frac{e}{r^2} + o\left(\frac{1}{r^2}\right), \tag{9.2.9}$$

$$N(r) = 1 + \frac{e'}{r^4} + o\left(\frac{1}{r^4}\right), \tag{9.2.10}$$

$$A(r) = 1 + \frac{e''}{r^4} + o\left(\frac{1}{r^4}\right), \tag{9.2.11}$$

where e, e' and e'' are some fixed constants.

One concludes that there is no term to the first inverse power of r in the expansion (9.2.10) of N, meaning that the Komar mass is zero according to the relation (9.2.4). This fact may be checked numerically by extracting the asymptotic slope of $1 - N$ in a log-log graph (figure 9.5a), which corresponds to the asymptotically dominant power of r; the resulting numerical value is perfectly consistent with -4. The function $A - 1$ does have a very similar log-log graph, and one may check on figure 9.5b that, for the function Z, the asymptotic slope is numerically consistent with -2.

Such asymptotic behaviours seem to be maintained in the rotating case although the dominant power for N might not be exactly -4, but still smaller than -3.5, hence no mass term can be extracted either. One is thus led to conclude that the presence of a scalar field with structure (7.2.5) in the cubic Galileon theory generically hides the

mass of an asymptotically flat black hole from infinity. Note that this could not be the case whenever asymptotic flatness is abandoned, i.e. non-zero Λ and/or η, since the asymptotic expansions (4.17) of [239] require a standard mass term from the first inverse power of r.

9.2.2 Angular momentum

Similarly to the definition (9.2.1), the Komar angular momentum of an asymptotically flat axisymmetric spacetime is defined as

$$J_{\text{Komar}} \equiv \frac{1}{16\pi} \int_{\mathcal{S}} *d\chi, \tag{9.2.12}$$

where ξ is the axisymmetric Killing vector.

Using the quasi-isotropic coordinates, the definition (9.2.12) reexpresses as

$$J_{\text{Komar}} = -\frac{1}{8} \lim_{r\to\infty} \int_0^\pi \partial_r \omega \; r^4 \sin^3\theta d\theta. \tag{9.2.13}$$

Therefore, if ω has the following asymptotic behaviour:

$$\omega = \frac{\omega_1}{r^3} + o\left(\frac{1}{r^3}\right), \tag{9.2.14}$$

where ω_1 is a constant, then

$$J_{\text{Komar}} = \frac{\omega_1}{2}. \tag{9.2.15}$$

Again, one may try to extract a Komar angular momentum from the asymptotic expansion of ω although, in the cubic Galileon theory, such a value would have no reason to be common to all other 2-surfaces $\mathcal{S}$. Figure 9.6a confirms that $\bar{\omega}$ has the asymptotic behaviour (9.2.14) (asymptotic slope equal to -3) so that the Komar angular momentum is non-zero. Since only dimensionless quantities are processed numerically, one has

$$\bar{\omega} \equiv r_{\mathcal{H}}\omega \sim \frac{2\bar{J}_{\text{Komar}}}{\bar{r}^3}, \tag{9.2.16}$$

where $\bar{J}$ is the dimensionless Komar angular momentum:

$$\bar{J}_{\text{Komar}} = \frac{J_{\text{Komar}}}{r_{\mathcal{H}}^2}. \tag{9.2.17}$$

The values of $\bar{J}_{\text{Komar}}$ extracted for all the $\bar{\Omega}_{\mathcal{H}}$ that were reached for $\bar{\gamma} = 10^{-2}$ and 1 are marked in figure 9.6b. The relation between $\bar{\Omega}_{\mathcal{H}}$ and $\bar{J}_{\text{Komar}}$ can be expressed explicitly in the case of the Kerr family, and it is represented by the solid red curve to highlight the deviations from GR.

As mentioned in section 9.1.2, $r_{\mathcal{H}}$ tends to zero for the extremal Kerr solutions while J_{Komar} tends to the finite value M^2. Therefore $\bar{\Omega}_{\mathcal{H}}$ goes to zero while $\bar{J}_{\text{Komar}}$ diverges according to the relation (9.2.17). This is why the curve corresponding to Kerr in figure 9.6b is defined all over $\mathbb{R}_+$ and converges to zero at infinity. Since $\bar{\Omega}_{\mathcal{H}} = 0$

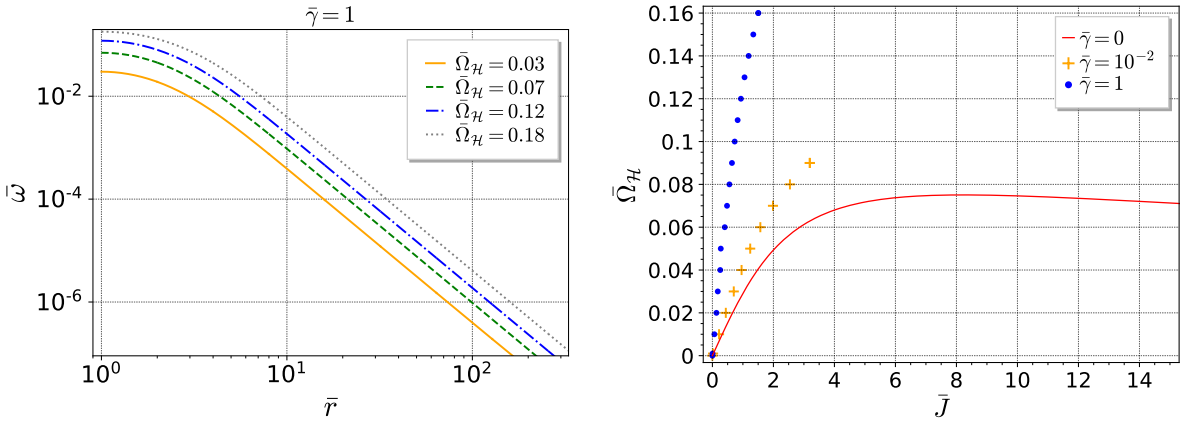

(a) log-log graph of function $\bar{\omega}$.

(b) Angular velocity with respect to angular momentum.

Figure 9.6: Angular momentum extracted from the asymptotic behaviour of $\bar{\omega}$.

for $\bar{J}_{\text{Komar}} = 0$ and $\bar{\Omega}_{\mathcal{H}}$ is positive, it must also have a maximum which is reached for $\bar{J}_{\text{Komar}} \simeq 8$ according to figure 9.6b. One can see that some cubic Galileon solutions exceed this maximum value, which clearly shows why it was not possible to provide a Kerr analog for the metric functions in figure 9.2 for $\bar{\gamma} = 0.12$ and 0.18.

Yet the existence of a maximum value for $\bar{\Omega}_{\mathcal{H}}$ in the Kerr case reveals that this quantity does not provide a bijective parametrization of the families of dimensionless black hole solutions. This represents a numerical difficulty: the solutions are gradually constructed by increasing the parameter $\bar{\Omega}_{\mathcal{H}}$ starting from the static and spherically symmetric solution $(\bar{\Omega}_{\mathcal{H}}, \bar{J}_{\text{Komar}}) = (0, 0)$ (left part of the curve, i.e. located before the maximum). The algorithm no longer converges when the maximum value is reached. From then on, $\bar{\Omega}_{\mathcal{H}}$ should be lowered to explore more and more rapidly rotating solutions (right part of the curve). But numerically, using the "maximum" solution as initial guess to reach a solution with a smaller value of $\bar{\Omega}_{\mathcal{H}}$ will actually yield the less rapidly rotating solution (i.e. going backward on the left part of the curve) rather than the more rapidly rotating solution that has the same dimensionless angular velocity $\bar{\Omega}_{\mathcal{H}}$ but located to the right of the maximum.

Finding a way to "jump" over the maximum in order to explore the right part of the curve is a non-trivial issue: one must use another quantity, easily handled numerically, which does parametrize the black hole solutions in a bijective way at least in a neighborhood of the maximum, unlike $\bar{\Omega}_{\mathcal{H}}$. Attempts using the dimensionless surface gravity (discussed in the following section) and other parameters fulfilling this condition were unsuccessful so far. This is why the highest points marked on figure 9.6b for $\bar{\gamma} = 0.12$ and 0.18 represent the last solutions that could be reached, beyond which the numerical algorithm does not converge anymore, revealing the proximity of a maximum value.

Of course, other notions of mass and angular momentum than the Komar quantities exist. In particular, some of them are more appropriate, but more technical, to take into account contributions from the scalar field. Some of these quantities are for instance introduced in [297] and the references cited therein.

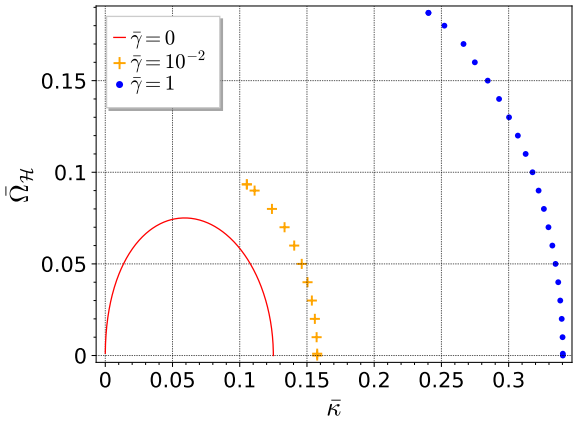

Figure 9.7: Angular velocity with respect to surface gravity.

9.2.3 Surface gravity

In a circular spacetime, the zeroth law of black hole mechanics holds [103, 110, 111], i.e. the surface gravity is constant on the horizons of stationary black holes. To check this for the solutions presented here, the dimensionless quantity $\bar{\kappa}$ corresponding to surface gravity κ was extracted according to the following formula:

$$\bar{\kappa} \equiv r_{\mathcal{H}}\kappa = \frac{1}{A}\partial_{\bar{r}}N_{|_1}. \tag{9.2.18}$$

In all solutions, the relative variations of $\bar{\kappa}$ on the horizon are smaller than 10^{-6}, confirming that the surface gravity is numerically homogeneous on the horizon.

The relation between $\bar{\kappa}$ and $\bar{\Omega}_{\mathcal{H}}$ is represented on figure 9.7. For each $\bar{\gamma}$, the static and spherically symmetric case corresponds to the only point such that $\bar{\Omega}_{\mathcal{H}} = 0$ but $\bar{\kappa} \neq 0$, while the origin of the graph, i.e. $(\bar{\Omega}_{\mathcal{H}}, \bar{\kappa}) = (0, 0)$ corresponds to extremal cases. The explicit case of Kerr is again represented by a solid red curve for comparison with GR.

9.2.4 Ergoregion

Recall that the ergoregion is the domain over which the pseudo-stationary Killing vector ∂_t is non-timelike, i.e. $N^2 \leq (\omega Br\sin\theta)^2$. Thus, realistic observers can no longer have constant spatial coordinates. Theoretically, this region allows to use particles to extract rotational energy from a black hole, as described by the Penrose process. In practice, the latter is not efficient enough to be significantly involved in astrophysical processes such as the relativistic jets emerging e.g. from quasars, although this used to be conjectured. Yet higher efficiencies might be reached around other objects, such as naked singularities or wormholes, or through more elaborate avatars of the process, such as the collisional Penrose process or superradiance. One may consult [298, 299] and references therein for discussions of these topics.

Locating the ergoregions of the Galileon solutions provides another evidence of deviations from GR. Figure 9.8a displays the ergoregions corresponding to various angular velocities $\bar{\Omega}_{\mathcal{H}}$ at fixed coupling $\bar{\gamma} = 1$ and figure 9.8b compares two of them with Kerr (same color meaning same angular velocity). On both figures, the ergospheres are

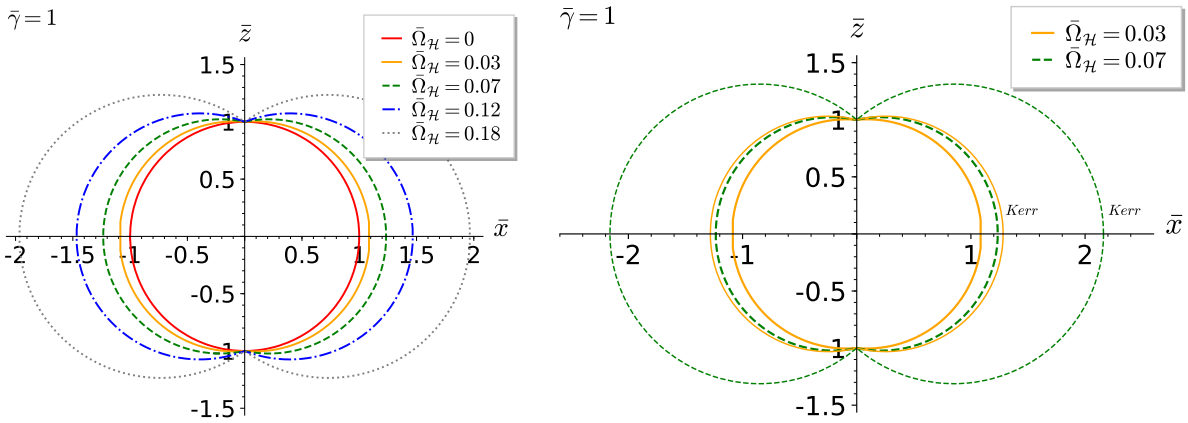

(a) Ergoregions of the cubic Galileon solutions.

(b) Comparison with Kerr.

Figure 9.8: Location of the ergoregion.

plotted in terms of Cartesian-like coordinates yet based on the quasi-isotropic coordinates: $(\bar{x}, \bar{z}) = (\bar{r}\sin\theta, \bar{r}\cos\theta)$. This explains the irregularities observed at the poles even in the case of Kerr, although none is observed in the familiar Boyer-Lindquist coordinates: the change of coordinates from Boyer-Lindquist to quasi-isotropic coordinates is not regular at the poles.

The ergoregions of the cubic Galileon solutions generically have the same shape as Kerr: they coincide with the horizon at the poles and get thicker towards the equator. They grow as $\bar{\Omega}_{\mathcal{H}}$ increases, yet they are thinner than Kerr for a given angular velocity.

Chapter 10

Equatorial geodesics in circular spacetimes

Contents

Before investigating the geodesics of the black hole configurations constructed in chapter 9, general results on equatorial geodesics are exposed in the present chapter.

One of the first reference works on equatorial geodesics date back to the investigations of Boyer and Price [300], who focused on the Kerr metric just before the seminal articles of Carter on general Kerr geodesics [105–107]. Later on, Bardeen [301], Press and Teukolsky [302] considered equatorial geodesics in circular spacetimes (7.2.2).

At the time, these authors were interested in the precession of the periapsis of bounded orbits, stability of thin dust disks and other processes around rotating black holes. In regard of the highly accurate observations realized by instruments like GRAVITY and the Event Horizon Telescope (see section 3.2), such investigations are still essential today e.g. to examine orbits of stars, accretion disks around massive black holes and the images they produce. Contemporary discussions on these topics can be found in references [288, 292, 303–305].

Beside circularity, the present chapter will further assume the equatorial reflection symmetry

$$\forall \mu, \nu, \;\; g_{\mu\nu}(r, \pi/2 - \theta) = g_{\mu\nu}(r, \theta). \tag{10.0.1}$$

Such metrics still include the Kerr family and the numerical black hole metrics [252, 253, 295], models of rotating neutron stars [291] and boson stars [292] earlier mentioned. Yet, note for instance that Kerr-Newman-Taub-NUT metric [306–308] does not fall into this family as equatorial symmetry (10.0.1) cannot hold in presence of the gravitomagnetic parameter.

In the sections below, the way the geodesic equation equivalently rewrites in terms of an effective potential is explicitly recalled for circular and non-circular equatorial

geodesics. This then provides a practical tool to discuss their stability. Statements are illustrated in Kerr spacetime.

10.1 Conservation equations

This section recalls the elements relevant in investigating the existence and properties of the trajectory of a free massive (resp. massless) particle in the equatorial plane of a circular spacetime. To effectively search for such a trajectory, its parametrization is set to be the only one whose corresponding tangent vector is the 4-momentum p of the particle. More explicitly, one looks for a timelike (resp. null), future-oriented curve

$$\mathcal{C}: \ \lambda \mapsto (x^\mu(\lambda)) = (t(\lambda),\ r(\lambda),\ \theta(\lambda),\ \phi(\lambda)) \tag{10.1.1}$$

such that the 4-momentum of the particle is $p^\mu = \dot{x}^\mu$, where a dot denotes differentiation with respect to the parameter λ. In addition, the particle is free *iff* its 4-momentum is parallely transported along its trajectory $\mathcal{C}$:

$$\nabla_p p = 0, \tag{10.1.2}$$

so that $\mathcal{C}$ is an affinely parametrized geodesic by definition.

The geodesic equation (10.1.2) implies that the mass

$$m = \sqrt{-p^2} \quad \text{is conserved along } \mathcal{C}. \tag{10.1.3}$$

In particular, if $m > 0$, λ is necessarily the curvilinear abscissa (i.e. proper time) τ along $\mathcal{C}$ divided by m.

In a stationary and axisymmetric spacetime such as (7.2.2), equation (10.1.2) also implies conservation of the Killing energy and angular momentum:

$$E = -\partial_t \cdot p \quad \text{is conserved along } \mathcal{C}, \tag{10.1.4}$$
$$L = \partial_\phi \cdot p \quad \text{is conserved along } \mathcal{C}. \tag{10.1.5}$$

Such quantities are actual observables only if the particle ever reaches spacelike infinity, where they are the energy and angular momentum effectively measured by a zero angular momentum observer (ZAMO)[44]. In this case, $E \geq 0$ necessarily.

Finally, the trajectory is requested to be equatorial:

$$\theta = \pi/2 \quad \text{is conserved along } \mathcal{C}. \tag{10.1.6}$$

This implies $p^\theta = 0$, which is equivalent to $p_\theta = 0$ in the quasi-isotropic coordinates (7.2.2).

The conservation equations (10.1.3), (10.1.4), (10.1.5) and (10.1.6) are thus four necessary conditions for a curve $\mathcal{C}$ to describe an equatorial trajectory of a free particle.

[44]The ZAMO are characterized by a 4-velocity colinear to ∇t; as a result, one may check that the ZAMO are not freely falling, yet they fulfill property (10.1.5) with $L = 0$, hence their name.

10.2 Non circular geodesics

For non-circular orbits, i.e. for any trajectory such that $p^r \neq 0$ ($\Leftrightarrow p_r \neq 0$ in coordinates (7.2.2)) almost everywhere (p^r may only cancel at periapsis and apoapsis, when they exist), these four conservation equations are sufficient, i.e. they imply the geodesic equation (10.1.2) for the following reasons. First, the Killing equation for ∂_t

$$[\nabla_\mu \partial_t]_\nu + [\nabla_\nu \partial_t]_\mu = 0 \tag{10.2.1}$$

and the Killing energy conservation (10.1.4) establish the covariant t component of the geodesic equation:

$$[\nabla_p p]_t = \partial_t \cdot \nabla_p p = \nabla_p (\partial_t \cdot p) = -\nabla_p E = 0. \tag{10.2.2}$$

The analogous argument for ∂_ϕ and (10.1.5) yields $[\nabla_p p]_\phi = 0$.

Besides, the covariant θ component of the geodesic equation also vanishes:

$$[\nabla_p p]_\theta = A^2 r^2 [\nabla_p p]^\theta = A^2 r^2 p^\mu p^\nu \Gamma^\theta{}_{\mu\nu} = 0 \tag{10.2.3}$$

since $\Gamma^\theta{}_{r\theta}$ gets multiplied by $p^\theta = 0$, and all the other Christoffel symbols $\Gamma^\theta{}_{\mu\nu}$ vanish in the equatorial plane as sums of terms that are proportional either to $\cos\theta$, or to some angular derivative of the metric $\partial_\theta g_{\mu\nu}$, which is necessarily zero under the natural assumption of equatorial symmetry (10.0.1). When the latter does not hold, e.g. in Kerr-Newman-Taub-NUT spacetime, the covariant θ component of the geodesic equation might not come out so simply: it may require alternative constraints on the metric components, or invoke some of the other conservation equations. It is indeed interesting to note that each of the above three covariant components of the geodesic equation do not require any of the two other conservation equations to be derived. As a result, any trajectory satisfying conservation of E (resp. L, resp. $\theta = \pi/2$ when equatorial symmetry holds) always satisfies the covariant t (resp. ϕ, resp. θ) component of the geodesic equation.

Finally, mass conservation (10.1.3) rewrites as

$$0 = \nabla_p (p \cdot p) = p^\mu [\nabla_p p]_\mu = p^r [\nabla_p p]_r , \tag{10.2.4}$$

which implies $[\nabla_p p]_r = 0$ since $p^r \neq 0$ almost everywhere.

Before treating the circular case $p^r = 0$, it is very useful to note that equations (10.1.4), (10.1.5) and (10.1.6) allow to rewrite the mass conservation equation (10.1.3) as a familiar first order ordinary differential equation on the radial coordinate function r:

$$\frac{\dot{r}^2}{2} + \mathcal{V}(r, m, E, L) = 0 \tag{10.2.5}$$

where the effective potential $\mathcal{V}$ is defined as

$$\mathcal{V}(r, m, E, L) = \frac{1}{2A^2}\left[m^2 - \left(\frac{E - \omega L}{N}\right)^2 + \left(\frac{L}{Br}\right)^2\right]. \tag{10.2.6}$$

Since $\lambda = \tau/m$ for massive particles, note that (10.2.5) rewrites as

$$\frac{1}{2}\left(\frac{dr}{d\tau}\right)^2 + \mathcal{V}(r, 1, \bar{E}, \bar{L}) = 0 \tag{10.2.7}$$

where $\bar{E} = E/m$ and $\bar{L} = L/m$, so that the trajectories of free massive particles only depend on their Killing energy and angular momentum per unit mass.

Based on the explicit form (10.2.5) of the mass conservation equation, conditions on $\mathcal{V}$ and its partial derivatives will also allow to characterize the circular geodesics (see section 10.3) and study their stability (see section 10.4). So far, simply note that non-circular geodesics necessarily have $\mathcal{V} < 0$ almost everywhere, while circular geodesics necessarily have $\mathcal{V} = 0$ everywhere.

Finally, the procedure to explicitly construct all non-circular equatorial trajectories of free particles is to first pick an initial radial coordinate r_0, a Killing energy E, a Killing angular momentum L and a mass m such that $\mathcal{V}(r_0, m, E, L) < 0$ and $E - \omega(r_0)L > 0$ to guarantee that the trajectory is initially causal future-oriented (see equation (10.2.9) below); in particular, this necessarily requires $E > 0$ if r_0 is outside the ergoregion. Secondly, the right-hand side of

$$\dot{r} = \pm\sqrt{-2\mathcal{V}(r, m, E, L)} \tag{10.2.8}$$

is sufficiently regular for equation (10.2.8) to admit a unique solution $\lambda \mapsto r_s(\lambda)$ once the $\pm$ sign is chosen (to determine whether the initial direction is ingoing or outgoing). Conservation of E and L then provide the solutions for t and ϕ:

$$t_s(\lambda) = \int \frac{E - \omega(r_s)L}{N(r_s)^2} d\lambda, \tag{10.2.9}$$

$$\phi_s(\lambda) = \int \left[\frac{L}{(B(r_s)r_s)^2} + \omega(r_s)\frac{E - \omega(r_s)L}{N(r_s)^2}\right] d\lambda, \tag{10.2.10}$$

where the second argument $\theta_s = \pi/2$ of the metric functions is omitted without loss of clarity. Note that frame dragging can be read off from relation (10.2.10): radial free fall from infinity (hence $L = 0$) does not remain radial in a rotating spacetime as ϕ_s receives contribution from the non-vanishing metric function ω.

10.3 Circular geodesics

As mentioned earlier, $p^r = 0$ (circular orbit) forbids to establish the radial geodesic equation from mass conservation, which is then redundant as a linear combination of the E and L conservation equations (i.e. the covariant t and ϕ geodesic equations). Therefore, one additional equation is missing to realize a geodesic. Indeed, there are so far multiple solutions to the problem $\{(10.1.4), (10.1.5), (10.1.6), p^r = 0\}$ (which implies mass conservation): for any E, L and r_0, the curve

$$\lambda \mapsto \left(\frac{E - \omega_0 L}{N_0^2}\lambda,\ r_0,\ \pi/2,\ \left[\frac{L}{(B_0 r_0)^2} + \omega_0\frac{E - \omega_0 L}{N_0^2}\right]\lambda\right) \tag{10.3.1}$$

is circular (an index 0 means that the metric function is evaluated at r_0, in the equatorial plane) with conserved Killing energy E and angular momentum L. Additionally, one may simply require $E \geq \omega_0 L + N_0|L|/(B_0 r_0)$ (which is always positive outside the ergoregion) to describe a causal future-oriented trajectory; this amounts to requiring that mass conservation $\mathcal{V}(r_0, m, E, L) = 0$ holds for a real constant m (i.e. $m^2 > 0$).

All these circular orbits are distinct solutions to the same problem, but at most one of them is a geodesic, sometimes none (intuitively, the other orbits are accelerated

inward if they rotate "faster" than a geodesic to compensate for the centrifugal effect, outward otherwise). To search for a geodesic among them, one obtains an additional prescription from differentiating equation (10.2.5):

$$\dot{r}\left[\ddot{r}+\mathcal{V}'(r,m,E,L)\right]=0, \tag{10.3.2}$$

where $'$ denotes differentiation with respect to the first argument (the radial coordinate).

Of course, for any circular orbit (10.3.1), equation (10.3.2) holds because $\dot{r}=0$, while it implies

$$\ddot{r}+\mathcal{V}'(r,m,E,L)=0, \tag{10.3.3}$$

for all non-circular geodesics. The missing condition to realize a circular geodesic at r_0 is then obtained by requiring equation (10.3.3) to hold even in the circular limit, i.e. when $\ddot{r}=0$, yielding

$$\mathcal{V}'(r_0,m,E,L)=0. \tag{10.3.4}$$

On figure 10.1a for instance, circular geodesics exist at the zeros of the bottom red and top blue curves since the latter cancel in a stationary way (the corresponding geodesics are respectively represented by the red and blue dashed lines in figure 10.1b), while the zeros of the two other curves can only correspond to accelerated circular orbits or to the periapsis and apoapsis of a non-circular geodesic; more precisely, the smallest (resp. greatest) zero of the top red curve is the unique apoapsis (resp. periapsis) of a geodesic reaching the event horizon (resp. infinity, as represented by the red solid line in figure 10.1b) while the smallest (resp. greatest) zero of the bottom blue curve is the periapsis (resp. apoapsis) of a bounded geodesic (represented by the blue solid line in figure 10.1b). Note here that, in the asymptotically flat case, $N\to 1$, $A\to 1$, $B\to 1$ and $\omega\to 0$ at infinity, so that $\mathcal{V}(r,m,E,L)\to(1-E^2)/2$; therefore, a non-circular unbounded geodesic (such as the one represented by the red solid line on figure 10.1b ruled by the right negative branch of the top red curve of figure 10.1a) requires $E>1$.

To show that the additional condition (10.3.4) allows to establish the r geodesic equation, define

$$\mathcal{W}(r,m,E,L)=m^2-\left(\frac{E-\omega L}{N}\right)^2+\left(\frac{L}{Br}\right)^2 \tag{10.3.5}$$

so that $\mathcal{V}(r,m,E,L)=\mathcal{W}(r,m,E,L)/(2A^2)$, and hence

$$\mathcal{V}'(r_0,m,E,L)=\left(\frac{1}{2A^2}\right)'_0\mathcal{W}(r_0,m,E,L)+\frac{\mathcal{W}'(r_0,m,E,L)}{2A_0^2} \tag{10.3.6}$$

$$=\frac{\mathcal{W}'(r_0,m,E,L)}{2A_0^2} \tag{10.3.7}$$

since mass conservation $\mathcal{V}(r_0,m,E,L)=0$ is equivalent to $\mathcal{W}(r_0,m,E,L)=0$. Therefore, condition (10.3.4) is equivalent to

$$0=\frac{\mathcal{W}'(r_0,m,E,L)}{2} \tag{10.3.8}$$

$$=\frac{E-\omega_0 L}{N_0^2}\left[(E-\omega_0 L)\frac{N_0'}{N_0}+L\omega_0'\right]-\left(\frac{L}{B_0 r_0}\right)^2\left(\frac{B_0'}{B_0}+\frac{1}{r_0}\right). \tag{10.3.9}$$

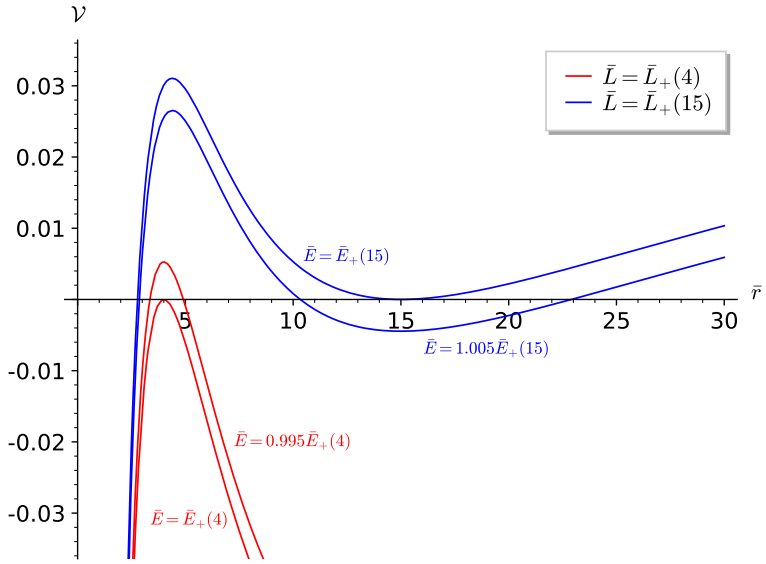

(a) Effective potentials of timelike orbits with respect to $\bar{r} = r/r_{\mathcal{H}}$ for different Killing energy and angular momentum per unit mass (only the ratios $\bar{E} = E/m$ and $\bar{L} = L/m$ are relevant in the massive case). The bottom red (resp. top blue) curve corresponds to the Killing energy and angular momentum of the timelike circular geodesic at $4r_{\mathcal{H}}$ (resp. $15r_{\mathcal{H}}$) while the other red (resp. blue) curve has same $\bar{L}$ but a slightly smaller (resp. greater) $\bar{E}$.

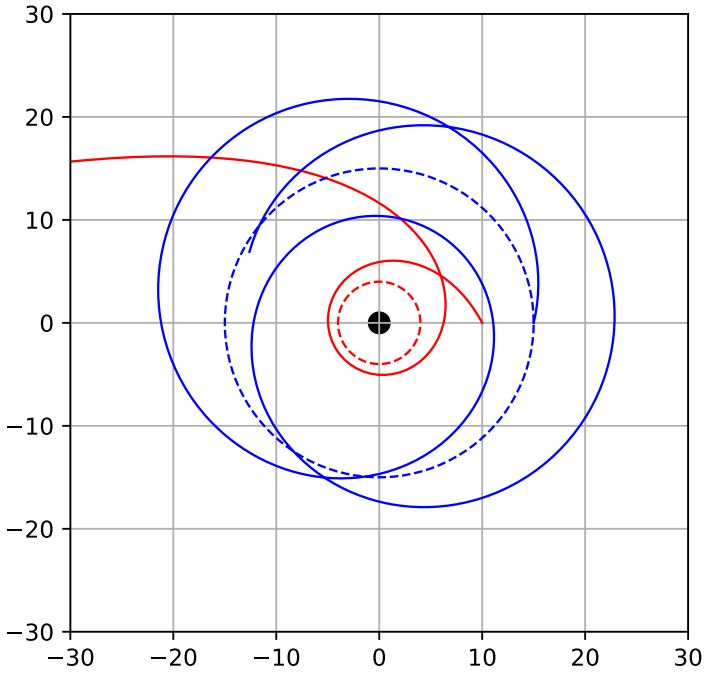

(b) The red (resp. blue) dashed circle corresponds to the zero of the bottom red (resp. top blue) curve of figure 10.1a. The red (resp. blue) solid line is ruled by the right, negative, unbounded (resp. bounded) branch of the top red (resp. bottom blue) curve of figure 10.1a. Plot realized with the ray-tracing code *GYOTO* [309].

Figure 10.1: Potentials and spatial projections of timelike circular and non-circular equatorial geodesics in a Kerr spacetime ($a/M \simeq 0.52$).

Then, injecting the explicit expressions

$$L = B_0^2 r_0^2 \left(p^\phi - \omega_0 p^t\right), \tag{10.3.10}$$
$$E = N_0^2 p^t + \omega_0 L, \tag{10.3.11}$$

into (10.3.8) immediately yields

$$0 = p^t \left[N_0 N_0' p^t + B_0^2 r_0^2 \left(p^\phi - \omega_0 p^t\right) \omega_0'\right] - B_0^2 r_0^2 \left(p^\phi - \omega_0 p^t\right)^2 \left(\frac{B_0'}{B_0} + \frac{1}{r_0}\right) \tag{10.3.12}$$
$$= A_0^2 \left[\Gamma^r{}_{tt} (p^t)^2 + 2\Gamma^r{}_{t\phi} p^t p^\phi + \Gamma^r{}_{\phi\phi} (p^\phi)^2\right] \tag{10.3.13}$$
$$= A_0^2 \Gamma^r{}_{\mu\nu} p^\mu p^\nu = A_0^2 \left[\nabla_p p\right]^r = \left[\nabla_p p\right]_r . \tag{10.3.14}$$

Therefore, circular geodesics are precisely the circular orbits (10.3.1) that continue property (10.3.3) of non-circular geodesics. Gathered with the result of section 10.2, the circular and non-circular free trajectories are characterized as follows. A curve $\mathcal{C} : \lambda \mapsto (x^\mu(\lambda))$ describes an equatorial free particle with 4-momentum $p^\mu = \dot{x}^\mu$ *iff* it satisfies the three conservation equations {(10.1.4), (10.1.5), (10.1.6)} and either one of the two following conditions:

- the fourth conservation equation (10.1.3) and $\mathcal{V} \neq 0$ almost everywhere on $\mathcal{C}$ (in this case, $\mathcal{C}$ is non-circular);
- $\mathcal{V} = 0$ and $\mathcal{V}' = 0$ everywhere on $\mathcal{C}$ (in this case, $\mathcal{C}$ is circular).

Finally, to explicitly construct all free circular equatorial trajectories, recall that all the curves (10.3.1) with $E \geq \omega L + N|L|/(Br)$ (the indices 0 are now removed although all the statements in the remaining of the section will only apply to circular orbits) are very good candidates because they satisfy the three conservation equations {(10.1.4), (10.1.5), (10.1.6)} and $\mathcal{V}(r, m, E, L) = 0$ as well since this relation is the definition of m for a circular orbit at r. It thus only remains to derive which final constraint emerges from requiring $\mathcal{V}'(r, m, E, L) = 0$ (in which m actually does not appear because of $\mathcal{V}(r, m, E, L) = 0$). This constraint will first be formulated in terms of the "signed norm" V of the spatial velocity v measured by the ZAMO, defined below. From V will then be deduced the values of E and L to be injected into (10.3.1) to define a free circular trajectory at r.

For a particle with mass m, first denote $\mathcal{E}$ and v the energy and spatial velocity measured by the ZAMO[45], and n the 4-velocity of the latter, so that the 4-momentum of the particle decomposes as

$$p = \mathcal{E}(n + v) \text{ with } n \cdot v = 0. \tag{10.3.15}$$

One obtains

$$\mathcal{E} = \frac{E - \omega L}{N} \tag{10.3.16}$$

and

$$v = \frac{V}{Br} \partial_\phi \tag{10.3.17}$$

[45]For a massive particle, $\mathcal{E} = \Gamma m$ where Γ is the Lorentz factor of the particle with respect to the ZAMO; for a massless particle, $\mathcal{E} = h\nu$ where ν is the frequency measured by the ZAMO.

where

$$V = \frac{L}{Br\mathcal{E}} \tag{10.3.18}$$

Note that $v^2 = V^2$, hence the name "signed norm" for V. Also recall here that a trajectory is defined to be prograde (resp. retrograde) when $\omega L > 0$ (resp. $\omega L < 0$); since ω does not generally cancel, the ϕ coordinate may be chosen so that $\omega > 0$, which then simplifies in the definition. Based on relations (10.3.17) and (10.3.18), and the fact that $\omega(r_{\mathcal{H}})$ equals the angular velocity $\Omega_{\mathcal{H}}$ of the event horizon, a prograde (resp. retrograde) trajectory intuitively rotates in the same (resp. opposite) direction as the black hole for the ZAMO. However, for an observer at infinity, the angular velocity p^ϕ/p^t of a circular orbit (10.3.1) is

$$\frac{p^\phi}{p^t} = \omega + \frac{NL}{Br\sqrt{(mBr)^2 + L^2}}, \tag{10.3.19}$$

so that one of the retrograde orbit may appear prograde from infinity *iff* it is outside the ergoregion and $L > -m\omega(Br)^2/\sqrt{-N^2 + (\omega Br)^2}$.

Note also that equation (10.3.8) (which is equivalent to $\mathcal{V}' = 0$ as $\mathcal{V} = 0$) is independent of m and hence homogeneous with respect to E and L. Therefore, injecting relations (10.3.16) and (10.3.18) into this expression allows to simplify all $\mathcal{E}$, which finally yields the following second order equation in V:

$$\left(\frac{B'}{B} + \frac{1}{r}\right) V^2 - \frac{Br\omega'}{N} V - \frac{N'}{N} = 0. \tag{10.3.20}$$

As announced, only the spatial velocity of the particle is constrained and not $\mathcal{E}$, which means that, where a circular timelike geodesic exists, it can be the worldline of any massive particle regardless of its mass provided it has the right velocity, and where a circular null geodesic exists (i.e. a photon ring), it can be the worldline of any photon regardless of its frequency (this all seems consistent with the equivalence principle). For a timelike circular geodesic to exist at r, the values at r of the metric functions involved in (10.3.20) need to be such that at least one of the roots, if any exists, belongs to $(-1, 1)$ (the ZAMO must measure subluminal velocities). In the massless case, $V = \pm 1$ so that at any photon ring, if any exists, the metric functions need to be such that 1 or -1 is a root of equation (10.3.20). One then only needs to study the roots $V_\pm$ of equation (10.3.20) to conclude about existence and location of timelike circular geodesics and photon rings. These roots exist *iff* the discriminant

$$D = \left(\frac{Br\omega'}{N}\right)^2 + \frac{4N'}{N}\left(\frac{B'}{B} + \frac{1}{r}\right) \tag{10.3.21}$$

of equation (10.3.20) is non-negative, in which case one has

$$V_\pm(r) = \frac{\frac{Br\omega'}{N} \pm \sqrt{D}}{2\left(\frac{B'}{B} + \frac{1}{r}\right)}. \tag{10.3.22}$$

In Kerr, for any angular velocity $\Omega_{\mathcal{H}}$, function D monotonically decreases from an infinite value at the horizon down to a zero limit as $r \to +\infty$ (see figure 10.2a). Therefore, each velocity function $V_\pm$ necessarily becomes luminal at some point corresponding

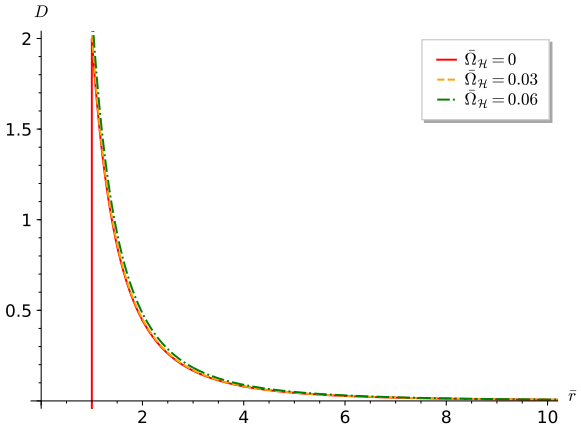

(a) Positivity of D allows (possibly superluminal) circular geodesics.

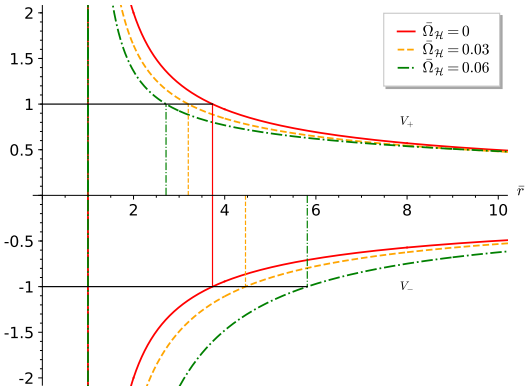

(b) Velocities and photon rings.

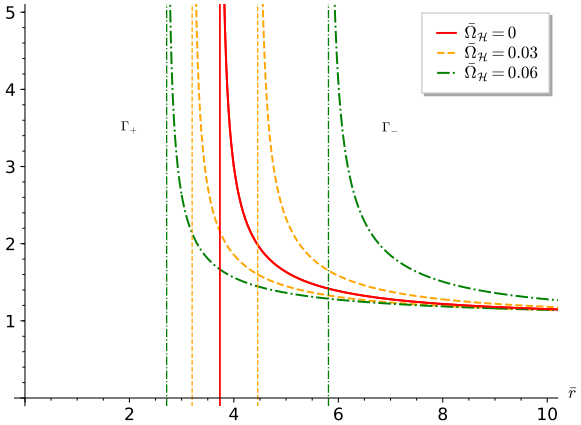

(c) Lorentz factor of timelike circular geodesics.

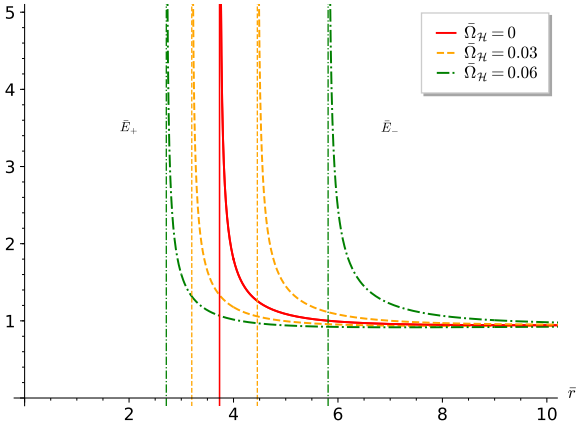

(d) Killing energy of timelike circular geodesics.

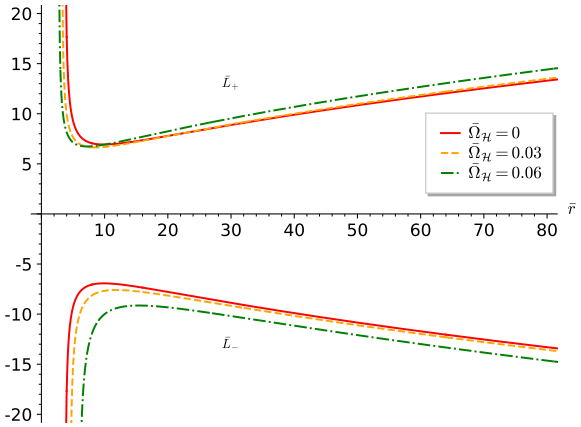

(e) Killing angular momentum of timelike circular geodesics.

Figure 10.2: Kinematic characteristics of circular geodesics in Kerr spacetime for different (dimensionless) angular velocities $\bar{\Omega}_{\mathcal{H}}$.

to a photon ring (marked with a vertical line from 0 to 1 in figure 10.2b), beyond which timelike circular geodesics exist everywhere.

Finally, relations (10.3.16) and (10.3.18) then yield

$$L_\pm = \mathcal{E} B r V_\pm, \tag{10.3.23}$$
$$E_\pm = \mathcal{E}(N + Br\omega V_\pm), \tag{10.3.24}$$

i.e. in the massive case,

$$L_\pm = \Gamma_\pm m B r V_\pm, \tag{10.3.25}$$
$$E_\pm = \Gamma_\pm m(N + Br\omega V_\pm), \tag{10.3.26}$$

with

$$\Gamma_\pm = (1 - V_\pm^2)^{-1/2}, \tag{10.3.27}$$

while in the massless case,

$$L_\pm = \pm h\nu B r, \tag{10.3.28}$$
$$E_\pm = h\nu(N \pm Br\omega). \tag{10.3.29}$$

These quantities are plotted on figure 10.2c, 10.2d and 10.2e in the massive case for different angular velocities $\bar{\Omega}_\mathcal{H}$ in Kerr spacetime. In particular, the "+" and "-" quantities are no longer merely equal or opposite in the rotating cases and respectively follow the evolution of the "+" and "-" photon rings in figure 10.2b: the "+" (resp. "-") Lorentz factor and Killing energy are for instance roughly shifted to the left (resp. right) of the Schwarzschild profile.

10.4 Stability of circular geodesics

For circular geodesics, the radial equation (10.2.5) expectedly provides a stability criterion based on convexity. A non-constant perturbation δ (a constant perturbation would not threaten stability) to a circular geodesic at r allows to use equation (10.3.3) instead:

$$\ddot{\delta} + \mathcal{V}'(r + \delta, m, E + \delta_E, L + \delta_L) = 0 \tag{10.4.1}$$

in which Taylor expanding and invoking condition (10.3.4) yields

$$\ddot{\delta} + \mathcal{V}''(r, m, E, L)\delta = O(\delta_E) + O(\delta_L) + O(\delta^2 + \delta_E^2 + \delta_L^2). \tag{10.4.2}$$

If $\mathcal{V}''(r, m, E, L) < 0$, then δ must be accelerating away from r to preserve the asymptotic orders in the right-hand side. To guarantee that any δ is bounded in some neighbourhood of r then requires positive $\mathcal{V}''(r, m, E, L)$.

Actually, the values of E and L for a circular geodesic at r are necessarily $E_\pm(r)$ and $L_\pm(r)$, explicitly given by relations (10.3.23) and (10.3.24). In practice, one should thus study the sign of the two functions

$$\mathcal{V}''_\pm : r \mapsto \mathcal{V}''\left(r, m, E_\pm(r), L_\pm(r)\right), \tag{10.4.3}$$

on the set on which the discriminant D is non-negative. Actually, the expressions $\mathcal{V}''(r, m, E_\pm(r), L_\pm(r))$ are homogeneous with respect to $\mathcal{E}$, so that their sign do not depend on $\Gamma_\pm m$ in the massive case nor on $h\nu$ in the massless case. Therefore, the stability of causal circular geodesics only depends on the sign of the two functions (10.4.3) and concerns massive particles where $V_\pm(r) \in (-1, 1)$ and massless ones where $V_\pm(r) = \pm 1$, regardless of whether the expressions used for $E_\pm$ and $L_\pm$ apply to a massive or a massless particle.

Figures 10.3a and 10.3b illustrate all this in the Schwarzschild case: for each radii r_0 marked with a dashed vertical line of a given colour in figure 10.3a, the potential $\mathcal{V}(\cdot, m, E_\pm(r_0), L_\pm(r_0))$, which corresponds to the geodesic at r_0, is plotted with the same colour, and thus cancels in a stationary way at r_0. Then, for each r_0, function $\mathcal{V}''_\pm$ in figure 10.3b extracts the convexity of $\mathcal{V}(\cdot, m, E_\pm(r_0), L_\pm(r_0))$ at the corresponding r_0: the purple curve is concave at $r_0 = 5r_\mathcal{H}$ on figure 10.3a (hence unstable circular geodesic), so that $\mathcal{V}''_\pm$ is negative at $5r_\mathcal{H}$ on figure 10.3b, whereas the turquoise curve is convex at $r_0 = 20r_\mathcal{H}$, so that $\mathcal{V}''_\pm$ is positive at $20r_\mathcal{H}$. The limiting case (grey lines) such that $\mathcal{V}(\cdot, m, E_\pm(r_0), L_\pm(r_0))$ cancels as an inflection point at $r_0 \simeq 9.9r_\mathcal{H}$ ($\mathcal{V}''_\pm(r_0) = 0$) defines the innermost stable circular orbit (ISCO)[46].

Finally, figure 10.3c gathers the functions $\mathcal{V}''_\pm$ for different angular velocities; the functions $\mathcal{V}''_+$ and $\mathcal{V}''_-$ are no longer equal in the rotating case ($\mathcal{V}''_+$ globally increases with rotation while $\mathcal{V}''_-$ globally decreases) and thus respectively define an ISCO. Based on figure 10.2b, both ISCO are always located beyond the corresponding photon ring, so that the latter are always unstable.

Note that for a stable circular geodesic (r_0, m, E, L), the function $\mathcal{V}(\cdot, m, E, L)$ realizes a local minimum (equal to zero) at r_0, so that it is strictly positive in a neighbourhood of r_0 except at r_0. Yet, one always has

$$\partial_E \mathcal{V}(r_0, m, E, L) = -\frac{\mathcal{E}}{N_0 A_0^2} < 0 \tag{10.4.4}$$

since $\mathcal{E}$ is always strictly positive for a causal future-oriented curve. Decreasing E thus increases $\mathcal{V}$ locally[47], so that $\mathcal{V}$ becomes strictly positive on a neighbourhood of r_0. But $\mathcal{V}$ is necessarily negative or zero on any orbit ruled by (10.2.5), which means that, m and L being fixed, there can be no geodesic close to (r_0, m, E, L) with smaller E: a stable circular geodesic at r_0 realizes a local minimum of E on the set of geodesics having same m and L.

As an additional note, fixing m and L also provides other interesting criteria to characterize circular geodesics among circular orbits (instead of $\mathcal{V}' = 0$), and investigate their stability (instead of $\mathcal{V}'' > 0$). For illustrative purposes, the function $\mathcal{V}^{(m,L)} : (r, E) \mapsto \mathcal{V}(r, m, E, L)$ is plotted for a Kerr spacetime in figure 10.4.

From this point of view, circular geodesics lie on the set of points (r, E) such that $\mathcal{V}^{(m,L)}(r, E) = 0$ (black horizontal curve in figure 10.4): it is the intersection of the image of $\mathcal{V}^{(m,L)}$ (yellow surface) with the $\mathcal{V} = 0$ plane (green horizontal plane). For any of these points (r_0, E_0) to actually correspond to a circular geodesic (rather than an accelerated circular orbit), condition (10.3.4) must hold, meaning that r_0 must

[46] In Boyer-Lindquist coordinates, the ISCO radius R_0 of Schwarzschild spacetime is known to equal $6M$; injecting this value into equation (C.9) does yield $r_0 = (5 + 2\sqrt{6})M/2 \simeq 9.9r_\mathcal{H}$.

[47] This is illustrated on figure 10.1a: E is decreased to switch from the bottom curve to the top curve of a given color.

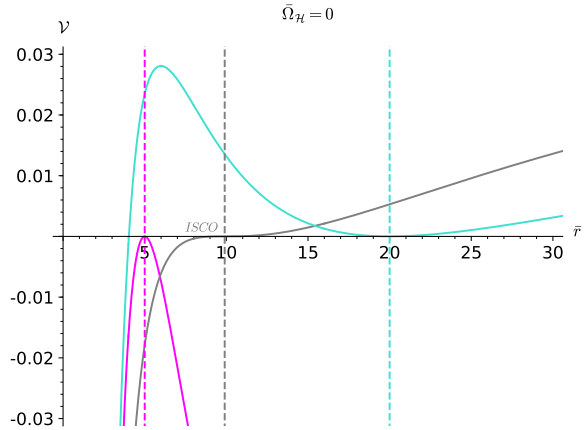

(a) Potentials $\mathcal{V}(\,\cdot\,, m, E_{\pm}(r_0), L_{\pm}(r_0))$ of circular geodesics at various r_0 in Schwarzschild spacetime.

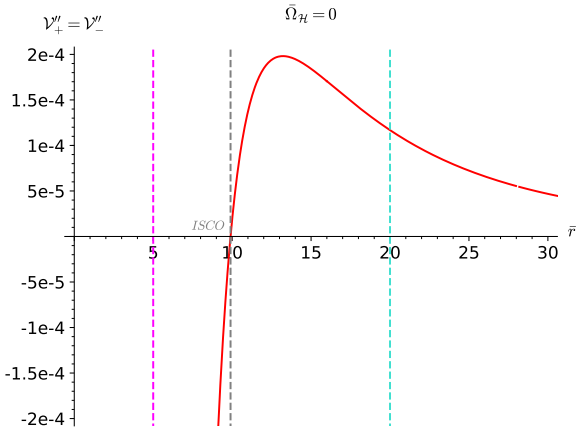

(b) $\mathcal{V}''_{\pm}(r_0)$ is the convexity of $\mathcal{V}(\,\cdot\,, m, E_{\pm}(r_0), L_{\pm}(r_0))$ evaluated at r_0.

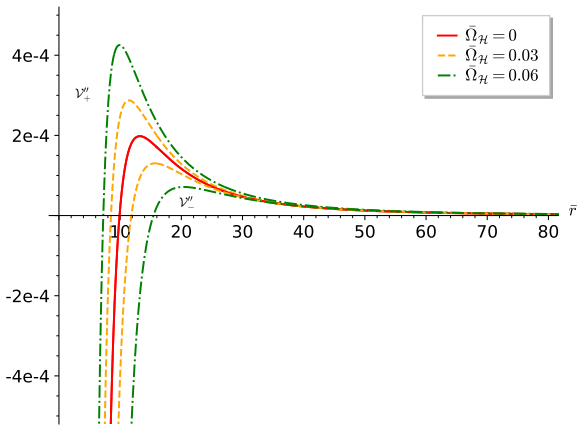

(c) Stability of circular geodesics from function $\mathcal{V}''_{\pm}$.

Figure 10.3: Positivity of $\mathcal{V}''_{\pm}$ rules stability and hence location of ISCO.

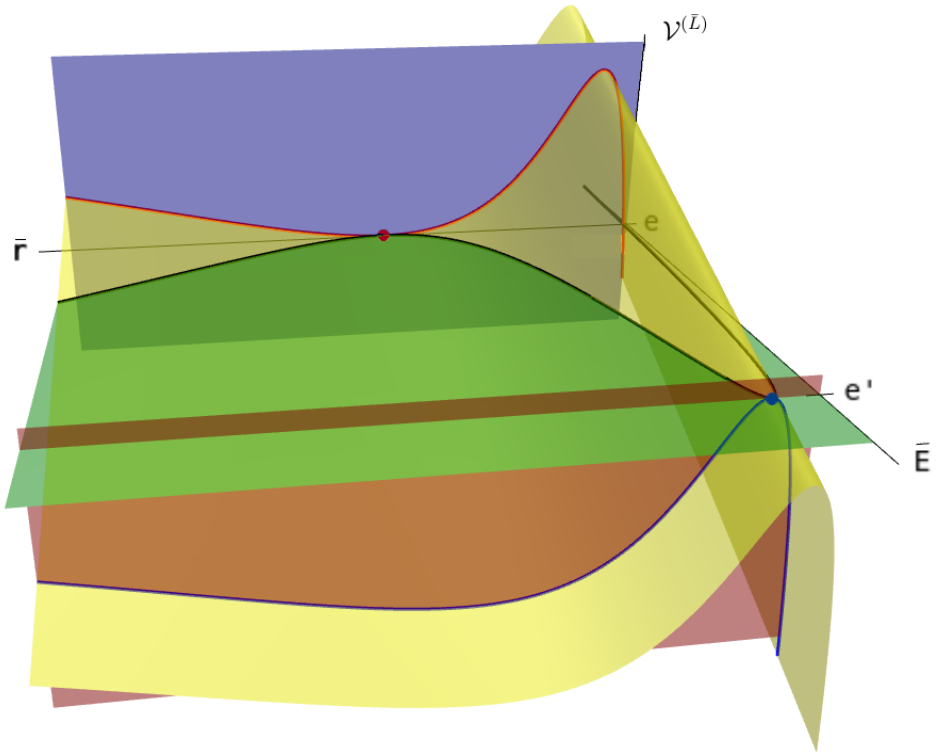

Figure 10.4: Effective potential $\mathcal{V}^{(\bar{L})}$ (yellow surface) of massive particles at fixed $\bar{L}$ in a Kerr spacetime ($a/M \simeq 0.52$). Its zeros lie on the black curve $E^{(\bar{L})}_{min}$. Its profile at fixed Killing energy per unit mass e (resp. e') is highlighted as a red (resp. blue) curve on the blue (resp. red) vertical plane. $\bar{L}$ being fixed, the only circular geodesics are marked with the red and blue dots, where both the two curves to which they respectively belong are stationary, and whose common convexity determines their stability.

be a stationary point of $\mathcal{V}^{(m,L)}(\,\cdot\,, E_0)$, whose graph is the intersection of the image of $\mathcal{V}^{(m,L)}$ (yellow surface) with the $E = E_0$ plane (blue or red vertical plane).

However, the set of points (r, E) such that $\mathcal{V}^{(m,L)}(r, E) = 0$ (black horizontal curve) is always the graph of a function well-defined with respect to r: $r \mapsto E(r)$. This comes from the fact that $\mathcal{V}^{(m,L)}$ is a second order polynomial with respect to E. For any r, the function $\mathcal{V}^{(m,L)}(r, \cdot\,)$ always admits two distinct roots

$$E^{(m,L)}_{min}(r) = \omega(r)L + N(r)\sqrt{m^2 + \left(\frac{L}{B(r)r}\right)^2}, \tag{10.4.5}$$

$$E^{(m,L)}_{neg}(r) = -E^{(m,-L)}_{min}(r). \tag{10.4.6}$$

Since $\mathcal{V}^{(m,L)}(r, \cdot\,)$ is a second order polynomial with negative dominant coefficient with respect to E, and since $E^{(m,L)}_{min}$ is always the greatest root, one has

$$\partial_E \mathcal{V}^{(m,L)}\left(r, E^{(m,L)}_{min}(r)\right) < 0, \tag{10.4.7}$$

$$\partial_E \mathcal{V}^{(m,L)}\left(r, E^{(m,L)}_{neg}(r)\right) > 0. \tag{10.4.8}$$

Based on equation (10.4.4), $E^{(m,L)}_{neg}$ can in no case correspond to a causal future-oriented curve. Actually, it merely corresponds to all the causal past-oriented circular and non-circular equatorial geodesics. This had to be expected since the effective potential $\mathcal{V}$ and the three other conservation equations can as well be used to describe them. More precisely, based on relations (10.2.6), (10.2.8), (10.2.9) and (10.2.10), the past-oriented version of a future-oriented non-circular geodesic is obtained by switching the sign of both E and L and taking the opposite sign in (10.2.8). This is even easier to check in the circular case (10.3.1), and relation (10.4.6) confirms that $E^{(m,L)}_{neg}$ is merely the Killing energy of the past-oriented version of the circular orbit having opposite Killing angular momentum. One may thus focus on $E^{(m,L)}_{min}$ alone, which can only be negative for retrograde orbits inside the ergoregion.

By definition, one has

$$\mathcal{V}^{(m,L)}\left(r, E^{(m,L)}_{min}(r)\right) = 0, \tag{10.4.9}$$

so that

$$E^{(m,L)'}_{min}(r) = -\frac{\mathcal{V}^{(m,L)'}\left(r, E^{(m,L)}_{min}(r)\right)}{\partial_E \mathcal{V}^{(m,L)}\left(r, E^{(m,L)}_{min}(r)\right)} \tag{10.4.10}$$

where division is allowed by (10.4.7). Therefore, the circular orbit $(r, m, E^{(m,L)}_{min}(r), L)$ is a geodesic *iff* $E^{(m,L)'}_{min}(r) = 0$ (instead of $\mathcal{V}'(r, m, E^{(m,L)}_{min}(r), L) = 0$). Graphically, one may check on figure 10.4 that at the circular geodesic marked with a red (resp. blue) dot, both the red curve $\mathcal{V}^{(\bar{L})}(\,\cdot\,, e)$ (resp. blue curve $\mathcal{V}^{(\bar{L})}(\,\cdot\,, e')$) and function $E^{(\bar{L})}_{min}$ are stationary.

The second derivative of relation (10.4.9) at a circular geodesic $(r_0, m, E^{(m,L)}_{min}(r_0), L)$ (to use $E^{(m,L)'}_{min}(r_0) = 0$) merely yields

$$E^{(m,L)''}_{min}(r_0) = -\frac{\mathcal{V}^{(m,L)''}\left(r_0, E^{(m,L)}_{min}(r_0)\right)}{\partial_E \mathcal{V}^{(m,L)}\left(r_0, E^{(m,L)}_{min}(r_0)\right)} \tag{10.4.11}$$

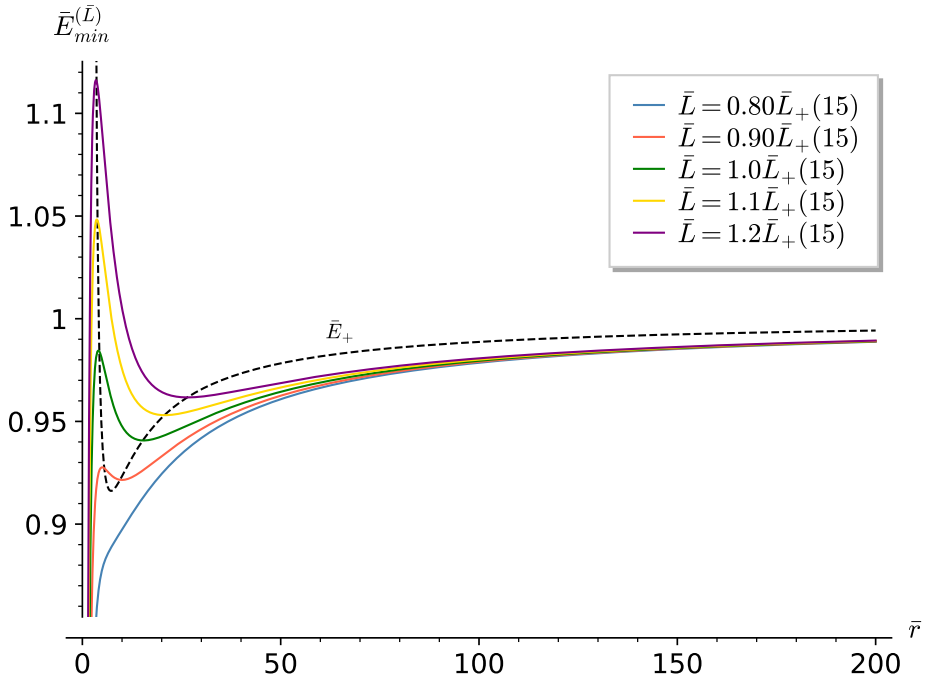

Figure 10.5: Function $\bar{E}_{min}^{(\bar{L})}$ of massive particles for various positive $\bar{L}$ in a Kerr spacetime ($a/M \simeq 0.52$).

which has the same sign has $\mathcal{V}^{(m,L)\prime\prime}(r_0, E_{min}^{(m,L)}(r_0))$ because of (10.4.7). Therefore, such circular geodesic is stable *iff* $E_{min}^{(m,L)\prime\prime}(r_0) > 0$ (instead of $\mathcal{V}''(r_0, m, E_{min}^{(m,L)}(r_0), L) > 0$). Graphically, one may check on figure 10.4 that at the stable (resp. unstable) circular geodesic marked with a red (resp. blue) dot, both the red curve $\mathcal{V}^{(\bar{L})}(\,\cdot\,, e)$ (resp. blue curve $\mathcal{V}^{(\bar{L})}(\,\cdot\,, e')$) and function $E_{min}^{(\bar{L})}$ are convex (resp. concave).

It is thus possible to determine the location and stability of circular geodesics at fixed m and L from the function $E_{min}^{(m,L)}$ rather than $\mathcal{V}^{(m,L)}$. In this case, one would then study the dependence of $E_{min}^{(m,L)}$ on the parameter L (graphically, changing L deforms the yellow surface in figure 10.4 and hence the black curve). Figure 10.5 illustrates this for a Kerr spacetime. At fixed $L = L_0$, circular geodesics correspond to the stationary points. But then, for any stationary point (r_0, E_0), E_0 is necessarily equal to $E_\pm(r_0)$ (the sign depending on whether the orbit is prograde or retrograde) which is why the black dashed curve intersects each coloured curve at its stationary points.

Non circular geodesics with Killing energy E are possible where $E > E_{min}^{(m,L)}$. Graphically, such a geodesic covers the region where the horizontal line E is above $E_{min}^{(m,L)}$ while the abscissae of their intersections locate the periapsis and apoapsis of the geodesic.

Despite providing another interesting point of view on geodesics and stability criteria, using $E_{min}^{(m,L)}$ to investigate stability is laborious since it requires to locate the circular geodesics and evaluate convexity for each L. Instead, it is much more efficient and exhaustive to focus on the sign of the two functions $\mathcal{V}''_\pm$ given by (10.4.3), as illustrated for Kerr with figure 10.3c above.

Finally, it is interesting for practical use to mention that the existence of a bounded non-circular orbit strongly suggests the existence of a stable circular orbit at some radius

between its apsides, as one would expect intuitively. Denote m, E and L the mass, Killing energy and angular momentum of a particle following a bounded non-circular orbit such as the solid blue line in figure 10.1b ruled by the right, negative, bounded branch of the bottom blue curve of figure 10.1a. The argument is that $\mathcal{V}(\,\cdot\,, m, E, L))$ necessarily admits a local minimum at some r_0 between its apsides, i.e. such that

$$\mathcal{V}(r_0, m, E, L) < 0, \tag{10.4.12}$$
$$\mathcal{V}'(r_0, m, E, L) = 0, \tag{10.4.13}$$
$$\mathcal{V}''(r_0, m, E, L) > 0. \tag{10.4.14}$$

Since $\mathcal{V}(r, m, 0, 0) > 0$ and $\mathcal{V}(r, m, E, L) < 0$, there necessarily exists a strictly positive factor α rescaling E and L in such a way that

$$\mathcal{V}(r, m, \alpha E, \alpha L) = 0. \tag{10.4.15}$$

Defining

$$\mathcal{X}(r, m, E, L) = \frac{1}{2A^2}\left[-\left(\frac{E - \omega L}{N}\right)^2 + \left(\frac{L}{Br}\right)^2\right] \tag{10.4.16}$$

so that $\mathcal{V} = 1/(2A^2) + \mathcal{X}$, one has, for any β,

$$\mathcal{V}'(r_0, m, \beta E, \beta L) \approx \mathcal{X}'(r_0, m, \beta E, \beta L) = \beta^2 \mathcal{X}'(r_0, m, E, L), \tag{10.4.17}$$
$$\mathcal{V}''(r_0, m, \beta E, \beta L) \approx \mathcal{X}''(r_0, m, \beta E, \beta L) = \beta^2 \mathcal{X}''(r_0, m, E, L) \tag{10.4.18}$$

far from the strong-field region (so that A slowly varies) where most stars orbiting a central object would be observed. The quantities (10.4.17) and (10.4.18) cancel for $\beta = 1$ according to (10.4.13) and (10.4.14), which implies the same for $\beta = \alpha$. The parameters $(r_0, m, \alpha E, \alpha L)$ are thus close to define a stable circular orbit, and it should generally be possible to finish tuning them to obtain an exact stable circular orbit. This makes the previously discussed stability criteria for circular orbits relevant for observations although no exactly circular orbit exists; this means for instance that observing a star on a non-circular orbit around a black hole logically requires the ISCO to be located below the apoapsis of the star orbit.

Chapter 11

Orbits in cubic Galileon black hole spacetimes

Contents

As mentioned in section 3.2, trajectories of stars and images of accretion disks orbiting black holes provide some of the main observables to test strong-field gravity. For comparison, the theoretical predictions for these observables have been worked out within various frameworks, starting with the Kerr black hole but also other, more or less exotic objects like rotating black holes dressed with a complex scalar hair [310] (i.e. the "Kerr black holes with scalar-hair" mentioned in section 6.2), boson stars [311], regular black holes and wormholes [312]. In return, such analyses may constrain the nature of the observed objects, but also the theory in which they are modelled. This thus helps assessing the viability of modified theories of gravity. To this end, the present chapter compares geodesic motion around black holes in GR and the cubic Galileon theory, while chapter 12 will consider images produced by an accretion disk orbiting these black holes.

11.1 Static and spherically symmetric case

To study the geodesics of the cubic Galileon static and spherically symmetric spacetimes ($\omega = 0$ and metric independent of θ) obtained in section 9, the procedure is to first characterize the circular geodesics. As mentioned in section 10, regions of positive discriminant (10.3.21) are first checked on figure 11.1a for different couplings ($\bar{\gamma} = 0$ corresponds to Schwarzschild). Function D appears positive everywhere down to the horizon[48], where it diverges because of division by the lapse N which cancels at the horizon. Therefore, circular geodesics a priori exist everywhere for all couplings, but they necessarily become superluminal near the horizon according to (10.3.22).

This is what figure 11.1b confirms: for each coupling, velocity diverge at the horizon so that there exists a photon ring (marked with a vertical line from 0 to 1), only

[48]The fact that D and N' are positive everywhere implies that the denominator in (10.3.22) is positive. Therefore, $V_+ > 0$ (prograde orbit) and $V_- = -V_+ < 0$ (retrograde).

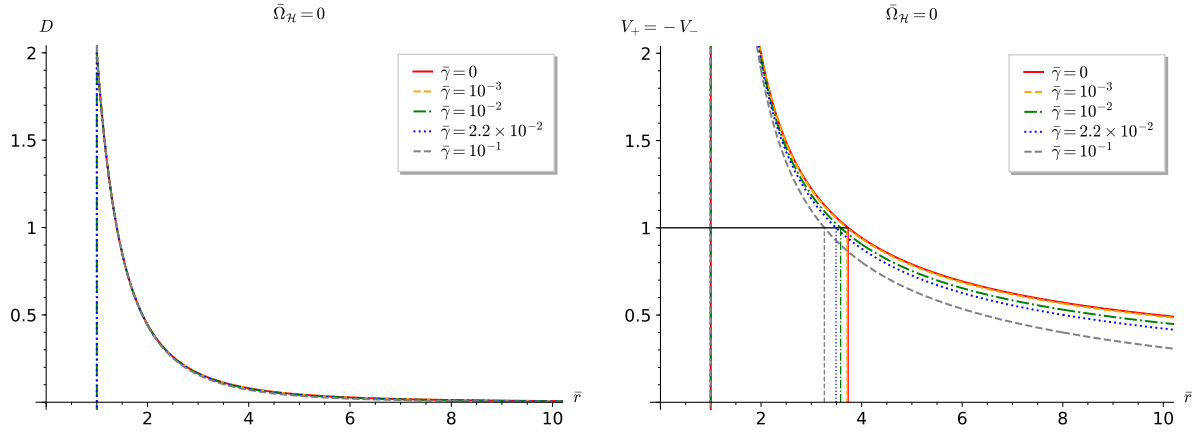

(a) Radial profile of function D whose positivity allows (possibly superluminal) circular geodesics.

(b) Velocities and photon rings.

Figure 11.1: Radial profiles of D and the resulting velocities of circular geodesics in the static, spherically symmetric case (i.e. vanishing dimensionless angular velocity of the event horizon $\bar{\Omega}_{\mathcal{H}} = r_{\mathcal{H}}\Omega_{\mathcal{H}}$) for various couplings.

beyond which timelike circular geodesics exist. Although D does not vary much with coupling on figure 11.1a, the velocities more strongly depend on $\bar{\gamma}$ because function B in the denominator does (see figure 9.1b, knowing that $B = A$ everywhere in spherical symmetry). More precisely, at fixed radius, the velocity of the circular geodesic decreases with coupling. As a consequence, the photon ring gets closer to the horizon as $\bar{\gamma}$ increases.

These results are related to the following facts, detailed in section 9.2.1. The metric functions N and $A = B$ converge faster to Minkowski at infinity as $\bar{\gamma}$ increases. Therefore, at fixed radius away from the strong-field region, gravitation gets naively weaker as $\bar{\gamma}$ increases, so that the velocity of the circular geodesic must be smaller. In addition, for any $\bar{\gamma} \neq 0$, convergence to Minkowski is always much faster than Schwarzschild: N and $A = B$ converge to 1 like $1/r^4$ rather than $1/r$, yielding a vanishing Komar mass at infinity. As a result, velocities given by (10.3.22) converge to zero like $r^{-\alpha/2}$ with $\alpha = 1$ for Schwarzschild and $\alpha = 4$ for the Galileon.

Such asymptotic behaviour are revealed in figures 11.2. In all cases, the Lorentz factor displayed in figure 11.2a logically converges to 1. However, the Killing angular momentum per unit mass $\bar{L}$ displayed in figure 11.2b behaves like $rV \simeq r^{1-\alpha/2}$ according to (10.3.23), hence the divergence for Schwarzschild and convergence to zero for any $\bar{\gamma} \neq 0$ (the numerical solutions contain information at infinity confirming this, even for small couplings like $\bar{\gamma} = 10^{-3}$ whose convergence to zero becomes apparent very far from the horizon). Finally, function ω converges to 0 like $1/r^3$ regardless of whether $\bar{\gamma}$ is zero or not, so that $\bar{E}$, given by (10.3.24), converges to 1 for all cases on figure 11.2c. At the photon ring, all the kinematic quantities displayed in figure 11.2 naturally diverge.

Figure 11.3 assesses the stability of circular orbits based on function $\mathcal{V}''_{\pm}$ given by (10.4.3). As explained in section 10, its sign at a given radial coordinate r_0 is the same as the second radial derivative of the potential evaluated at r_0 with the Killing energy and angular momentum of the circular geodesic at r_0. Figures 11.4a and 11.4b

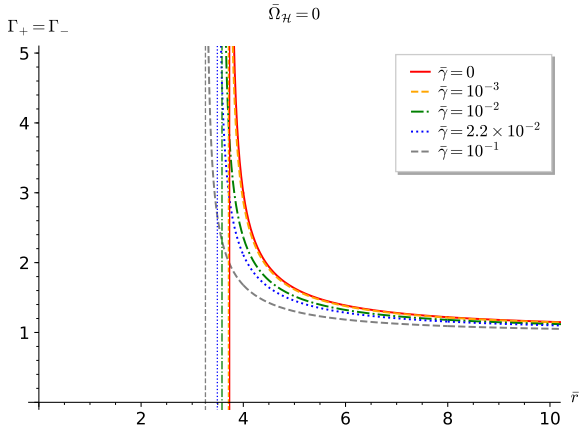

(a) Lorentz factor.

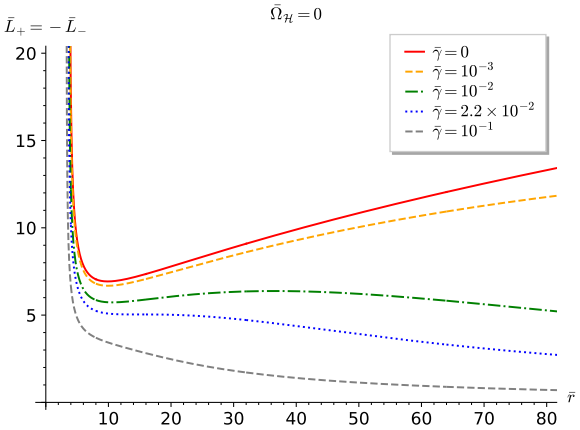

(b) Killing angular momentum.

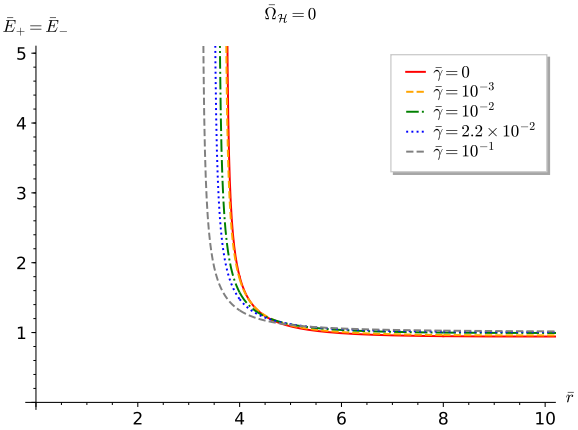

(c) Killing energy.

Figure 11.2: Radial profiles of kinematic quantities measured by the ZAMO for the timelike circular geodesics in the static, spherically symmetric case for various couplings. They all diverge at the photon ring (yet asymptotes are only plotted for the Lorentz factor).

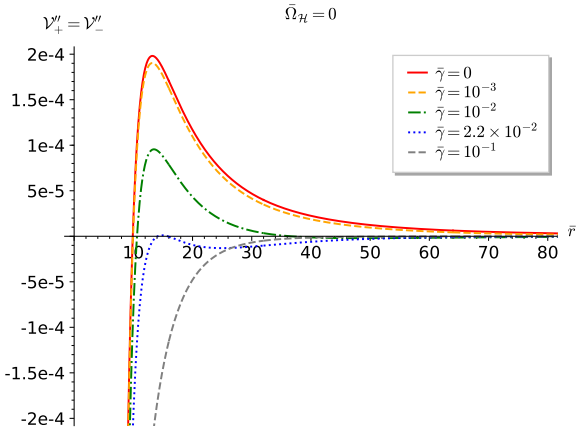

Figure 11.3: Radial profile of $\mathcal{V}''_\pm$; positivity determines stability of the geodesics.

illustrate this for $\bar{\gamma} = 10^{-2}$: for each radii r_0 marked with a dashed vertical line of a given colour, the potential $\mathcal{V}(\,\cdot\,, m, E_\pm(r_0), L_\pm(r_0))$ ruling the circular geodesic at r_0 is plotted with the same colour, and thus cancels in a stationary way at r_0. On figure 11.4c, function $\mathcal{V}''_\pm$ extracts the convexity of $\mathcal{V}(\,\cdot\,, m, E_\pm(r_0), L_\pm(r_0))$ at the corresponding r_0: the purple curve is strongly concave at $r_0 = 5r_{\mathcal{H}}$ on figure 11.4b (hence unstable circular geodesic), so that $\mathcal{V}''_\pm$ is strongly negative at $5r_{\mathcal{H}}$ on figure 11.4c, whereas the brown curve is convex at $r_0 = 20r_{\mathcal{H}}$, so that $\mathcal{V}''_\pm$ is positive at $20r_{\mathcal{H}}$.

Figure 11.3 thus gathers all this information for various couplings. It appears that for any non-zero γ, both an innermost and an outermost stable circular orbit (ISCO and OSCO) exist (they respectively correspond to the smallest and greatest r_0 such that $\mathcal{V}''_\pm(r_0) \geq 0$). However, the existence of an OSCO strongly constrains the Galileon model presently studied because of the mere observation of stars orbiting in a seemingly stable way far from *Sgr A** (yet still in its sphere of dominating influence, so that the orbits are legitimately described by geodesics of an isolated black hole whose stability does not depend on any other physical phenomenon). For instance, the well-known star S2 has a non-circular orbit beyond $280r_{ISCO}$.[49] Although it is non-circular, such a far stable orbit indicates that a stable circular orbit should also exist somewhere between its apsides for some $\bar{E}$ and $\bar{L}$. This strongly suggests that the OSCO should be beyond the orbit of any star ruled by *Sgr A** like S2, which requires $\bar{\gamma}$ much smaller than 10^{-2}.

In addition, $\mathcal{V}''_\pm$ globally decreases as $\bar{\gamma}$ increases. As a result, the ISCO radius increases while the OSCO decreases from infinity (where it is formally located in the Schwarzschild case $\bar{\gamma} = 0$), so that they eventually merge for a critical coupling $\bar{\gamma}^c \simeq 2.2 \times 10^{-2}$, beyond which no stable circular orbit exists anywhere. Therefore, the mere existence of stars orbiting black holes such as *Sgr A** suggests that the Galileon models presently studied are constrained to $\bar{\gamma} < \bar{\gamma}^c$ for viable static, spherically symmetric black holes to exist. Finally, since the photon ring radius decreases (figure 11.1b) while the ISCO radius increases (figure 11.3) when $\bar{\gamma}$ increases, the photon

[49] As the Galileon solutions have vanishing Komar mass at infinity and hence no reference gravitational radius, the ISCO radius provides an unambiguous scale. Besides, the instrument GRAVITY, which is capable of very high astrometric precision, observed flares [15] which are believed to materialize near the inner edge of the accretion disk of *Sgr A** and hence close to the ISCO. Such observation thus provides the ISCO scale for *Sgr A**.

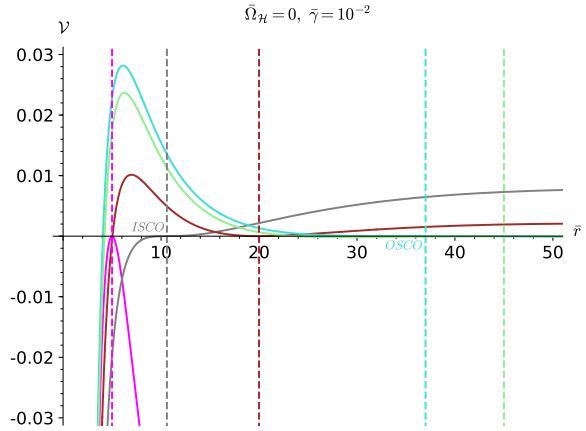

(a) Potentials $\mathcal{V}(\,\cdot\,, m, E_{\pm}(r_0), L_{\pm}(r_0))$ of circular geodesics at various r_0.

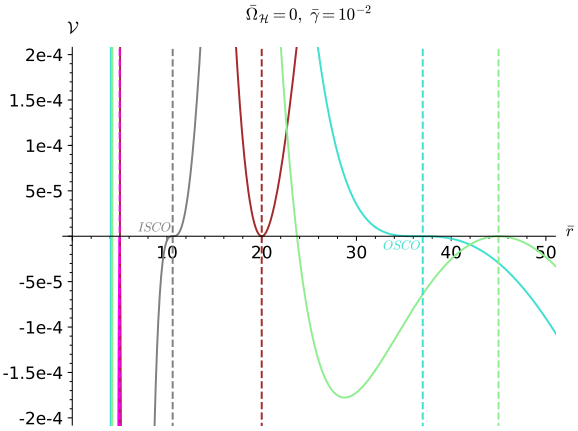

(b) Zoom in figure 11.4a.

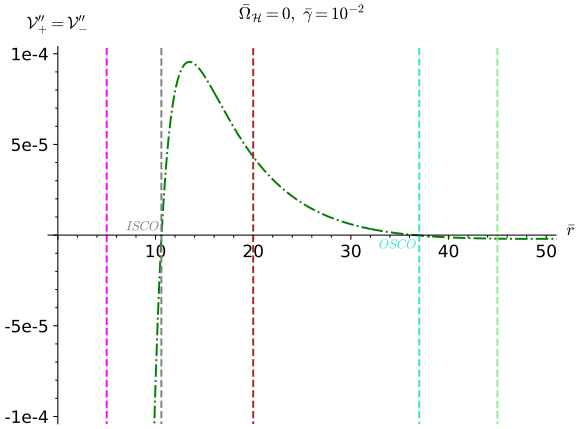

(c) Stability of circular geodesics from function $\mathcal{V}''_{\pm}$.

Figure 11.4: $\mathcal{V}''_{\pm}(r_0)$ is the convexity of $\mathcal{V}(\,\cdot\,, m, E_{\pm}(r_0), L_{\pm}(r_0))$ at r_0.

ring always remains unstable as it is in Schwarzschild.

11.2 Rotating case

Rotation breaks spherical symmetry so that the "+" and "-" quantities are no longer equal or opposite, as shown in figures 11.5 (in which solid lines correspond to the Kerr counterparts). Yet, all these quantities have the same behaviour at the boundaries as in the static, spherically symmetric case commented in section 11.1.

In the static, spherically symmetric case, the fact that $V_+ > 0$ (see footnote 48) means that $B(r) > B(r_{\mathcal{H}})/r$. The latter relation most likely holds in the rotating case[50], which would explain why $V_+ > 0$ and $V_- < 0$ everywhere in the rotating case as well, as is clear from figure 11.5a. However, contrary to the static, spherically symmetric case (red curves), $V_+ \neq V_-$, so that there exist a prograde photon ring and a distinct retrograde one for each angular velocity $\bar{\Omega}_{\mathcal{H}}$; as in Kerr, prograde and retrograde velocities decrease as $\bar{\Omega}_{\mathcal{H}}$ increases, so that the prograde (resp. retrograde) ring radius decreases (resp. increases). The dependence on $\bar{\Omega}_{\mathcal{H}}$ yet seems stronger for Kerr, meaning e.g. that the prograde ring radius decreases faster than for the Galileon solution. As a result, since the photon ring of the static, spherically symmetric Galileon spacetime is below that of Schwarzschild, the relative position of the Kerr and Galileon prograde rings is inverted at some $\bar{\Omega}_{\mathcal{H}}$ ($\simeq 0.03$ for $\bar{\gamma} = 10^{-2}$). On the contrary, the Kerr retrograde ring grows away from its Galileon counterpart.

The fact that the dependence on $\bar{\Omega}_{\mathcal{H}}$ is qualitatively the same for Kerr and the Galileon, but stronger for Kerr, also applies to L (figure 11.5b), E (figures 11.5c and 11.5d) and $\mathcal{V}''_{\pm}$ (figures 11.5e and 11.5f). Besides, $\mathcal{V}''_+$ (resp. $\mathcal{V}''_-$) globally increases (resp. decreases) as $\bar{\Omega}_{\mathcal{H}}$ increases; therefore, both the prograde ISCO and retrograde OSCO (resp. prograde OSCO and retrograde ISCO) radii decrease (resp. increase). Interestingly, $\mathcal{V}''_+$ may thus become positive even for $\bar{\gamma}$ greater than the critical coupling $\bar{\gamma}^c \simeq 2.2 \times 10^{-2}$ (beyond which function $\mathcal{V}''_{\pm}$ is negative everywhere in the non-rotating case) provided rotation is high enough, as illustrated in figure 11.6a for $\bar{\gamma} = 1 > \bar{\gamma}^c$. Therefore, for each coupling $\bar{\gamma} > \bar{\gamma}^c$, there is a minimal angular velocitiy $\bar{\Omega}^{min}_{\mathcal{H}}(\bar{\gamma})$ beyond which stable orbits reappear, yet only prograde ones.

On the contrary, since function $\mathcal{V}''_{\pm}$ is negative everywhere in the non-rotating case, $\mathcal{V}''_-$ gets even more negative with rotation. Therefore, the fact that stars stably orbit *Sgr A** in both directions (the spin direction of *Sgr A** is unknown) suggests that the present Galileon model is constrained to $\bar{\gamma} < \bar{\gamma}^c$ for viable rotating black holes to exist.

As final remarks, since the ISCO of the static, spherically symmetric Galileon spacetime is beyond the Schwarzschild's ISCO and Kerr's retrograde ISCO increases faster with $\bar{\Omega}_{\mathcal{H}}$, the Kerr and Galileon retrograde ISCO merge at some $\bar{\Omega}_{\mathcal{H}}$ ($\simeq 0.06$ for $\bar{\gamma} = 10^{-2}$). As $\bar{\Omega}_{\mathcal{H}}$ increases further, the Galileon retrograde ISCO and OSCO eventually merge for a critical angular velocity $\bar{\Omega}^c_{\mathcal{H}}$ ($\simeq 0.09$ for $\bar{\gamma} = 10^{-2}$), beyond which no stable retrograde orbit exists anywhere. Therefore, even for $\bar{\gamma} < \bar{\gamma}^c$, there exists a critical angular velocity $\bar{\Omega}^c_{\mathcal{H}}(\bar{\gamma})$ beyond which the black hole solutions are not viable.

[50] It is certain beyond $r = B(r_{\mathcal{H}})$ since B monotonically decreases to 1 in all solutions.

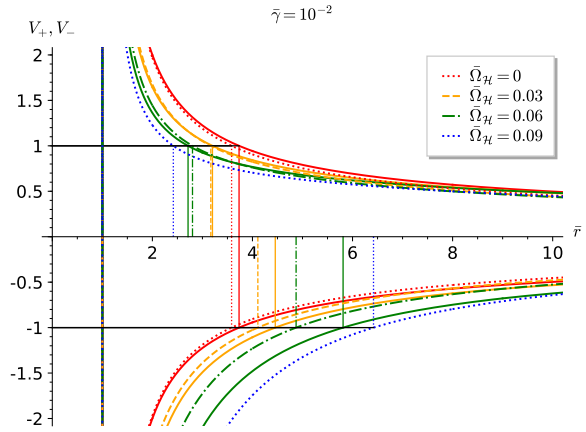

(a) Velocities ($V_+ > 0,\ V_- < 0$) and photon rings.

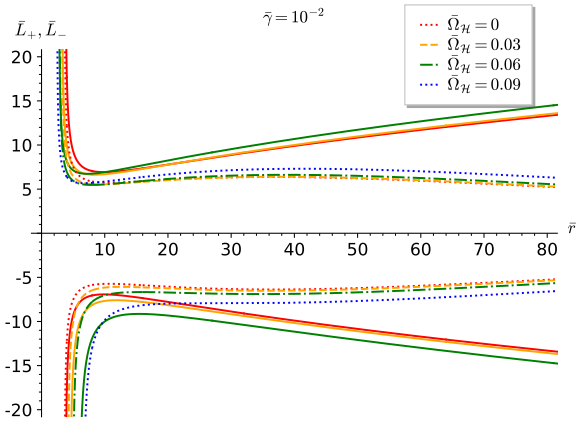

(b) Angular momentum ($\bar{L}_+ > 0,\ \bar{L}_- < 0$).

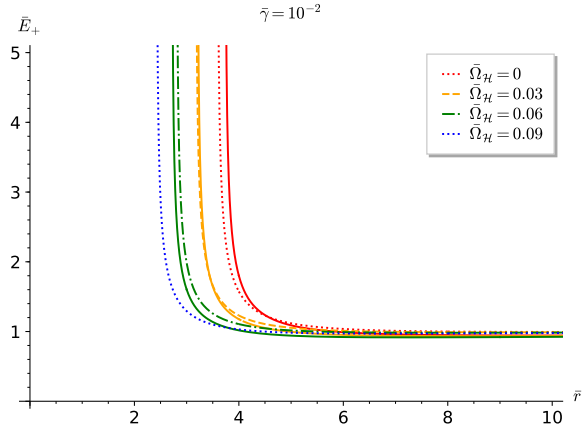

(c) Energy of prograde geodesics.

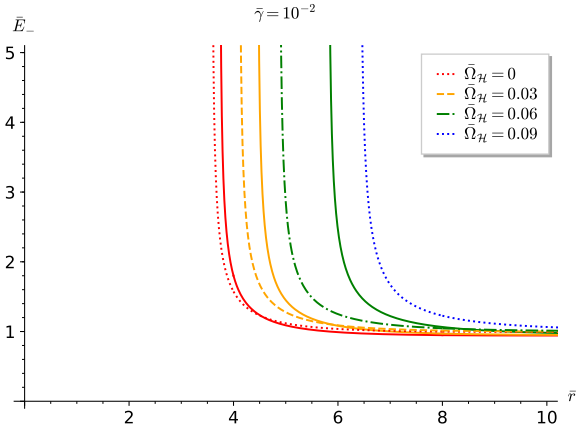

(d) Energy of retrograde geodesics.

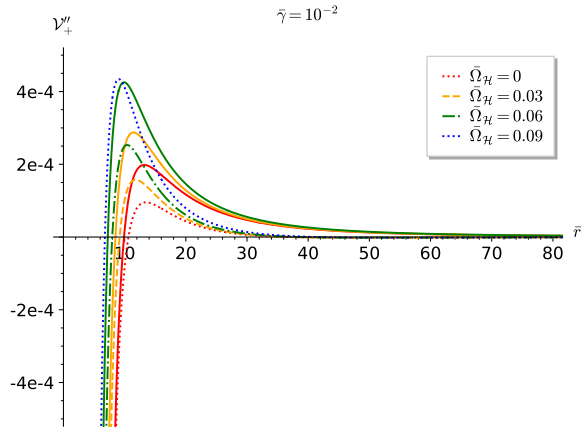

(e) Stability of prograde orbits from function $\mathcal{V}''_+$.

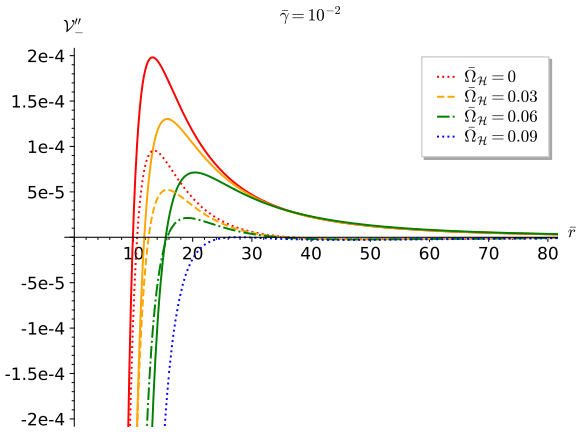

(f) Stability of retrograde orbits from function $\mathcal{V}''_-$.

Figure 11.5: Kinematic quantities measured by the ZAMO and stability of the timelike circular geodesics for different angular velocities $\bar{\Omega}_{\mathcal{H}}$ at fixed coupling $\bar{\gamma} = 10^{-2} < \bar{\gamma}^c$. For comparison at fixed $\bar{\Omega}_{\mathcal{H}}$, the profile in Kerr is plotted as a solid line with the same color.

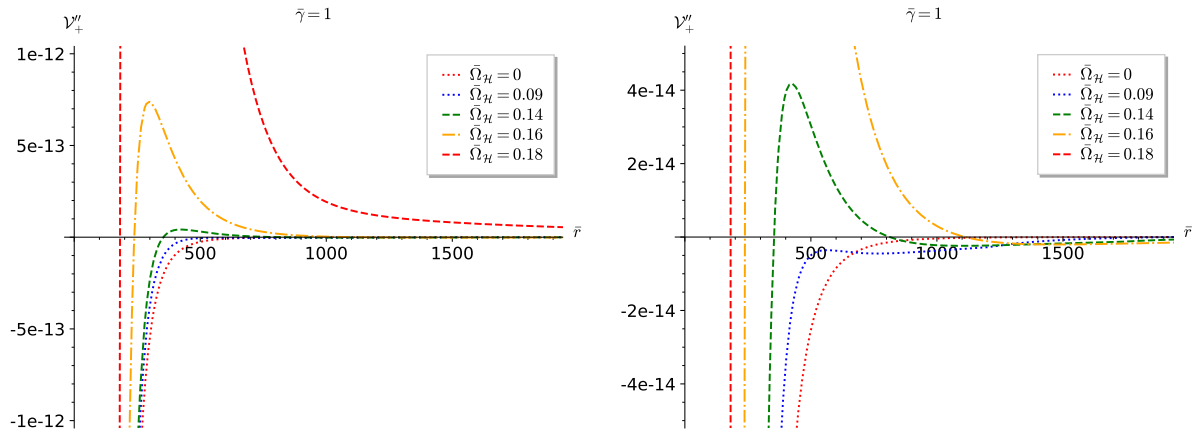

(a) Stability of prograde orbits for $\bar{\gamma} = 1 > \bar{\gamma}^c$.

(b) Zoom in figure 11.6a.

Figure 11.6: Rotation restores prograde stable orbits.

Chapter 12

Images of accretion flows in cubic Galileon black hole spacetimes

Contents

In the sections below, images of an accretion disk orbiting the black hole configurations presented in section 9 are computed numerically with the software *GYOTO*.

12.1 Principle of ray-tracing

GYOTO is a free open-source C++ software [309]. It notably features an efficient approach to integrate the geodesic equations from the knowledge of the 3+1 quantities decomposing the metric according to (3.1.1). This method, exposed in [313], is particularly well-suited for numerical metrics obtained within the 3+1 formalism, which is the case here: the shift β and spatial metric γ corresponding to the spacetime foliation induced by the quasi-isotropic time coordinate t, and the adapted spatial coordinates (r, θ, ϕ), are given by the relations (see e.g. section 2.2.3 of [288])

$$\beta = -\omega \partial_\phi, \tag{12.1.1}$$

$$\gamma = \mathrm{diag}(A^2, A^2 r^2, B^2 r^2 \sin^2\theta). \tag{12.1.2}$$

Images are computed in the following way. An explicit model of accretion flow is set around the black hole[51]. A refracting telescope with a screen in its focal plane is set at a certain point of the numerical metric. In both sections below, the orientation, field of view and distance to the black hole of the telescope qualitatively reproduces the situation of the Event Horizon Telescope with respect to *M87**. Each pixel of the screen

[51] Rough estimates, confirmed by simple exact models of accretion disks coupled to a black hole, show that the gravitational influence of an accretion disk is usually completely negligible with respect to the black hole. Thus, the vacuum metrics computed in section 9 are still completely valid in presence of an accretion disk. See section 6.5 of [11] for quantitative arguments.

corresponds to a spatial direction: space is Euclidean close to the telescope, so that parallel rays converge at the same point on the screen after crossing the converging lens of the instrument. Any of these spatial directions uniquely defines the initial tangent vector of a null affinely parametrized geodesic. The latter is integrated backward in time until a stopping condition is reached, e.g. it falls into the black hole or definitely leaves its neighbourhood. Yet, if the photon reaches the accretion disk at some point, the radiative transfer equations ruling the specific intensity start being integrated as well, as long as the geodesic lies inside the disk (which it can actually enter and leave several times). The geodesic thus accumulates the intensity that will hit the same initial pixel when going forward in time again.

12.2 Model of accretion flow

Determining the nature and properties of a compact object based on the image of its accretion flow is a very degenerate inverse problem. This is for instance evidenced in reference [311] in which the same model of accretion disk is set around either a boson star or a black hole: the differences between the resulting images are very subtle although the natures of the accreting objects are very different. Furthermore, the resolution of present and future instruments like the Event Horizon Telescope is limited, making it even harder to distinguish subtle features.

Then, the prime purpose of numerical images is not necessarily to check whether the exact image constructed by the Event Horizon Telescope [17] can be reproduced for different accreting compact objects. This would require full relativistic magnetohydrodynamics simulations, together with a model of the Event Horizon Telescope itself. Instead, strong efforts are made to propose fairly simple and yet realistic models of accretion disks [298, 314–316]. Comparing the resulting images for different compact objects provides a more efficient, and still relevant, method to evaluate how degenerate the problem is. The hope is that such an approach should help isolating the causes of differences between images, e.g. being able to guess the nature and amplitudes of the modifications that result from changing the accretion model or the theory used to describe it.

As a result, a simple model of accretion disk, recently introduced in [316], is used in the sections below. Like *Sgr A**, supermassive black hole *M87** features a very low-luminosity accretion flow, revealing an inefficient radiative cooling and hence a high temperature. It is consistently modelled as a low accretion rate, geometrically thick, optically thin disk[52] [317]. Besides these properties, only the thermal synchrotron emission is computed, following a method exposed in [318]. In the end, the complete model is described by very few input parameters: the opening angle and inner edge of the disk (which will be set at the ISCO in the next sections), the magnetization parameter (which determines the ambient magnetic field strength), the electron density and temperature at the inner edge (which determine the density and temperature profiles, since these are assumed to scale as $1/r^2$ and $1/r$ respectively).

[52] An accretion disk is geometrically (resp. optically) thin when the opening angle (resp. optical depth) is smaller than 1. It is geometrically (resp. optically) thick otherwise.

12.3 Static and spherically symmetric case

In the static and spherically symmetric case, the ISCO is read from figure 11.3 for each coupling. The resulting images are presented in figure 12.1, from the Schwarzschild limit $\bar{\gamma} = 0$ to the critical coupling $\bar{\gamma}^c \simeq 2.2 \times 10^{-2}$, beyond which no stable accretion disk may exist. The effects of coupling are subtle though perceivable. Before drawing conclusions about the implications and observability of such deviations, more precise investigations must be done. In particular, more realistic models of disk such as ion tori could be considered. These are still geometrically thick and optically thin structures, yet featuring more complex density and temperature profiles derived from first principles, as well as chaotic (i.e. isotropic) [314] or toroidal [315] magnetic fields.

12.4 Rotating case

Figure 12.2 compares the images obtained for rotating solutions in GR (i.e. Kerr black holes) and in the cubic Galileon case $\bar{\gamma} = 10^{-2} < \bar{\gamma}^c$. For these rotating configurations, the inner edge of the disk is set at the prograde ISCO, which is read from figure 11.5e for each angular velocity $\bar{\Omega}_{\mathcal{H}}$. Again, the effects of rotation and coupling are perceivable, but need further work. Furthermore, unsolved issues arose in trying to compute images for higher $\bar{\Omega}_{\mathcal{H}}$, so that the effects of rotation are necessarily weak on figure 12.2. These issues should be fixed soon, and more realistic accretion models should be considered as well.

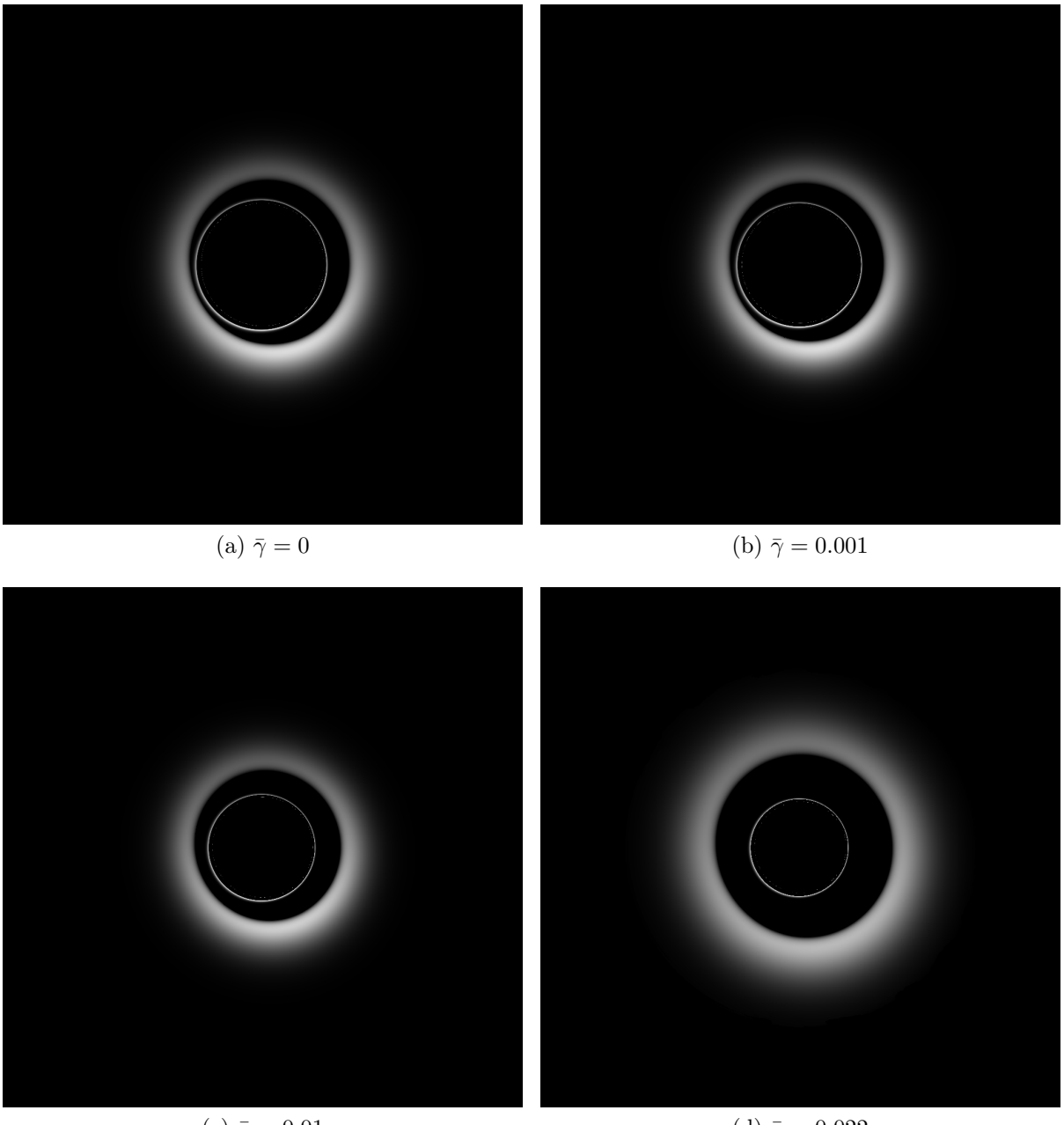

(a) $\bar{\gamma} = 0$ (b) $\bar{\gamma} = 0.001$

(c) $\bar{\gamma} = 0.01$ (d) $\bar{\gamma} = 0.022$

Figure 12.1: Images produced by a thick accretion disk orbiting static and spherically symmetric black holes for different couplings $\bar{\gamma}$.

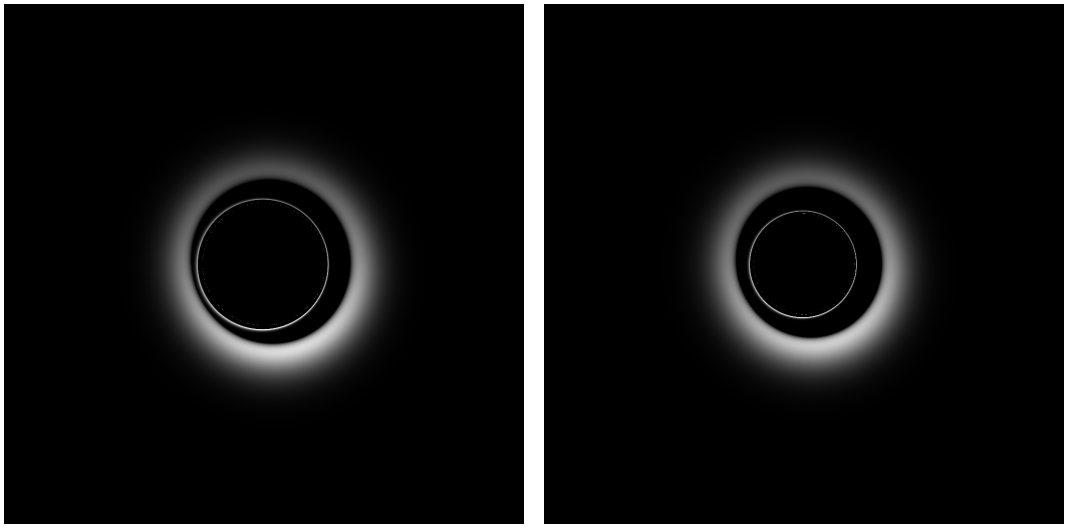

(a) $(\bar{\gamma}, \bar{\Omega}_{\mathcal{H}}) = (0, 0)$

(b) $(\bar{\gamma}, \bar{\Omega}_{\mathcal{H}}) = (0.01, 0)$

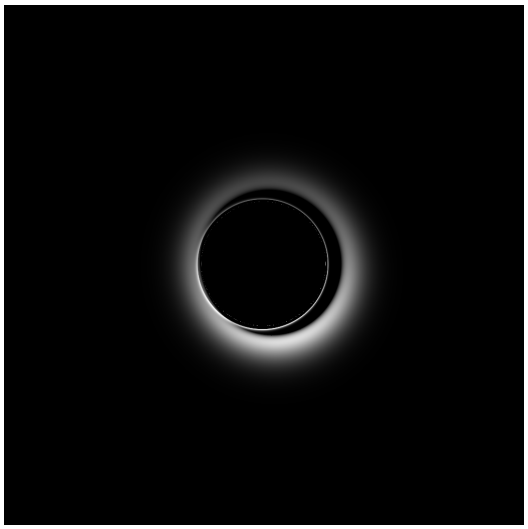

(c) $(\bar{\gamma}, \bar{\Omega}_{\mathcal{H}}) = (0, 0.02)$

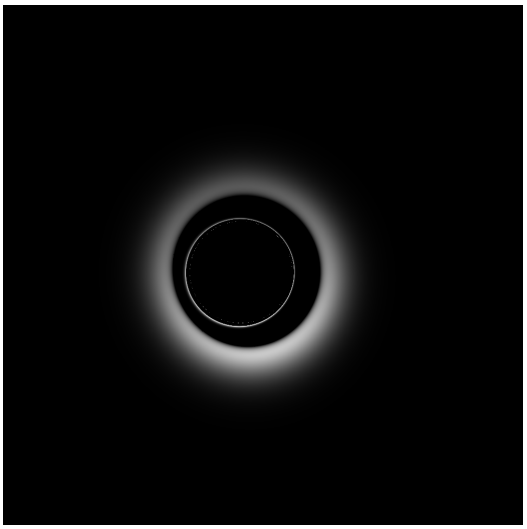

(d) $(\bar{\gamma}, \bar{\Omega}_{\mathcal{H}}) = (0.01, 0.02)$

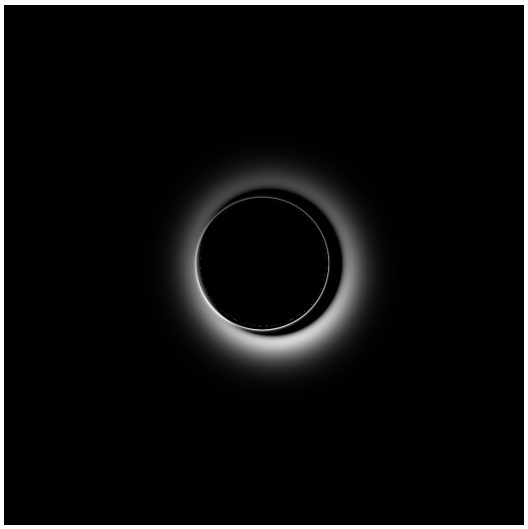

(e) $(\bar{\gamma}, \bar{\Omega}_{\mathcal{H}}) = (0, 0.03)$

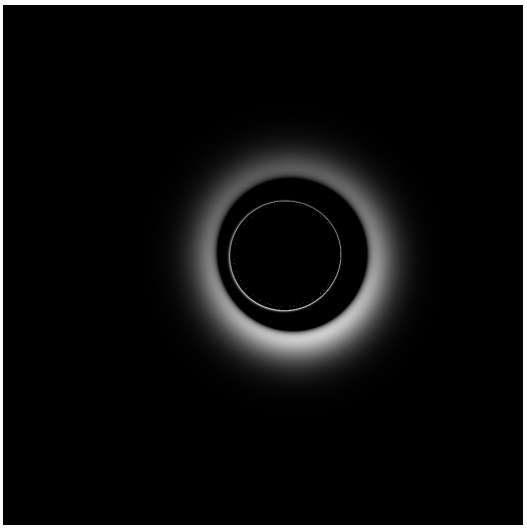

(f) $(\bar{\gamma}, \bar{\Omega}_{\mathcal{H}}) = (0.01, 0.03)$

Figure 12.2: Images produced by a thick accretion disk orbiting Kerr black holes (left images) and rotating black holes of the cubic Galileon theory (right images).

Conclusion

The results reported in this manuscript fall within the wide and long-term effort conducted to constrain theories of gravitation, notably by modelling the physics of compact objects and the different types of radiation they produce. To introduce this context, the objects and principles common to most theories of gravitation have been exposed and discussed, with the overall objective of sketching the arguments leading from these foundations to the (organized) profusion of theories of gravitation.

The actual contribution of the present project has then been presented: investigating possible deviations of the cubic Galileon theory in the neighbourhood of rotating black holes. Like most studies on strong-field phenomena, constructing such black hole metrics required a dedicated numerical approach. Determining the right numerical formulation of the problem (choice of unknown functions, boundary conditions, additional equations) was not straightforward. The resulting numerical configurations are the first ones that describe asymptotically flat hairy rotating black holes in the cubic Galileon theory. They are based on a scalar ansatz involving a linear time-dependence and a circular approximation of the metric. To realize asymptotic flatness, the bare cosmological constant Λ and kinetic coupling η must be set to zero. The solutions are thus dominated by the DGP term $(\partial\phi)^2\Box\phi$. The remaining parameter $\bar{\gamma}$ induces significant deviations from the Kerr metric on different physical quantities such as surface gravity and angular momentum. In addition, these asymptotically flat solutions feature convergence towards Minkowski faster than the Schwarzschild solution, which can be understood as a vanishing Komar mass at infinity.

Extreme angular velocities (and possibly extremal black holes) were not reached numerically, but could be the goal of future work. For consistency, one should then abandon the circular ansatz for the metric, as the corresponding approximation error would become worse for rapidly rotating configurations. A second natural extension of the work presented here would be the construction of asymptotically (anti-)de Sitter solutions, i.e. solutions featuring non-zero cosmological constant or canonical kinetic coupling.

Then, in searching for observable signatures of the cubic Galileon theory, stable bounded timelike geodesics around the Galileon black holes turned out to exist for sufficiently small coupling, in spite of the non-Schwarzschild asymptotics of these black hole metrics. Yet, their existence regions are generically bounded, i.e. they feature an outermost stable circular orbit in addition to the innermost stable circular orbit. Thus, compatibility with observations of stable star orbits around *Sgr A** clearly constrains the dimensionless coupling $\bar{\gamma}$. Finally, the astrophysical imaging of an emitting accretion disk surrounding the Galileon black holes has been simulated, notably based on numerical integration of null geodesics. Yet, further work is required before making quantitative statements about the images produced by such accreting Galileon black

holes. Both these investigations have today a clear astrophysical relevance in regards of the observations realized by the instrument GRAVITY and the Event Horizon Telescope, which test strong-field gravity by accurately monitoring supermassive black holes and their close environment.

As a final remark, all solutions considered in this work were stationary solutions of the cubic Galileon theory, in order to eventually derive predictions that could be compared with supermassive black hole observations. However, regarding accretion flow observations, constraining alternative theories is a highly degenerate problem given the very large number of accretion models and theories, and the relatively low accuracy of the Event Horizon Telescope. Furthermore, the Kerr metric is a solution not only of GR but of many alternative theories as well, including the cubic Galileon. In particular, accretion flows onto stationary supermassive black holes might still be described by the Kerr metric, even if another theory than GR turns out more successful to describe all classical gravitational phenomena. On the contrary, way less ambiguous tests of gravity than accretion flow imaging are provided by perturbative phenomena such as quasi-normal mode signatures in gravitational waves. Prior to such investigations in any given theory, and as mentioned several times in the core of the manuscript, the viability of a theory must notably be assessed from the stability of its stationary configurations. Thus, numerical studies of perturbations around the black holes presented in this work, in one dimension for a start (spherically symmetric perturbations of the static and spherically symmetric solutions), constitute one further future axis of research, which would complete existing analytical studies [242, 244].

Part III

Appendices

Appendix A

No-scalar-hair theorem for the cubic Galileon

A static and spherically symmetric spacetime admits coordinates (t, R, θ, φ) with respect to which the metric can be written as (7.4.1).

If the Galileon field features the same symmetries, it only depends on the radial coordinate R, and the (tR) metric equation (i.e. equation (7.4.2) in which q is set to 0) reads

$$\phi' \left[f\phi' \left(\frac{h'}{h} + \frac{4}{R} \right) - \frac{2\eta}{\gamma} \right] = 0. \tag{A.1}$$

The general no-hair theorem [232, 236] assumes the Galileon Lagrangian to contain a standard kinetic term, i.e. $\eta \neq 0$. Yet, for the cubic Galileon, the case $\eta = 0$ can be included in the theorem, or yields a non-trivial hairy solution if asymptotic flatness is abandoned (see below).

Case $\eta \neq 0$ The metric equation (7.4.3) in which q is set to 0 gives

$$\phi'^2 = -\frac{2\zeta}{\eta} \left[\frac{h'}{Rh} + \frac{1}{f} \left(\frac{f-1}{R^2} + \Lambda \right) \right]. \tag{A.2}$$

Then, the asymptotic flatness requirements (7.4.10)-(7.4.11) imply that $\phi'^2 \longrightarrow -2\zeta\Lambda/\eta$. In particular, ϕ' is bounded at infinity, so that

$$f\phi' \left(\frac{h'}{h} + \frac{4}{R} \right) \longrightarrow 0. \tag{A.3}$$

If the latter term was non-zero at some point, its absolute value would get smaller than e.g. η/γ at some other point while remaining strictly positive, which would require $\phi' \neq 0$. This would contradict (A.1), in which one could simplify the overall factor ϕ' while having no chance for $f\phi'(h'/h + 4/R) = 2\eta/\gamma$ to hold.

Therefore, $f\phi'(h'/h + 4/R)$ must vanish everywhere and equation (A.1) finally implies that ϕ is trivial (up to a meaningless constant shift).

Case $\eta = 0$ A hairy solution would feature non-zero ϕ' on some interval I, which can be assumed to either extend to infinity, or to be such that ϕ' is zero beyond some upper bound. According to (A.1) with $\eta = 0$, one would have

$$h = \frac{h_1}{R^4} \text{ over } I, \tag{A.4}$$

where h_1 is an integration constant (whose sign must be the same as f on I for the metric to be Lorentzian). Yet, the expression (A.4) does not meet with the asymptotic behaviour (7.4.10) so that I cannot extend to infinity. This can also be seen from the metric equation (7.4.3) in which η is set to 0:

$$f = \left(\frac{1}{R^2} - \Lambda\right)\left(\frac{h'}{Rh} + \frac{1}{R^2}\right)^{-1} = \frac{\Lambda R^2 - 1}{3} \text{ over } I, \tag{A.5}$$

which does not meet with the asymptotic behaviour (7.4.11) either.

Therefore ϕ' should vanish at some point R_0 and remain zero up to infinity; whether this is possible to realize in a smooth way or not relies on the equation (A.10) which provides the expression of ϕ' on I. But anyway, beyond R_0, h and f would become Schwarzschild, with no chance to match (A.4) and (A.5) at R_0 in a smooth way:

$$h = f = 1 - \frac{4R_0}{3R}, \ R \geq R_0, \tag{A.6}$$

so that only the Schwarzschild behaviour outside the event horizon located at $R = 4R_0/3$ and a trivial Galileon remain meaningful.

Solutions with $\eta = 0$ Abandoning asymptotic flatness allows us to use the expressions (A.4) and (A.5) everywhere up to infinity, and thus inject them into equation (7.4.4) in which q and η are set to 0. The resulting equation takes the form

$$\left[\left(R^2\sqrt{fh}\phi'\right)^3\right]' = \frac{2\zeta}{\gamma}G'_\Lambda, \tag{A.7}$$

where

$$G'_\Lambda = \left(\frac{2}{R^2} - 3\Lambda\right)\sqrt{\frac{3h_1^3}{\Lambda R^2 - 1}}, \tag{A.8}$$

which integrates into

$$G_\Lambda = \begin{cases} \sqrt{3h_1^3}\left[\frac{2\sqrt{\Lambda R^2-1}}{R} - 3\sqrt{\Lambda}\text{arcosh}\left(\sqrt{\Lambda}R\right)\right] & \text{if } \Lambda > 0,\ R > \frac{1}{\sqrt{\Lambda}} \text{ and hence } h_1 > 0, \\ -\sqrt{3|h_1|^3}\left[\frac{2\sqrt{1-\Lambda R^2}}{R} + 3\sqrt{\Lambda}\text{arcsin}\left(\sqrt{\Lambda}R\right)\right] & \text{if } \Lambda > 0,\ R < \frac{1}{\sqrt{\Lambda}} \text{ and hence } h_1 < 0, \\ \sqrt{3|h_1|^3}\left[-\frac{2\sqrt{1-\Lambda R^2}}{R} + 3\sqrt{|\Lambda|}\text{arsinh}\left(\sqrt{|\Lambda|}R\right)\right] & \text{if } \Lambda \leq 0 \text{ and hence } h_1 < 0. \end{cases} \tag{A.9}$$

In any case, one finally has

$$\phi' = \sqrt{\frac{3}{h_1\left(\Lambda R^2 - 1\right)}} \left(\frac{2\gamma}{\zeta} G_\Lambda + \alpha\right)^{1/3}, \tag{A.10}$$

where α is an integration constant.

If $\Lambda \leq 0$, then t is a spacelike coordinate and R is timelike, so that the expressions (A.4), (A.5) and (A.10) describe a time-dependent metric and a homogeneous, time-dependent scalar field. It is also the case if $\Lambda > 0$ and $R < 1/\sqrt{\Lambda}$, so that the time coordinate R is bounded, like the interior Schwarzschild solution. Finally, if $\Lambda > 0$, the expressions (A.4), (A.5) and (A.10) describe the exterior domain of a hairy black hole spacetime with an event horizon located at $R = 1/\sqrt{\Lambda}$. Asymptotically, ϕ' converges to zero as $\ln(R)/R$.

Appendix B

Source terms and scalar equation

The explicit expressions of the source terms and the scalar equation exposed below are justified in a Jupyter notebook based on the free software *SageMath*[53]. The notebook is available at the following url: https://share.cocalc.com/share/6cfa5f27-1564-4bd8-9b0c-fcb3c7d0f325/2019-09-29-155358/metric_and_scalar_equations_cubic_Galileon.ipynb?viewer=share (in which the equation numbers and references mentioned in the explanatory parts correspond to those of the article [281]). The steps are also summarized below, where the following notations are used for any functions f, g and h of $\bar{r}$ and θ:

$$\partial f \partial g = \partial_{\bar{r}} f \, \partial_{\bar{r}} g + \frac{1}{\bar{r}^2} \partial_\theta f \, \partial_\theta g, \tag{B.1}$$

$$\mathcal{H}_f^{(0)}[g,h] = \begin{pmatrix} \partial_{\bar{r}} g \\ \frac{1}{\bar{r}} \partial_\theta g \end{pmatrix}^T \begin{pmatrix} \partial^2_{\bar{r}\bar{r}} f & \frac{1}{\bar{r}} \partial^2_{\bar{r}\theta} f \\ \frac{1}{\bar{r}} \partial^2_{\bar{r}\theta} f & \frac{1}{\bar{r}^2} \partial^2_{\theta\theta} f \end{pmatrix} \begin{pmatrix} \partial_{\bar{r}} h \\ \frac{1}{\bar{r}} \partial_\theta h \end{pmatrix}, \tag{B.2}$$

$$\mathcal{H}_f^{(1)}[g,h] = \begin{pmatrix} \frac{1}{\bar{r}} \partial_\theta g \\ -\partial_{\bar{r}} g \end{pmatrix}^T \begin{pmatrix} \partial^2_{\bar{r}\bar{r}} f & \frac{1}{\bar{r}} \partial^2_{\bar{r}\theta} f \\ \frac{1}{\bar{r}} \partial^2_{\bar{r}\theta} f & \frac{1}{\bar{r}^2} \partial^2_{\theta\theta} f \end{pmatrix} \begin{pmatrix} \frac{1}{\bar{r}} \partial_\theta h \\ -\partial_{\bar{r}} h \end{pmatrix}, \tag{B.3}$$

$$\mathcal{H}_f^{(2)}[g,h] = \begin{pmatrix} \partial_{\bar{r}} g \\ \frac{1}{\bar{r}} \partial_\theta g \end{pmatrix}^T \begin{pmatrix} \partial^2_{\bar{r}\bar{r}} f & \frac{2}{\bar{r}} \partial^2_{\bar{r}\theta} f \\ \frac{2}{\bar{r}} \partial^2_{\bar{r}\theta} f & \frac{1}{\bar{r}^2} \partial^2_{\theta\theta} f \end{pmatrix} \begin{pmatrix} \partial_{\bar{r}} h \\ \frac{1}{\bar{r}} \partial_\theta h \end{pmatrix}. \tag{B.4}$$

Then, the right-hand side terms of equations (7.3.10)-(7.3.13) read

$$\begin{aligned} \mathcal{S}_N = & \frac{N \left(B \bar{r} \sin\theta\right)^2}{2} \partial\bar{\omega}\partial\bar{\omega} - \frac{N^2}{B} \partial N \partial B - N A^2 \left(\bar{\eta} + \bar{\Lambda} N^2\right) \\ & - \frac{\bar{\gamma}}{2} \left(1 + \frac{N^2 \partial\bar{\Psi}\partial\bar{\Psi}}{A^2}\right) \left(N \Delta_3 \bar{\Psi} + \partial\bar{\Psi}\partial N + \frac{N \partial\bar{\Psi}\partial B}{B}\right), \end{aligned} \tag{B.5}$$

$$\begin{aligned} \mathcal{S}_A = & \frac{N^4}{A} \partial A \partial A + 2 N^3 \partial A \partial N + \frac{3A(NB\bar{r}\sin\theta)^2}{4} \partial\bar{\omega}\partial\bar{\omega} \\ & + \frac{\bar{\eta} N^2 A}{2} \left(N^2 \partial\bar{\Psi}\partial\bar{\Psi} - A^2\right) - \bar{\Lambda} A^3 N^4 \\ & - \bar{\gamma} \left(N A \partial\bar{\Psi}\partial N - \frac{N^4 \partial\bar{\Psi}\partial\bar{\Psi}\ \partial\bar{\Psi}\partial A}{A^2} \right. \\ & \left. + \frac{1}{A} \left[N^4 \mathcal{H}^{(0)}_{\bar{\Psi}}[\bar{\Psi},\bar{\Psi}] - \frac{N^4 \partial_r \bar{\Psi}}{\bar{r}^3} \left(\partial_\theta \bar{\Psi}\right)^2 \right] \right), \end{aligned} \tag{B.6}$$

[53] https://www.sagemath.org, https://sagemanifolds.obspm.fr

$$\mathcal{S}_B = -B\bar{r}\sin\theta\left[NA^2\left(\bar{\eta}+2\bar{\Lambda}N^2\right) + \frac{\bar{\gamma}N^2\partial\bar{\Psi}\partial\bar{\Psi}}{A^2}\left(N\Delta_3\bar{\Psi}+\partial\bar{\Psi}\partial N+\frac{N\partial\bar{\Psi}\partial B}{B}\right)\right], \quad \text{(B.7)}$$

$$\mathcal{S}_{\bar{\omega}} = \frac{N\bar{\omega}}{\bar{r}\sin\theta} + \bar{r}\sin\theta\left(\partial\bar{\omega}\partial N - \frac{3N}{B}\partial\bar{\omega}\partial B\right) \quad \text{(B.8)}$$

and the scalar equation takes the form

$$\begin{aligned}
0 =& -\bar{\eta}N^3A^2\left(N\Delta_3\bar{\Psi}+\partial\bar{\Psi}\partial N+\frac{N\partial\bar{\Psi}\partial B}{B}\right)\\
&+\bar{\gamma}\left\{A^2\left(N\Delta_3 N+\frac{N}{B}\partial N\partial B-2\partial N\partial N\right)\right.\\
&\quad+2N\left(N\Delta_3\bar{\Psi}+\partial\bar{\Psi}\partial N+\frac{N\partial\bar{\Psi}\partial B}{B}\right)\left(\frac{N^2\partial\bar{\Psi}\partial A}{A}-N\partial\bar{\Psi}\partial N\right)\\
&\quad-2\left(N^2\Delta_2\bar{\Psi}+\frac{N^2\partial\bar{\Psi}\partial B}{B}\right)\left(N^2\Delta_3\bar{\Psi}-\frac{N^2\partial_{\bar{r}}\bar{\Psi}}{\bar{r}}\right)\\
&\quad+\frac{2N^2}{\bar{r}^2}\partial^2_{\theta\theta}\bar{\Psi}\left(N^2\Delta_2\bar{\Psi}-\frac{N^2\partial\bar{\Psi}\partial A}{A}\right)\\
&\quad-N^3\partial\bar{\Psi}\partial\bar{\Psi}\left(\frac{N}{A}\left[\Delta_3 A-\frac{4}{\bar{r}}\partial_{\bar{r}}A\right]+\frac{N}{B}\Delta_2 B+\frac{\partial N\partial A}{A}-\frac{3N}{A^2}\partial A\partial A+\frac{N}{AB}\partial A\partial B\right)\\
&\quad+2\left(N\partial\bar{\Psi}\partial N\right)^2\\
&\quad-N^3\,\mathcal{H}^{(0)}_N[\bar{\Psi},\bar{\Psi}]\\
&\quad+\frac{N^4\mathcal{H}^{(1)}_B[\bar{\Psi},\bar{\Psi}]}{B}\\
&\quad-\frac{2N^4\mathcal{H}^{(2)}_{\bar{\Psi}}[\bar{\Psi},A]}{A}\\
&\quad+2\left(\left[N^2\partial^2_{\bar{r}\bar{r}}\bar{\Psi}\right]^2+\left[\frac{N^2}{\bar{r}^2}\partial_\theta\bar{\Psi}-\frac{N^2\partial_{\bar{r}\theta}\bar{\Psi}}{\bar{r}}\right]^2\right)\\
&\quad-\frac{2N^2\partial_{\bar{r}}\bar{\Psi}\partial_{\bar{r}}A}{A}\left(N^2\partial^2_{\bar{r}\bar{r}}\bar{\Psi}+\frac{2N^2\partial_{\bar{r}}\bar{\Psi}}{\bar{r}}-\frac{N^2}{\bar{r}^2}\partial^2_{\theta\theta}\bar{\Psi}\right)\\
&\quad-\frac{N^4(\partial_{\bar{r}}\bar{\Psi})^2}{\bar{r}}\frac{\partial_{\bar{r}}B}{B}\\
&\quad\left.+\frac{N^2}{\bar{r}^3}\partial_\theta\bar{\Psi}\left(2N\partial_{\bar{r}}\bar{\Psi}\partial_\theta N-N\partial_\theta\bar{\Psi}\partial_{\bar{r}}N\right)\right\}. \quad \text{(B.9)}
\end{aligned}$$

The function N could be factored out in many places but instead it is explicitly left everywhere it is needed to counterbalance divergences on the horizon. More precisely, it appears as a factor in front of all the quantities that involve the radial derivative of $\bar{\Psi}$, in order to form terms that remain finite on the horizon.

Appendix C

Kerr metric in quasi-isotropic coordinates

Denoting M the mass and a the spin parameter, the four metric functions involved in the quasi-isotropic expression (7.2.2) of the Kerr metric explicitly write as

$$N^2 = \frac{\Sigma\Delta}{\Sigma(R^2+a^2)+2a^2MR\sin^2\theta}, \tag{C.1}$$

$$A^2 = \frac{\Sigma}{r^2}, \tag{C.2}$$

$$B^2 = \frac{1}{r^2}\left(R^2+a^2+\frac{2a^2MR\sin^2\theta}{\Sigma}\right), \tag{C.3}$$

$$\omega = \frac{2aMR}{\Sigma(R^2+a^2)+2a^2MR\sin^2\theta}, \tag{C.4}$$

$$\tag{C.5}$$

where

$$R = r + \frac{M^2-a^2}{4r} + M, \tag{C.6}$$

$$\Sigma = R^2 + a^2\cos^2\theta, \tag{C.7}$$

$$\Delta = R^2 + a^2 - 2MR. \tag{C.8}$$

The function R defined by relation (C.6) actually corresponds to the radial coordinate of the Boyer-Lindquist system (which is presented e.g. in section 33.2 of [52]). It is inverted as

$$r = \frac{1}{2}\left(R + \sqrt{R^2-2MR+a^2} - M\right). \tag{C.9}$$

The remaining coordinates are identical in the quasi-isotropic and Boyer-Lindquist systems.

Bibliography

[1] B. P. Abbott et al. 'Gravitational Waves and Gamma-Rays from a Binary Neutron Star Merger: GW170817 and GRB170817A'. *ApJ* **848**.2 (2017), p. L13.

[2] B. P. Abbott et al. 'GW170817: Observation of Gravitational Waves from a Binary Neutron Star Inspiral'. *Phys. Rev. Lett.* **119**.16 (2017), p. 161101.

[3] B. P. Abbott et al. 'GWTC-1: A Gravitational-Wave Transient Catalog of Compact Binary Mergers Observed by LIGO and Virgo during the First and Second Observing Runs' (2018).

[4] B. P. Abbott et al. 'Observation of Gravitational Waves from a Binary Black Hole Merger'. *Phys. Rev. Lett.* **116**.6 (2016), p. 061102.

[5] A. Goldstein et al. 'An Ordinary Short Gamma-Ray Burst with Extraordinary Implications: Fermi-GBM Detection of GRB 170817A'. *ApJ* **848**.2 (2017), p. L14.

[6] V. Savchenko et al. 'INTEGRAL Detection of the First Prompt Gamma-Ray Signal Coincident with the Gravitational-wave Event GW170817'. *ApJ* **848**.2 (2017), p. L15.

[7] P. F. Michelson, W. B. Atwood and S. Ritz. 'Fermi Gamma-ray Space Telescope: high-energy results from the first year'. *Rep. Prog. Phys.* **73**.7 (2010), p. 074901.

[8] J. Strobl, R. Hudec, V. Simon and F. Hroch. 'ESA INTEGRAL and Cataclysmic Variables'. *Odessa Astronomical Publications* **16** (2003), p. 77.

[9] I. H. Stairs. 'Testing General Relativity with Pulsar Timing'. *Living Rev. Relativ.* **6**.1 (2003), p. 5.

[10] C. M. Will. 'The Confrontation between General Relativity and Experiment'. *Living Rev. Relativ.* **17**.1 (2014), p. 4.

[11] C. Bambi. 'Black Holes: A Laboratory for Testing Strong Gravity'. Springer, 2017.

[12] R. Abuter et al. 'First light for GRAVITY: Phase referencing optical interferometry for the Very Large Telescope Interferometer'. *A&A* **602** (2017), A94.

[13] S. Doeleman et al. 'Imaging an Event Horizon: submm-VLBI of a Super Massive Black Hole'. *ASTRO2010 Decadal Review Panels* (2009).

[14] GRAVITY Collaboration. 'Detection of the gravitational redshift in the orbit of the star S2 near the Galactic centre massive black hole'. *A&A* **615** (2018), p. L15.

[15] GRAVITY Collaboration. 'Detection of orbital motions near the last stable circular orbit of the massive black hole SgrA*'. *A&A* **618** (2018), p. L10.

[16] S. Issaoun et al. 'The Size, Shape, and Scattering of Sagittarius A* at 86 GHz: First VLBI with ALMA'. *ApJ* **871**.1 (2019), p. 30.

[17] The EHT Collaboration et al. 'First M87 Event Horizon Telescope Results. I. The Shadow of the Supermassive Black Hole'. *ApJL* **875** (2019), p. 1.

[18] C. P. Burgess. 'Quantum Gravity in Everyday Life: General Relativity as an Effective Field Theory'. *Living Rev. Relativ.* **7**.1 (2004), p. 5.

[19] C.P. Burgess. 'An Introduction to Effective Field Theory'. *Ann. Rev. Nucl. Part. Sci.* **57**.1 (2007), pp. 329–362.

[20] C. Kiefer. 'Quantum Gravity'. 3rd ed. International series of monographs on physics. Oxford Univ. Pr., 2012.

[21] K. Krasnov and R. Percacci. 'Gravity and unification: a review'. *Class. Quantum Gravity* **35**.14 (2018), p. 143001.

[22] I. Saltas, L. Amendola, M. Kunz and I. Sawicki. 'Modified gravity, gravitational waves and the large-scale structure of the Universe: A brief report'. *15th Marcel Grossmann Meeting on Recent Developments in Theoretical and Experimental General Relativity, Astrophysics, and Relativistic Field Theories (MG15) Rome, Italy, July 1-7, 2018*. 2018.

[23] S. Nojiri, S. Odintsov and V. Oikonomou. 'Modified Gravity Theories on a Nutshell: Inflation, Bounce and Late-time Evolution'. *Phys. Rep.* **692** (2017).

[24] T. Clifton, P. Ferreira, A. Padilla and C. Skordis. 'Modified Gravity and Cosmology'. *Phys. Rep.* **513** (2011).

[25] E. Berti et al. 'Testing general relativity with present and future astrophysical observations'. *Class. Quantum Gravity* **32**.24 (2015), p. 243001.

[26] K. Koyama. 'Cosmological tests of modified gravity'. *Rep. Prog. Phys.* **79**.4 (2016), p. 046902.

[27] E. Papantonopoulos, ed. 'Modifications of Einstein's Theory of Gravity at Large Distances'. Lecture Notes in Physics. Springer, 2015.

[28] C. M. Will. 'Theory and Experiment in Gravitational Physics'. 2nd ed. Cambridge Univ. Pr., 2018.

[29] S. Kobayashi and K. Nomizu. 'Foundations of Differential Geometry. Vol. 1'. Wiley Classics Library. Wiley InterScience, 1996.

[30] S. Kobayashi and K. Nomizu. 'Foundations of Differential Geometry. Vol. 2'. Wiley Classics Library. Wiley InterScience, 1996.

[31] M. Nakahara. 'Geometry, topology and physics'. 2nd ed. Graduate Student Series in Physics. Institue of Physics Publishing, 2003.

[32] G. Rudolph and M. Schmidt. 'Differential Geometry and Mathematical Physics: Part I. Manifolds, Lie Groups and Hamiltonian Systems'. Theoretical and Mathematical Physics. Springer, 2013.

[33] G. Rudolph and M. Schmidt. 'Differential Geometry and Mathematical Physics: Part II. Fibre Bundles, Topology and Gauge Fields'. Theoretical and Mathematical Physics. Springer, 2017.

[34] P. Godfrey-Smith. 'Theory and Reality: An Introduction to Philosophy of Science'. Chicago Univ. Pr., 2003.

[35] C. Cohen-Tannoudji, B. Diu and F. Laloë. 'Quantum Mechanics. Vol. 1: Basic Concepts, Tools, and Applications'. 2nd ed. Wiley, 2019.

[36] C. Cohen-Tannoudji, B. Diu and F. Laloë. 'Quantum Mechanics. Vol. 2: Angular Momentum, Spin, and Approximation Methods'. 2nd ed. Wiley, 2019.

[37] C. Cohen-Tannoudji, B. Diu and F. Laloë. 'Quantum Mechanics. Vol. 3: Fermions, Bosons, Photons, Correlations, and Entanglement'. 2nd ed. Wiley, 2019.

[38] S. Weinberg. 'Lectures on Quantum Mechanics'. 2nd ed. Cambridge Univ. Pr., 2015.

[39] D. Nawarajan and M. Visser. 'Global properties of physically interesting Lorentzian spacetimes'. *Int. J. Mod. Phys. D* **25**.14 (2016), p. 1650106.

[40] N. Deruelle and J.-P. Uzan. 'Relativity in Modern Physics'. Oxford Graduate Texts. Oxford Univ. Pr., 2018.

[41] J. L. Anderson. 'Principles of relativity physics'. Academic Pr., 1967.

[42] M. Friedman. 'Foundations of Space-Time Theories: Relativistic Physics and Philosophy of Science'. Princeton Univ. Pr., 1983.

[43] C. N. Yang and R. L. Mills. 'Conservation of Isotopic Spin and Isotopic Gauge Invariance'. *Phys. Rev.* **96**.1 (1954), pp. 191–195.

[44] M. E. Peskin and D. V. Schroeder. 'An Introduction to quantum field theory'. Addison-Wesley, 1995.

[45] S. Weinberg. 'The Quantum Theory of Fields. Vol. 1: Foundations'. Vol. 1. Cambridge Univ. Pr., 1995.

[46] S. Weinberg. 'The Quantum Theory of Fields. Vol. 2: Modern applications'. Vol. 2. Cambridge Univ. Pr., 1996.

[47] A. Zee. 'Quantum field theory in a nutshell'. 2nd ed. Princeton Univ. Pr., 2010.

[48] E. Gourgoulhon. 'Special Relativity in General Frames'. Graduate Texts in Physics. Springer, 2013.

[49] E. Minguzzi. 'Lorentzian causality theory'. *Living Rev. Relativ.* **22**.1 (2019), p. 3.

[50] R. Penrose. 'Techniques of differential topology in relativity'. 3rd ed. Vol. 7. CBMS-NSF Regional Conference Series in Applied Mathematics. Society for Industrial and Applied Mathematics, 1987.

[51] S. W. Hawking and G. F. R. Ellis. 'The Large Scale Structure of Space-Time'. Cambridge Monographs on Mathematical Physics. Cambridge Univ. Pr., 1973.

[52] C. W. Misner, K. S. Thorne and J. A. Wheeler. 'Gravitation'. W. H. Freeman, 1973.

[53] K. Thorne and R. Blandford. 'Modern Classical Physics - Optics, Fluids, Plasmas, Elasticity, Relativity, and Statistical Physics'. Princeton Univ. Pr., 2017.

[54] S. Weinberg. 'Gravitation and Cosmology: Principles and Applications of the General Theory of Relativity'. John Wiley and Sons, 1972.

[55] R. M. Wald. 'General Relativity'. Chicago Univ. Pr., 1984.

[56] J. B. Hartle. 'An introduction to Einstein's general relativity'. Pearson Education, 2003.

[57] N. Straumann. 'General Relativity'. 2nd ed. Graduate Texts in Physics. Springer, 2013.

[58] S. Weinberg. 'Cosmology'. Oxford Univ. Pr., 2008.

[59] G. Wolschin, ed. 'Lectures on Cosmology - Accelerated Expansion of the Universe'. Vol. 800. Lecture Notes in Physics. Springer, 2010.

[60] P. Peter and J.-P. Uzan. 'Primordial Cosmology'. Oxford Graduate Texts. Oxford Univ. Pr., 2013.

[61] L. Rezzolla and O. Zanotti. 'Relativistic Hydrodynamics'. Oxford Univ. Pr., 2013.

[62] L. Rezzolla, P. Pizzochero, D. I. Jones, N. Rea and I. Vidaña, eds. 'The Physics and Astrophysics of Neutron Stars'. Astrophysics and Space Science Library. Springer, 2018.

[63] A. Ashtekar and V. Petkov, eds. 'Springer Handbook of Spacetime'. Springer, 2014.

[64] J. D. Norton. 'General covariance and the foundations of general relativity: eight decades of dispute'. *Rep. Prog. Phys.* **56**.7 (1993), pp. 791–858.

[65] B. Carter and N. Chamel. 'Covariant analysis of Newtonian multi-fluid models for neutron stars: I Milne-Cartan structure and variational formulation'. *Int. J. Mod. Phys. D* **13**.2 (2004), 291–325.

[66] B. Carter and N. Chamel. 'Covariant analysis of Newtonian multi-fluid models for neutron stars: II Stress-Energy Tensors and Virial Theorems'. *Int. J. Mod. Phys. D* **14**.5 (2005), 717–748.

[67] B. Carter and N. Chamel. 'Covariant analysis of Newtonian multi-fluid models for neutron stars: III Transvective, viscous, and superfluid drag dissipation'. *Int. J. Mod. Phys. D* **14**.5 (2005), 749–774.

[68] B. Carter, E. Chachoua and N. Chamel. 'Covariant Newtonian and relativistic dynamics of (magneto)-elastic solid model for neutron star crust'. *Gen. Relativ. Gravit.* **38**.1 (2006), 83–119.

[69] C. Cardall. 'Minkowski and Galilei/Newton Fluid Dynamics: A Geometric 3 + 1 Spacetime Perspective'. *Fluids* **4**.1 (2018), p. 1.

[70] E. Di Casola, S. Liberati and S. Sonego. 'Nonequivalence of equivalence principles'. *Am. J. Phys.* **83**.1 (2015), 39–46.

[71] I. M. Anderson. 'The principle of minimal gravitational coupling'. *Arch. Ration. Mech. Anal.* **75**.4 (1981), pp. 349–372.

[72] T. P. Sotiriou and V. Liberati S. an Faraoni. 'Theory of gravitation theories: a no-progress report'. *Int. J. Mod. Phys. D* **17**.03n04 (2008), pp. 399–423.

[73] A. Delhom. *Minimal coupling in presence of non-metricity and torsion*. 2020.

[74] W.-T. Ni. 'One Hundred Years of General Relativity: From Genesis and Empirical Foundations to Gravitational Waves, Cosmology and Quantum Gravity'. World Scientific, 2017.

[75] E. Di Casola, S. Liberati and S. Sonego. 'Weak equivalence principle for self-gravitating bodies: A sieve for purely metric theories of gravity'. *Phys. Rev. D* **89**.8 (2014), p. 084053.

[76] J. Bergé, P. Touboul and M. Rodrigues. 'Status of MICROSCOPE, a mission to test the Equivalence Principle in space'. *J. Phys. Conf. Ser.* **610** (2015), p. 012009.

[77] P. Touboul et al. 'MICROSCOPE Mission: First Results of a Space Test of the Equivalence Principle'. *Phys. Rev. Lett.* **119**.23 (2017), p. 231101.

[78] P. Touboul et al. 'Space test of the equivalence principle: first results of the MICROSCOPE mission'. *Class. Quantum Gravity* **36**.22 (2019), p. 225006.

[79] G. S. Hall and D. P. Lonie. 'The principle of equivalence and projective structure in spacetimes'. *Class. Quantum Gravity* **24**.14 (2007), pp. 3617–3636.

[80] G. S. Hall and D. P. Lonie. 'Projective structure and holonomy in four-dimensional Lorentz manifolds'. *J. Geom. Phys.* **61**.2 (2011), pp. 381 –399.

[81] G. S. Hall and D. P. Lonie. 'Projective structure and holonomy in general relativity'. *Class. Quantum Gravity* **28**.8 (2011), p. 083101.

[82] E. Seiler and I.-O. Stamatescu, eds. 'Approaches to Fundamental Physics: An Assessment of Current Theoretical Ideas'. Vol. 721. Lecture Notes in Physics. Springer, 2007.

[83] C. Rovelli and M. Gaul. 'Loop Quantum Gravity and the Meaning of Diffeomorphism Invariance'. *Towards Quantum Gravity*. Ed. by J. Kowalski-Glikman. Vol. 541. Lecture Notes in Physics. Springer, 2000, p. 277.

[84] H. Westman and S. Sonego. 'Coordinates, observables and symmetry in relativity'. *Ann. Phys.* **324**.8 (2009), 1585–1611.

[85] O. Pooley. 'Background Independence, Diffeomorphism Invariance, and the Meaning of Coordinates'. *Towards a Theory of Spacetime Theories*. Ed. by D. Lehmkuhl, G. Schiemann and E. Scholz. Vol. 13. Einstein studies book series. Springer, 2017, pp. 105–143.

[86] D Lovelock. 'The Einstein Tensor and Its Generalizations'. *J. Math. Phys.* **12**.3 (1971), pp. 498–501.

[87] D. Lovelock. 'The Four-Dimensionality of Space and the Einstein Tensor'. *J. Math. Phys.* **13**.6 (1972), pp. 874–876.

[88] C. Lanczos. *Z. Phys.* **73** (1932), p. 147.

[89] C. Lanczos. 'A Remarkable Property of the Riemann-Christoffel Tensor in Four Dimensions'. *Ann. Math.* **39**.4 (1938), pp. 842–850.

[90] R. P. Woodard. 'The Theorem of Ostrogradsky' (2015).

[91] F. Sbisà. 'Classical and quantum ghosts'. *Eur. J. Phys.* **36**.1 (2014), p. 015009.

[92] M. Hadamard. 'Les problèmes aux limites dans la théorie des équations aux dérivées partielles'. *J. Phys. Theor. Appl.* **6**.1 (1907), pp. 202–241.

[93] D. Hilditch. 'An introduction to well-posedness and free-evolution'. *Int. J. Mod. Phys. A* **28**.22n23 (2013), p. 1340015.

[94] E. Gourgoulhon. '3+1 Formalism in General Relativity'. Lecture Notes in Physics. Springer, 2012.

[95] Y. Choquet-Bruhat and R. Geroch. 'Global aspects of the Cauchy problem in general relativity'. *Commun. Math. Phys.* **14**.4 (1969), pp. 329–335.

[96] Y. Choquet-Bruhat. 'General Relativity and the Einstein Equations'. Oxford Mathematical Monographs. Oxford Univ. Pr., 2009.

[97] E. Gourgoulhon. *Geometry and physics of black holes*. 2020. URL: https://luth.obspm.fr/~luthier/gourgoulhon/bh16/ (visited on 12/04/2020).

[98] W. Israel. 'Event Horizons in Static Vacuum Space-Times'. *Phys. Rev.* **164**.5 (1967), pp. 1776–1779.

[99] W. Israel. 'Event Horizons in Static Electrovac Space-Times'. *Commun. Math. Phys.* **8**.3 (1968), pp. 245–260.

[100] B. Carter. 'Axisymmetric Black Hole Has Only Two Degrees of Freedom'. *Phys. Rev. Lett.* **26**.6 (1971), pp. 331–333.

[101] S. W. Hawking. 'Black holes in general relativity'. *Commun. Math. Phys.* **25**.2 (1972), pp. 152–166.

[102] D. C. Robinson. 'Uniqueness of the Kerr Black Hole'. *Phys. Rev. Lett.* **34**.14 (1975), pp. 905–906.

[103] M. Heusler. 'Black Hole Uniqueness Theorems'. Cambridge Lecture Notes in Physics. Cambridge Univ. Pr., 1996.

[104] P. T. Chruściel, J. L. Costa and M. Heusler. 'Stationary Black Holes: Uniqueness and Beyond'. *Living Rev. Relativ.* **15**.1 (2012), p. 7.

[105] B. Carter. 'Complete Analytic Extension of the Symmetry Axis of Kerr's Solution of Einstein's Equations'. *Phys. Rev.* **141**.4 (1966), pp. 1242–1247.

[106] B. Carter. 'Global Structure of the Kerr Family of Gravitational Fields'. *Phys. Rev.* **174**.5 (1968), pp. 1559–1571.

[107] B. Carter. 'Hamilton-Jacobi and Schrödinger separable solutions of Einstein's equations'. *Commun. Math. Phys.* **10**.4 (1968), pp. 280–310.

[108] B. Carter. 'Killing Horizons and Orthogonally Transitive Groups in Space-Time'. *J. Math. Phys.* **10** (1969), pp. 70–81.

[109] B. Carter. 'Republication of: Black hole equilibrium states. Part I Analytic and geometric properties of the Kerr solutions'. *Gen. Relativ. Gravit.* **41**.12 (2009), pp. 2873–2938.

[110] B. Carter. 'Republication of: Black hole equilibrium states Part II. General theory of stationary black hole states'. *Gen. Relativ. Gravit.* **42**.3 (2010), pp. 653–744.

[111] J. M. Bardeen, B. Carter and S. W. Hawking. 'The Four laws of black hole mechanics'. *Commun. Math. Phys.* **31**.2 (1973), pp. 161–170.

[112] S. Chandrasekhar. 'The mathematical theory of black holes'. International series of monographs on physics. Oxford Univ. Pr., 1983.

[113] V. P. Frolov and I. D. Novikov. 'Black hole physics: Basic concepts and new developments'. Vol. 96. Fundamental Theories of Physics. Springer, 1998, pp. 1–624.

[114] E. Poisson. 'A Relativist's Toolkit: The Mathematics of Black-Hole Mechanics'. Cambridge Univ. Pr., 2009.

[115] V. Frolov and A. Zelnikov. 'Introduction to Black Hole Physics'. Oxford Univ. Pr., 2011.

[116] D. Christodoulou and S. Klainerman. 'The Global Nonlinear Stability of the Minkowski Space'. Princeton Univ. Pr., 1993.

[117] F. Nicolò and S. Klainerman. 'The Evolution Problem in General Relativity'. 2003.

[118] P. G. LeFloch and Y. Ma. 'The global nonlinear stability of Minkowski space. Einstein equations, f(R)-modified gravity, and Klein-Gordon fields' (2017).

[119] P. G. LeFloch and Y. Ma. 'The Global Nonlinear Stability of Minkowski Space for Self-Gravitating Massive Fields'. World Scientific, 2017.

[120] T. Regge and J. A. Wheeler. 'Stability of a Schwarzschild Singularity'. *Phys. Rev.* **108** (4 1957), pp. 1063–1069.

[121] C. V. Vishveshwara. 'Stability of the Schwarzschild Metric'. *Phys. Rev. D* **1** (10 1970), pp. 2870–2879.

[122] M. Dafermos, G. Holzegel and I. Rodnianski. 'The linear stability of the Schwarzschild solution to gravitational perturbations'. *Acta Math.* **222**.1 (2019), 1–214.

[123] Bernard F. Whiting. 'Mode stability of the Kerr black hole'. *J. Math. Phys.* **30**.6 (1989), pp. 1301–1305.

[124] Mihalis Dafermos, Igor Rodnianski and Yakov Shlapentokh-Rothman. 'Decay for solutions of the wave equation on Kerr exterior spacetimes III: The full subextremal case $|a| < M$' (2014).

[125] L. Blanchet, A. Spallicci and B. Whiting, eds. 'Mass and motion in general relativity'. Vol. 162. Fundamental Theories of Physics. Springer, 2011, pp. 1–624.

[126] L. B. Szabados. 'Quasi-Local Energy-Momentum and Angular Momentum in General Relativity'. *Living Rev. Rel.* **12**.1 (2009), p. 4.

[127] S. G. Turyshev. 'Experimental Tests of General Relativity'. *Ann. Rev. Nucl. Part. Sci.* **58**.1 (2008), pp. 207–248.

[128] E. Poisson and C. M. Will. 'Gravity: Newtonian, Post-Newtonian, Relativistic'. Cambridge Univ. Pr., 2014.

[129] L. Blanchet. 'Gravitational Radiation from Post-Newtonian Sources and Inspiralling Compact Binaries'. *Living Rev. Relativ.* **17**.1 (2014), p. 2.

[130] T. Damour. 'Introductory lectures on the Effective One Body formalism'. *Int. J. Mod. Phys. A* **23**.08 (2008), pp. 1130–1148.

[131] E. Berti, K. Yagi and N. Yunes. 'Extreme gravity tests with gravitational waves from compact binary coalescences: (I) inspiral–merger'. *General Relativity and Gravitation* **50**.4 (2018), p. 46.

[132] E. Berti, K. Yagi, H. Yang and N. Yunes. 'Extreme gravity tests with gravitational waves from compact binary coalescences: (II) ringdown'. *General Relativity and Gravitation* **50**.5 (2018), p. 49.

[133] K. D. Kokkotas and B. G. Schmidt. 'Quasi-Normal Modes of Stars and Black Holes'. *Living Rev. Relativ.* **2**.1 (1999), p. 2.

[134] E. Berti, V. Cardoso and A. O. Starinets. 'Quasinormal modes of black holes and black branes'. *Class. Quantum Gravity* **26**.16 (2009), p. 163001.

[135] C. Rovelli and F. Vidotto. 'Covariant Loop Quantum Gravity: An Elementary Introduction to Quantum Gravity and Spinfoam Theory'. Cambridge Monographs on Mathematical Physics. Cambridge Univ. Pr., 2014.

[136] K. Ming, Triyanta and J. S. Kosasih. 'Possibility of gravitational quantization under the teleparallel theory of gravitation'. *AIP Conf. Proc.* Ed. by N. N. Rupiasih, W. G. Suharta and H. Suyanto. Vol. 1719. 1. 2016, p. 030004.

[137] F. T. Brandt, D. G. C. McKeon and Chenguang Zhao. 'Quantizing the Palatini action using a transverse traceless propagator'. *Phys. Rev. D* **96**.12 (2017), p. 125009.

[138] V. C. de Andrade, L. C. T. Guillen and J. G. Pereira. 'Teleparallel Gravity: An Overview' (2000).

[139] R. Aldrovandi and J. G. Pereira. 'Teleparallel Gravity'. Vol. 173. Fundamental Theories of Physics. Springer, 2013.

[140] A. Golovnev. 'Introduction to teleparallel gravities'. *9th Mathematical Physics Meeting: Summer School and Conference on Modern Mathematical Physics*. 2018.

[141] M. Fontanini, E. Huguet and M. Le Delliou. 'Teleparallel gravity equivalent of general relativity as a gauge theory: Translation or Cartan connection?' *Phys. Rev. D* **99**.6 (2019), p. 064006.

[142] J. G. Pereira and Yuri N. Obukhov. 'Gauge Structure of Teleparallel Gravity'. *Universe* **5**.6 (2019), p. 139.

[143] M. Le Delliou, E. Huguet and M. Fontanini. 'Teleparallel theory as a gauge theory of translations: Remarks and issues'. *Phys. Rev. D* **101**.2 (2020), p. 024059.

[144] B. Janssen, A. Jimenez-Cano, J. A. Orejuela and P. Sanchez-Moreno. '(Non-)uniqueness of Einstein-Palatini Gravity'. 2019.

[145] V. Vitagliano, T. P. Sotiriou and S. Liberati. 'The dynamics of metric-affine gravity'. *Ann. Phys.* **326**.5 (2011), 1259–1273. [Erratum: Annals Phys. 329, 186–187 (2013)].

[146] K. Shimada, K. Aoki and K. Maeda. 'Metric-affine gravity and inflation'. *Phys. Rev. D* **99**.10 (2019), p. 104020.

[147] F.W. Hehl, P. von der Heyde, G.D. Kerlick and J.M. Nester. 'General relativity with spin and torsion: Foundations and prospects'. *Rev. Mod. Phys.* **48**.3 (1976), pp. 393–416.

[148] A. Trautman. 'Einstein-Cartan Theory'. *Encyclopedia of Mathematical Physics* **2** (2006).

[149] T. Padmanabhan and D. Kothawala. 'Lanczos–Lovelock models of gravity'. *Phys. Rep.* **531**.3 (2013), 115–171.

[150] R. P. Kerr. 'Gravitational Field of a Spinning Mass as an Example of Algebraically Special Metrics'. *Phys. Rev. Lett.* **11**.5 (1963), pp. 237–238.

[151] F.R. Tangherlini. 'Schwarzschild field in n dimensions and the dimensionality of space problem'. *Nuovo Cim.* **27** (1963), pp. 636–651.

[152] R. C. Myers and M. J. Perry. 'Black holes in higher dimensional space-times'. *Ann. Phys.* **172**.2 (1986), pp. 304 –347.

[153] R. Emparan and H. S. Reall. 'Black Holes in Higher Dimensions'. *Living Rev. Relativ.* **11**.1 (2008), p. 6.

[154] G. Horowitz, ed. 'Black Holes in Higher Dimensions'. Cambridge Univ. Pr., 2012.

[155] P. Binetruy. 'Supersymmetry: Theory, experiment and cosmology'. Oxford Univ. Pr., 2006.

[156] T. Kaluza. 'On the Unification Problem in Physics'. *Int. J. Mod. Phys. D* **27**.14 (2018), p. 1870001.

[157] O. Klein. 'Quantum Theory and Five-Dimensional Relativity Theory'. *The Oskar Klein memorial lectures. Vol. 1: Lectures by C.N. Yang and S. Weinberg with translated reprints by O. Klein.* Ed. by G. Ekspong. World Scientific Pub. Co. Pte. Lt., 1991, p. 67.

[158] O. Klein. 'The Atomicity of Electricity as a Quantum Theory Law'. *The Oskar Klein memorial lectures. Vol. 1: Lectures by C.N. Yang and S. Weinberg with translated reprints by O. Klein.* Ed. by G. Ekspong. World Scientific Pub. Co. Pte. Lt., 1991, p. 81.

[159] P. S. Wesson. 'Space - time - matter: Modern Kaluza-Klein theory'. 1999.

[160] P. S. Wesson. 'Five-Dimensional Physics: Classical and quantum consequences of Kaluza-Klein cosmology'. World Scientific Pub. Co. Pte. Lt., 2006.

[161] P. S. Wesson and J. M. Overduin. 'Principles of Space-Time-Matter'. World Scientific Pub. Co. Pte. Lt., 2018.

[162] M. Fierz. 'On the relativistic theory of force-free particles with any spin'. *Helv. Phys. Acta* **12** (1939), pp. 3–37.

[163] M. Fierz and W. Pauli. 'On relativistic wave equations for particles of arbitrary spin in an electromagnetic field'. *Proc. Roy. Soc. Lond.* **A173** (1939), pp. 211–232.

[164] V. I. Ogievetsky and I. V. Polubarinov. 'Interacting field of spin 2 and the Einstein equations'. *Ann. Phys.* **35**.2 (1965), pp. 167–208.

[165] H. van Dam and M. J. G. Veltman. 'Massive and mass-less Yang-Mills and gravitational fields'. *Nucl. Phys.* **B22**.2 (1970), pp. 397–411.

[166] V. I. Zakharov. 'Linearized gravitation theory and the graviton mass'. *JETP Lett.* **12** (1970). [Pisma Zh. Eksp. Teor. Fiz.12,447(1970)], p. 312.

[167] A.I. Vainshtein. 'To the problem of nonvanishing gravitation mass'. *Phys. Lett. B* **39**.3 (1972), pp. 393 –394.

[168] D. G. Boulware and S. Deser. 'Can Gravitation Have a Finite Range?' *Phys. Rev. D* **6**.12 (1972), pp. 3368–3382.

[169] G. Dvali, G. Gabadadze and M. Porrati. '4D Gravity on a Brane in 5D Minkowski Space'. *Phys. Lett. B* **485** (2000), pp. 208–214.

[170] C. de Rham. 'Massive Gravity'. *Living Rev. Relativ.* **17**.1 (2014), p. 7.

[171] C. Deffayet, G. Dvali, G. Gabadadze and A. Vainshtein. 'Nonperturbative continuity in graviton mass versus perturbative discontinuity'. *Phys. Rev. D* **65**.4 (2002), p. 044026.

[172] C. Deffayet and J.-W. Rombouts. 'Ghosts, strong coupling, and accidental symmetries in massive gravity'. *Phys. Rev. D* **72**.4 (2005), p. 044003.

[173] C. de Rham, G. Gabadadze and A. J. Tolley. 'Resummation of Massive Gravity'. *Phys. Rev. Lett.* **106**.23 (2011), p. 231101.

[174] K. Hinterbichler. 'Theoretical aspects of massive gravity'. *Rev. Mod. Phys.* **84**.2 (2012), pp. 671–710.

[175] E. Babichev and R. Brito. 'Black holes in massive gravity'. *Class. Quantum Gravity* **32**.15 (2015), p. 154001.

[176] E. Babichev, C. Deffayet and R. Ziour. 'The Vainshtein mechanism in the decoupling limit of massive gravity'. *J. High Energy Phys.* **2009**.5 (2009), 098–098.

[177] E. Babichev, C. Deffayet and R. Ziour. 'Recovering General Relativity from Massive Gravity'. *Phys. Rev. Lett.* **103**.20 (2009), p. 201102.

[178] E. Babichev, C. Deffayet and R. Ziour. 'The recovery of general relativity in massive gravity via the Vainshtein mechanism'. *Phys. Rev. D* **82**.10 (2010), p. 104008.

[179] E. Babichev and M. Crisostomi. 'Restoring general relativity in massive bigravity theory'. *Phys. Rev. D* **88**.8 (2013), p. 084002.

[180] E. Babichev, C. Deffayet and R. Ziour. 'k-Mouflage gravity'. *Int. J. Mod. Phys. D* **18**.14 (2009), 2147–2154.

[181] C. de Rham. 'Galileons in the Sky'. *Comptes Rendus Physique* **13** (2012), pp. 666–681.

[182] D. Tong. 'Lectures on String Theory' (2009).

[183] Y. Fujii and K. Maeda. 'The Scalar-Tensor Theory of Gravitation'. Cambridge Monographs on Mathematical Physics. Cambridge Univ. Pr., 2003.

[184] D. Langlois. 'Dark energy and modified gravity in degenerate higher-order scalar–tensor (DHOST) theories: A review'. *Int. J. Mod. Phys. D* **28**.05 (2019), p. 1942006.

[185] T. Jacobson and D. Mattingly. 'Gravity with a dynamical preferred frame'. *Phys. Rev. D* **64**.2 (2001), p. 024028.

[186] T. Jacobson. 'Einstein-Æther gravity: A status report'. *Proceedings of Science* **043-QG-PH** (2008), p. 020.

[187] O. Sarbach, E. Barausse and J. A. Preciado-López. 'Well-posed Cauchy formulation for Einstein-Æther theory'. *Class. Quantum Gravity* **36**.16 (2019), p. 165007.

[188] Y. Gong, S. Hou, D. Liang and E. Papantonopoulos. 'Gravitational waves in Einstein-Æther and generalized TeVeS theory after GW170817'. *Phys. Rev. D* **97**.8 (2018), p. 084040.

[189] C. Ding. 'Gravitational quasinormal modes of black holes in Einstein-aether theory'. *Nucl. Phys. B* **938** (2019), 736–750.

[190] J. D. Bekenstein. 'Relativistic gravitation theory for the modified Newtonian dynamics paradigm'. *Phys. Rev. D* **70**.8 (2004), p. 083509. [Erratum: Phys. Rev. D 71, 069901 (2005)].

[191] M. Milgrom. 'A modification of the Newtonian dynamics as a possible alternative to the hidden mass hypothesis.' *ApJ* **270** (1983), pp. 365–370.

[192] M. Milgrom. 'A modification of the Newtonian dynamics - Implications for galaxies.' *ApJ* **270** (1983), pp. 371–389.

[193] M. Milgrom. 'A modification of the newtonian dynamics : implications for galaxy systems.' *ApJ* **270** (1983), pp. 384–389.

[194] J. Polchinski. 'String Theory. Vol. 1: An introduction to the bosonic string'. Cambridge Monographs on Mathematical Physics. Cambridge Univ. Pr., 1998.

[195] J. Polchinski. 'String Theory. Vol. 2: Superstring theory and beyond'. Cambridge Monographs on Mathematical Physics. Cambridge Univ. Pr., 1998.

[196] T. Ortín. 'Gravity and Strings'. 2nd ed. Cambridge Monographs on Mathematical Physics. Cambridge Univ. Pr., 2015.

[197] C. Rovelli. 'Quantum Gravity'. Cambridge Monographs on Mathematical Physics. Cambridge Univ. Pr., 2004.

[198] N. Bodendorfer. 'An elementary introduction to loop quantum gravity' (2016).

[199] J. F. Donoghue. 'The effective field theory treatment of quantum gravity'. *AIP Conf. Proc.* **1483**.1 (2012), pp. 73–94.

[200] J. F. Donoghue, M. M. Ivanov and A. Shkerin. 'EPFL Lectures on General Relativity as a Quantum Field Theory' (2017).

[201] A. Eichhorn. 'Asymptotically safe gravity' (2020).

[202] F. Dowker. 'Causal sets and the deep structure of spacetime'. *100 Years Of Relativity: space-time structure: Einstein and beyond*. Ed. by A. Ashtekar. 2005, pp. 445–464.

[203] S. Surya. 'The causal set approach to quantum gravity'. *Living Rev. Relativ.* **22**.1 (2019), p. 5.

[204] A. Connes. *Noncommutative Geometry*. URL: `https://www.alainconnes.org/fr/downloads.php` (visited on 12/04/2020).

[205] A. Connes and M. Marcolli. *Noncommutative Geometry, Quantum Fields and Motives*. URL: `https://www.alainconnes.org/fr/downloads.php` (visited on 12/04/2020).

[206] R. Penrose and M. A. H. MacCallum. 'Twistor theory: An approach to the quantisation of fields and space-time'. *Phys. Rep.* **6**.4 (1973), pp. 241 –315.

[207] S. Weinberg. 'The Quantum Theory of Fields. Vol. 3: Supersymmetry'. Vol. 3. Cambridge Univ. Pr., 2000.

[208] G. W. Horndeski. 'Second-order scalar-tensor field equations in a four-dimensional space'. *Int. J. Theor. Phys.* **10** (1974), pp. 363–384.

[209] C. Charmousis, E. J. Copeland, A. Padilla and P. M. Saffin. 'General Second-Order Scalar-Tensor Theory and Self-Tuning'. *Phys. Rev. Lett.* **108**.5 (2012), p. 051101.

[210] T. Kobayashi, M. Yamaguchi and J. Yokoyama. 'Generalized G-inflation: Inflation with the most general second-order field equations'. *Prog. Theor. Phys.* **126** (2011), pp. 511–529.

[211] M. A. Luty, M. Porrati and R. Rattazzi. 'Strong interactions and stability in the DGP model'. *J. High Energy Phys.* **2003**.09 (2003), pp. 029–029.

[212] A. Nicolis and R. Rattazzi. 'Classical and Quantum Consistency of the DGP Model'. *J. High Energy Phys.* **2004**.06 (2004), pp. 059–059.

[213] A. Nicolis, R. Rattazzi and E. Trincherini. 'The Galileon as a local modification of gravity'. *Phys. Rev. D* **79**.6 (2009), p. 064036.

[214] C. Deffayet, S. Deser and G. Esposito-Farèse. 'Generalized Galileons: All scalar models whose curved background extensions maintain second-order field equations and stress tensors'. *Phys. Rev. D* **80**.6 (2009), p. 064015.

[215] C. Deffayet and D. A. Steer. 'A formal introduction to Horndeski and Galileon theories and their generalizations'. *Class. Quantum Gravity* **30**.21 (2013), p. 214006.

[216] J. E. Chase. 'Event Horizons in Static Scalar-Vacuum Space-Times'. *Commun. Math. Phys.* **19**.4 (1970), pp. 276–288.

[217] J. D. Bekenstein. 'Transcendence of the Law of Baryon-Number Conservation in Black-Hole Physics'. *Phys. Rev. Lett.* **28**.7 (1972), pp. 452–455.

[218] J. D. Bekenstein. 'Nonexistence of Baryon Number for Static Black Holes'. *Phys. Rev. D* **5**.6 (1972), pp. 1239–1246.

[219] J. D. Bekenstein. 'Nonexistence of Baryon Number for Black Holes. II'. *Phys. Rev. D* **5**.10 (1972), pp. 2403–2412.

[220] I. Peña and D. Sudarsky. 'Do collapsed boson stars result in new types of black holes?' *Class. Quantum Gravity* **14**.11 (1997), pp. 3131–3134.

[221] Carlos A. R. Herdeiro and Eugen Radu. 'Kerr Black Holes with Scalar Hair'. *Phys. Rev. Lett.* **112**.22 (2014), p. 221101.

[222] C. Herdeiro and E. Radu. 'Construction and physical properties of Kerr black holes with scalar hair'. *Class. Quantum Gravity* **32**.14 (2015), p. 144001.

[223] S. W. Hawking. 'Black holes in the Brans-Dicke theory of gravitation'. *Commun. Math. Phys.* **25**.2 (1972), pp. 167–171.

[224] B. C. Xanthopoulos and T. Zannias. 'The uniqueness of the Bekenstein black hole'. *J. Math. Phys.* **32**.7 (1991), pp. 1875–1880.

[225] T. Zannias. 'Black holes cannot support conformal scalar hair'. *J. Math. Phys.* **36**.12 (1995), 6970–6980.

[226] J. D. Bekenstein. 'Novel "no-scalar-hair" theorem for black holes'. *Phys. Rev. D* **51**.12 (1995), R6608–R6611.

[227] Alberto Saa. 'New no-scalar-hair theorem for black holes'. *J. Math. Phys.* **37**.5 (1996), 2346–2351.

[228] T. P. Sotiriou and V. Faraoni. 'Black Holes in Scalar-Tensor Gravity'. *Phys. Rev. Lett.* **108**.8 (2012), p. 081103.

[229] V. Faraoni and T. P. Sotiriou. 'Absence of scalar hair in scalar-tensor gravity'. *The Thirteenth Marcel Grossmann Meeting*. Ed. by Kjell Rosquist, Robert T Jantzen and Remo Ruffini. World Scientific, 2015, pp. 1119–1121.

[230] C. Herdeiro and E. Radu. 'Asymptotically flat black holes with scalar hair: A review'. *Proceedings, 7th Black Holes Workshop 2014: Aveiro, Portugal, December 18-19, 2014*. Ed. by C. A. R. Herdeiro, V. Cardoso, J. P. S. Lemos and F. C. Mena. Vol. 24. 09. 2015, p. 1542014.

[231] M. S. Volkov. 'Hairy black holes in the XX-th and XXI-st centuries'. *Proceedings, 14th Marcel Grossmann Meeting on Recent Developments in Theoretical and Experimental General Relativity, Astrophysics, and Relativistic Field Theories (MG14) (In 4 Volumes): Rome, Italy, July 12-18, 2015*. Ed. by M. Bianchi, R. T. Jantzen and R. Ruffini. Vol. 2. 2017, pp. 1779–1798.

[232] L. Hui and A. Nicolis. 'No-Hair Theorem for the Galileon'. *Phys. Rev. Lett.* **110**.24 (2013), p. 241104.

[233] T. P. Sotiriou and S. Zhou. 'Black Hole Hair in Generalized Scalar-Tensor Gravity'. *Phys. Rev. Lett.* **112**.25 (2014), p. 251102.

[234] T. P. Sotiriou and S. Zhou. 'Black hole hair in generalized scalar-tensor gravity: An explicit example'. *Phys. Rev. Lett.* **90**.12 (2014), p. 124063.

[235] E. Babichev, C. Charmousis and A. Lehébel. 'Black holes and stars in Horndeski theory'. *Class. Quantum Gravity* **33**.15 (2016), p. 154002.

[236] A. Maselli, H. O. Silva, M. Minamitsuji and E. Berti. 'Slowly rotating black hole solutions in Horndeski gravity'. *Phys. Rev. D* **92**.10 (2015), p. 104049.

[237] A. Lehébel, E. Babichev and C. Charmousis. 'A no-hair theorem for stars in Horndeski theories'. *JCAP* **1707**.07 (2017), p. 037.

[238] E. Babichev and C. Charmousis. 'Dressing a black hole with a time-dependent Galileon'. *J. High Energy Phys.* **08** (2014), p. 106.

[239] E. Babichev, C. Charmousis, A. Lehébel and T. Moskalets. 'Black holes in a cubic Galileon universe'. *J. Cosmol. Astropart. Phys.* **1609**.09 (2016), p. 011.

[240] E. Babichev, C. Deffayet and G. Esposito-Farèse. 'Constraints on Shift-Symmetric Scalar-Tensor Theories with a Vainshtein Mechanism from Bounds on the Time Variation of G'. *Phys. Rev. Lett.* **107**.25 (2011), p. 251102.

[241] E. Babichev. 'Galileon accretion'. *Phys. Rev. D* **83**.2 (2011), p. 024008.

[242] E. Babichev and G. Esposito-Farèse. 'Time-dependent spherically symmetric covariant Galileons'. *Phys. Rev. D* **87**.4 (2013), p. 044032.

[243] E. Babichev, C. Charmousis and M. Hassaine. 'Charged Galileon black holes'. *J. Cosmol. Astropart. Phys.* **2015**.05 (2015), pp. 031–031.

[244] E. Babichev and G. Esposito-Farèse. 'Cosmological self-tuning and local solutions in generalized Horndeski theories'. *Phys. Rev. D* **95**.2 (2017), p. 024020.

[245] E. Babichev, C. Charmousis and A. Lehébel. 'Asymptotically flat black holes in Horndeski theory and beyond'. *JCAP* **1704**.04 (2017), p. 027.

[246] C. Charmousis, M. Crisostomi, R. Gregory and N. Stergioulas. 'Rotating Black Holes in Higher Order Gravity'. *Phys. Rev. D* **100**.8 (2019), p. 084020.

[247] P. Kanti, N. E. Mavromatos, J. Rizos, K. Tamvakis and E. Winstanley. 'Dilatonic black holes in higher curvature string gravity'. *Phys. Rev. D* **54** (8 1996), pp. 5049–5058.

[248] S. O. Alexeyev and M. V. Pomazanov. 'Black hole solutions with dilatonic hair in higher curvature gravity'. *Phys. Rev. D* **55** (4 1997), pp. 2110–2118.

[249] P. Kanti, N. E. Mavromatos, J. Rizos, K. Tamvakis and E. Winstanley. 'Dilatonic black holes in higher curvature string gravity. II. Linear stability'. *Phys. Rev. D* **57** (10 1998), pp. 6255–6264.

[250] Paolo Pani and Vitor Cardoso. 'Are black holes in alternative theories serious astrophysical candidates? The case for Einstein-dilaton-Gauss-Bonnet black holes'. *Phys. Rev. D* **79** (8 2009), p. 084031.

[251] B. Kleihaus, J. Kunz and E. Radu. 'Rotating Black Holes in Dilatonic Einstein-Gauss-Bonnet Theory'. *Phys. Rev. Lett.* **106**.15 (2011), p. 151104.

[252] B. Kleihaus, J. Kunz, S. Mojica and E. Radu. 'Spinning black holes in Einstein-Gauss-Bonnet-dilaton theory: Nonperturbative solutions'. *Phys. Rev. D* **93**.4 (2016), p. 044047.

[253] J. F. M. Delgado, C. A. R. Herdeiro and E. Radu. 'Spinning black holes in shift-symmetric Horndeski theory'. *J. High Energy Phys.* **2020**.4 (2020), p. 180.

[254] G. Antoniou, A. Bakopoulos and P. Kanti. 'Evasion of No-Hair Theorems and Novel Black-Hole Solutions in Gauss-Bonnet Theories'. *Phys. Rev. Lett.* **120** (13 2018), p. 131102.

[255] G. Antoniou, A. Bakopoulos and P. Kanti. 'Black-hole solutions with scalar hair in Einstein-scalar-Gauss-Bonnet theories'. *Phys. Rev. D* **97** (8 2018), p. 084037.

[256] A. Bakopoulos, G. Antoniou and P. Kanti. 'Novel black-hole solutions in Einstein-scalar-Gauss-Bonnet theories with a cosmological constant'. *Phys. Rev. D* **99** (6 2019), p. 064003.

[257] G. Papallo and H. S. Reall. 'On the local well-posedness of Lovelock and Horndeski theories'. *Phys. Rev. D* **96**.4 (2017), p. 044019.

[258] Á. D. Kovács. 'Well-posedness of cubic Horndeski theories'. *Phys. Rev. D* **100**.2 (2019), p. 024005.

[259] A. D. Kovacs and H. S. Reall. *Well-posed formulation of Lovelock and Horndeski theories*. 2020.

[260] D. Bettoni, J. M. Ezquiaga, K. Hinterbichler and M. Zumalacárregui. 'Speed of gravitational waves and the fate of scalar-tensor gravity'. *Phys. Rev. D* **95**.8 (2017), p. 084029.

[261] P. Creminelli and F. Vernizzi. 'Dark Energy after GW170817 and GRB170817A'. *Phys. Rev. Lett.* **119**.25 (2017), p. 251302.

[262] J. M. Ezquiaga and M. Zumalacárregui. 'Dark Energy after GW170817: dead ends and the road ahead'. *Phys. Rev. Lett.* **119**.25 (2017), p. 251304.

[263] E. J. Copeland, M. Kopp, A. Padilla, P. M. Saffin and C. Skordis. 'Dark Energy after GW170817 Revisited'. *Phys. Rev. Lett.* **122**.6 (2019), p. 061301.

[264] C. de Rham and S. Melville. 'Gravitational Rainbows: LIGO and Dark Energy at its Cutoff'. *Phys. Rev. Lett.* **121**.22 (2018), p. 221101.

[265] K. Van Acoleyen and J. Van Doorsselaere. 'Galileons from Lovelock actions'. *Phys. Rev.* **D83** (2011), p. 084025.

[266] C. Charmousis. 'From Lovelock to Horndeski's Generalized Scalar Tensor Theory'. *Proceedings of the 7th Aegean Summer School : Beyond Einstein's theory of gravity. Modifications of Einstein's Theory of Gravity at Large Distances.: Paros, Greece, September 23-28, 2013*. Vol. 892. 2015, pp. 25–56.

[267] C. Deffayet, O. Pujolàs, I. Sawicki and A. Vikman. 'Imperfect dark energy from kinetic gravity braiding'. *J. Cosmol. Astropart. Phys.* **2010**.10 (2010), pp. 026–026.

[268] A. Barreira, B. Li, C. M. Baugh and S. Pascoli. 'The observational status of Galileon gravity after Planck'. *J. Cosmol. Astropart. Phys.* **2014**.08 (2014), pp. 059–059.

[269] J. Renk, M. Zumalacárregui, F. Montanari and A. Barreira. 'Galileon gravity in light of ISW, CMB, BAO and H0 data'. *J. Cosmol. Astropart. Phys.* **2017**.10 (2017), pp. 020–020.

[270] J. Neveu, V. Ruhlmann-Kleider, P. Astier, M. Besançon, J. Guy, A. Möller and E. Babichev. 'Constraining the and Galileon models with recent cosmological data'. *A&A* **600** (2017), A40.

[271] C. Leloup, V. Ruhlmann-Kleider, J. Neveu and A. de Mattia. 'Observational status of the Galileon model general solution from cosmological data and gravitational waves'. *J. Cosmol. Astropart. Phys.* **2019**.05 (2019), pp. 011–011.

[272] A. Barreira, M. Cautun, B. Li, C. M. Baugh and S. Pascoli. 'Weak lensing by voids in modified lensing potentials'. *J. Cosmol. Astropart. Phys.* **2015**.08 (2015), pp. 028–028.

[273] S. P. E. Bergliaffa and R. Maier. 'On the Stability of Cubic Galileon Accretion'. *Ann. Phys. (N.Y.)* **384** (2017), pp. 1–10.

[274] S. Appleby and E. V. Linder. 'The paths of gravity in galileon cosmology'. *J. Cosmol. Astropart. Phys.* **2012**.03 (2012), pp. 043–043.

[275] P. Brax, C. Burrage and A.-C. Davis. 'Laboratory tests of the Galileon'. *J. Cosmol. Astropart. Phys.* **2011**.09 (2011), pp. 020–020.

[276] A. Barreira, B. Li, W. A. Hellwing, C. M. Baugh and S. Pascoli. 'Nonlinear structure formation in the cubic Galileon gravity model'. *J. Cosmol. Astropart. Phys.* **2013**.10 (2013), pp. 027–027.

[277] A. De Felice and S. Tsujikawa. 'Conditions for the cosmological viability of the most general scalar-tensor theories and their applications to extended Galileon dark energy models'. *J. Cosmol. Astropart. Phys.* **2012**.02 (2012), pp. 007–007.

[278] T. Kobayashi, H. Tashiro and D. Suzuki. 'Evolution of linear cosmological perturbations and its observational implications in Galileon-type modified gravity'. *Phys. Rev. D* **81**.6 (2010), p. 063513.

[279] A. Ijjas, F. Pretorius and P. J. Steinhardt. 'Stability and the gauge problem in non-perturbative cosmology'. *J. Cosmol. Astropart. Phys.* **1901**.01 (2019), pp. 015–015.

[280] L. Bernard, L. Lehner and R. Luna. 'Challenges to global solutions in Horndeski's theory'. *Phys. Rev. D* **100**.2 (2019), p. 024011.

[281] K. Van Aelst, E. Gourgoulhon, P. Grandclément and C. Charmousis. 'Hairy rotating black holes in cubic Galileon theory'. *Class. Quantum Gravity* **37**.3 (2020), p. 035007.

[282] E. Babichev and C. Deffayet. 'An introduction to the Vainshtein mechanism'. *Class. Quantum Gravity* **30**.18 (2013), p. 184001.

[283] A. De Felice, R. Kase and S. Tsujikawa. 'Vainshtein mechanism in second-order scalar-tensor theories'. *Phys. Rev. D* **85**.4 (2012), p. 044059.

[284] N. Kaloper, A. Padilla and N. Tanahashi. 'Galileon hairs of Dyson spheres, Vainshtein's coiffure and hirsute bubbles'. *J. High Energy Phys.* **2011**.10 (2011), p. 148.

[285] A. Avilez-Lopez, A. Padilla, Paul M. Saffin and C. Skordis. 'The Parametrized Post-Newtonian-Vainshteinian formalism'. *J. Cosmol. Astropart. Phys.* **2015**.06 (2015), pp. 044–044.

[286] C. Deffayet and T. Jacobson. 'On horizon structure of bimetric spacetimes'. *Class. Quantum Gravity* **29**.6 (2012), p. 065009.

[287] M. Saravani and T. P. Sotiriou. 'Classification of shift-symmetric Horndeski theories and hairy black holes'. *Phys. Rev. D* **99**.12 (2019), p. 124004.

[288] E. Gourgoulhon. 'An introduction to the theory of rotating relativistic stars'. *CompStar 2010: School and Workshop on Computational Tools for Compact Star Astrophysics Ganil, Caen, France, February 8-16, 2010*. 2010.

[289] E. Gourgoulhon and S. Bonazzola. 'Noncircular axisymmetric stationary spacetimes'. *Phys. Rev. D* **48**.6 (1993), pp. 2635–2652.

[290] S. Bonazzola, E. Gourgoulhon, M. Salgado and J. A. Marck. 'Axisymmetric rotating relativistic bodies: A new numerical approach for 'exact' solutions'. *A&A* **278** (1993), pp. 421–443.

[291] L. Villain, J. A. Pons, P. Cerdá-Durán and E. Gourgoulhon. 'Evolutionary sequences of rotating protoneutron stars'. *A&A* **418**.1 (2004), pp. 283–294.

[292] P. Grandclément, C. Somé and E. Gourgoulhon. 'Models of rotating boson stars and geodesics around them: New type of orbits'. *Phys. Rev. D* **90**.2 (2014), p. 024068.

[293] A. Lanza. 'Multigrid in general relativity. II. Kerr spacetime'. *Class. Quantum Gravity* **9**.3 (1992), pp. 677–696.

[294] B. Kleihaus and J. Kunz. 'Rotating Hairy Black Holes'. *Phys. Rev. Lett.* **86**.17 (2001), pp. 3704–3707.

[295] B. Kleihaus, J. Kunz and F. Navarro-Lérida. 'Rotating Einstein-Yang-Mills black holes'. *Phys. Rev. D* **66**.10 (2002), p. 104001.

[296] P. Grandclément. 'Kadath: A Spectral solver for theoretical physics'. *J. Comput. Phys.* **229** (2010), pp. 3334–3357.

[297] G. Compère and A. Fiorucci. 'Advanced Lectures on General Relativity' (2018).

[298] M. A. Abramowicz and P. C. Fragile. 'Foundations of Black Hole Accretion Disk Theory'. *Living Rev. Relativ.* **16**.1 (2013), p. 1.

[299] R. Brito, V. Cardoso and P. Pani. 'Superradiance'. *Lect. Notes Phys.* (2015).

[300] R. H. Boyer and T. G. Price. 'An interpretation of the Kerr metric in general relativity'. *Math. Proc. Camb. Philos. Soc.* **61**.2 (1965), 531–534.

[301] J.M. Bardeen. 'Stability of circular orbits in stationary, axisymmetric space-times'. *ApJ* **161** (1970), pp. 103–9.

[302] J.M. Bardeen, W.H. Press and S.A. Teukolsky. 'Rotating black holes: Locally nonrotating frames, energy extraction, and scalar synchrotron radiation'. *ApJ* **178** (1972), p. 347.

[303] D. Pugliese, H. Quevedo and R. Ruffini. 'Equatorial circular motion in Kerr spacetime'. *Phys. Rev. D* **84**.4 (2011), p. 044030.

[304] S. E. Gralla, D. E. Holz and R. M. Wald. 'Black hole shadows, photon rings, and lensing rings'. *Phys. Rev. D* **100**.2 (2019), p. 024018.

[305] A. Das, A. Saha and S. Gangopadhyay. 'Shadow of charged black holes in Gauss-Bonnet gravity'. *Eur. Phys. J. C* **80**.3 (2020), p. 180.

[306] A. Abdujabbarov, F. Atamurotov, Y. Kucukakca, B. Ahmedov and U. Camci. 'Shadow of Kerr-Taub-NUT black hole'. *Astrophys. Space Sci.* **344**.2 (2013), pp. 429–435.

[307] H. Cebeci, N. Özdemir. 'Motion of the charged test particles in Kerr-Newman-Taub-NUT spacetime and analytical solutions'. *Phys. Rev. D* **93**.10 (2016), p. 104031.

[308] C. Chakraborty and S. Bhattacharyya. 'Circular orbits in Kerr-Taub-NUT space-time and their implications for accreting black holes and naked singularities'. *J. Cosmol. Astropart. Phys.* **2019**.05 (2019), pp. 034–034.

[309] F. H. Vincent, T. Paumard, E. Gourgoulhon and G. Perrin. 'GYOTO: a new general relativistic ray-tracing code'. *Class. Quantum Gravity* **28**.22 (2011), p. 225011.

[310] F. H. Vincent, E. Gourgoulhon, C. Herdeiro and E. Radu. 'Astrophysical imaging of Kerr black holes with scalar hair'. *Phys. Rev. D* **94**.8 (2016), p. 084045.

[311] F. H. Vincent, Z. Meliani, P. Grandclément, E. Gourgoulhon and O. Straub. 'Imaging a boson star at the Galactic center'. *Class. Quantum Gravity* **33**.10 (2016), p. 105015.

[312] F. Lamy, E. Gourgoulhon, T. Paumard and F. H. Vincent. 'Imaging a non-singular rotating black hole at the center of the Galaxy'. *Class. Quantum Gravity* **35**.11 (2018), p. 115009.

[313] F. H. Vincent, E. Gourgoulhon and J. Novak. '3+1 geodesic equation and images in numerical spacetimes'. *Class. Quantum Gravity* **29**.24 (2012), p. 245005.

[314] Straub, O., Vincent, F. H., Abramowicz, M. A., Gourgoulhon, E. and Paumard, T. 'Modelling the black hole silhouette in Sagittarius A* with ion tori'. *A&A* **543** (2012), A83.

[315] Vincent, F. H., Yan, W., Straub, O., Zdziarski, A. A. and Abramowicz, M. A. 'A magnetized torus for modeling Sagittarius A* millimeter images and spectra'. *A&A* **574** (2015), A48.

[316] F. H. Vincent, M. Wielgus, M. A. Abramowicz, E. Gourgoulhon, J. P. Lasota, T. Paumard and G. Perrin. 'Geometric modeling of M87* as a Kerr black hole or a non-Kerr compact object' (2020).

[317] F. Yuan and R. Narayan. 'Hot Accretion Flows Around Black Holes'. *Annu. Rev. Astron. Astrophys.* **52**.1 (2014), pp. 529–588.

[318] A. Pandya, Z. Zhang, M. Chandra and C. F. Gammie. 'Polarized synchrotron emissivities and aborptivities for relativistic thermal, power-law, and kappa distribution functions'. *ApJ* **822**.1 (2016), p. 34.

Abstract

The present project falls within the wide effort conducted to study theories of gravitation, notably by modelling the physics of compact objects like black holes. The long-term objective of this approach is to determine all theories that are either incompatible with observations, or theoretically inconsistent. The first part of the manuscript thus presents the essential concepts and principles that are common to all these theories, and introduces some of these theories which connect to the project. In the second part, the actual contribution of the project is exposed: comparing rotating black holes of the cubic Galileon theory with the Kerr family of the general theory of relativity. The latter was developed by Albert Einstein more than a century ago, while the cubic Galileon is a much more recent theory.

First, the rotating black holes are constructed numerically. Then, the properties of the orbits around them are investigated, in particular their stability. Finally, the images of a simple model of accretion disk orbiting the black holes are simulated. Such orbits and images directly relate the observations realized by instruments like GRAVITY or the Event Horizon Telescope, which monitor supermassive black holes. The present project thus allows to identify possible tensions between the predictions of the cubic Galileon theory and observational data on black holes.

Keywords: modified gravity, cubic Galileon, hairy black hole, rotating black hole, geodesics

Résumé

Ce projet de thèse s'inscrit dans un large contexte : l'étude des théories de la gravitation, notamment par la modélisation d'objets compacts tels que les trous noirs. Le but ultime de cette démarche est de déterminer toutes les théories incompatibles avec les observations, ou présentant des pathologies théoriques. En conséquence, la première partie de ce manuscrit présente les concepts et principes essentiels communs à toutes ces théories, et introduit certaines d'entre elles entretenant un lien avec le projet. La deuxième partie expose les résultats propres au projet : une comparaison entre une famille de trous noirs en rotation issue de la théorie du Galileon cubique, et les trous noirs de Kerr de la théorie de la relativité générale. Le Galileon cubique est une théorie bien plus récente que la relativité générale, cette dernière ayant été développée par Albert Einstein il y a plus d'un siècle.

Tout d'abord, ces trous noirs sont construits numériquement. Les orbites autour de ces trous noirs, notamment leur stabilité, sont ensuite étudiées. Enfin, les images produites par un modèle simple de disque d'accrétion en orbite autour de ces trous noirs sont simulées numériquement. Ces géodésiques et images sont directement liées aux observations réalisées par certains instruments en activité, tels que GRAVITY ou l'Event Horizon Telescope, qui sont dédiés à l'étude des trous noirs supermassifs. Ce projet permet ainsi d'identifier de possibles tensions entre les prédictions de la théorie du Galileon cubique et certaines observations liées aux trous noirs.

Mots-clés: gravité modifiée, Galileon cubique, trou noir chevelu, trou noir en rotation, géodésiques